

Norwegian University
of Life Sciences

Master's Thesis 2020 60 ECTS

Faculty of Environmental Sciences and Natural Resource Management

Paleoclimatic reconstruction from laminated lake sediments, Bødalsvatnet, Nordenskiöld Land, Svalbard

Inger Marie Fausa Aasberg
Environmental Science and Natural Resources

**Paleoclimatic reconstruction from laminated lake
sediments, Bødalsvatnet, Nordenskiöld Land,
Svalbard**

Inger Marie Fausa Aasberg

This thesis was conducted in connection with the
University Centre in Svalbard:



August, 2020

Abstract

One predicted consequence of the current warming in the Arctic is an increase of heavy precipitation events. Svalbard have experienced an increase in total annual precipitation and air temperature have affected Svalbard's environment, in particular the regional hydroclimate. The varved proglacial sediment record preserved in Bødalsvatnet, Nordenskiöld Land, Svalbard, contains a valuable climate signal that in this study is used to reconstruct changes in precipitation and temperature the last 150 years. The thesis uses a multi-proxy approach with varve count, physical parameters (grain size, magnetic susceptibility, dry bulk density, loss-on-ignition and water content) and geochemical analysis through X-ray fluorescence (K, Ca, Mn, Fe, Ti and Zr) of surface core BSV – 2019 – 1. Age determination of the surface core were cross correlated with a 2012 by varve count and plutonium ($^{239+240}\text{Pu}$) measurement.

Six turbidites (E1 – E6) were identified and dated to 1936, 1945, 1957, 1983 and 1993. The six turbidites relating to mass movement events lead on by intense precipitation thought to have exceeded the 2,5 mm per hour. The current threshold for the formation of mass moment events in Svalbard. The presence of a dropstone > 1 mm within deposits from the 1957 event was likely caused by an avalanche. The 1993 and 1983 events were likely triggered by high intensity warm rainstorms related to south westerly cyclones in November and March, respectively. The mass movement event of 1974 is connected to an intense heavy precipitation event where 34 mm of rain fell during a period of 12 hours.

By cross-correlation to a longer - percussion core from 2012 the paleoclimatic record was extended to approximately 1844. The change in temperature and precipitation in combination with thicker lamina during the end of LIA has similarities to the current sedimentary record and needs to be investigated further.

Sammendrag

En forventet konsekvens av dagens oppvarming i Arktis er flere hendelser med intens nedbør. På Svalbard er det vært en økning i total årlig nedbør og temperatur som har påvirket miljøet og da særlig hydroklimaet. Den proglasiale, årlige laminerte sedimenthistorien er bevart i Bødalsvatnet, Nordenskiöld Land, Svalbard. Den inneholder et viktig klimasignal som denne studien har brukt for å rekonstruere forandringer i nedbør og temperatur de siste 150 år. Denne oppgaven bruker en multi-proxy metode på overflatekjernen BVS-2019-1 basert på fysiske parametere (kornstørrelse, magnetisk susceptibilitet, tetthet, glødetap og vanninnhold) og kjemiske parameter ved røntgen-fluorescens (K, Ca, Mn, Fe, Ti og Zr). Aldersbestemmelse av sedimentkjernen er gjort ved å korrelere varv-telling fra 2019 med varv-telling og plutonium ($^{239+240}\text{Pu}$) målinger fra et sediment kjerne tatt i 2012.

Seks turbiditeter (E1 til E6) er identifisert og datert til 1936, 1945, 1957, 1974, 1981 og 1993. Turbiditetene er relatert til massebevegelseshendelser forårsaket av nedbør med en intensitet over 2,5 mm i timen, som er grenseverdi for massebevegelseshendelser på Svalbard. Forekomst av droppstein > 1mm er knyttet til hendelse i 1974, forårsaket av et snøskred. Hendelsene i 1983 og 1993 er knyttet til sør-vestlig sykloner som har ført til mild regnstorm med høy intensitet i henholdsvis mars og november. Hendelsen i 1974 er knyttet til intenst regnvær hvor det falt 34 mm regn over en periode på 12 timer.

Ved å korrelere den lengre sediment kjernen fra 2012 ble den paleoklimatiske historien utvidet ytterligere, til ca. 1844. Forandringen i temperatur og nedbør sammen med tykkere lamina ved utgangen av LIA har likheter ved det nåværende sedimentære historien og trenger å bli studert ytterligere.

Acknowledgements

I would like to thank my supervisor at the Norwegian University of Life Sciences, Mona Henriksen for supporting my choices, her guidance and knowledge.

I am grateful to my University of Svalbard supervisor, Michael Retelle for his supervision, generosity and guidance. Thank you, Mike, your encouragement led me through this project.

This research was supported by a grant to Retelle from the U.S. National Science Foundation, Office of Polar Programs, Arctic Natural Sciences (award number 1744433).

I would like to thank Jan Christensen's Endowment for supporting my stay in Svalbard.

Further I would like to thank Phil Dostie, for your guidance in the laboratory and lab technician Pete Dawson and Professor Mike Rhodes at the Ronald B. Gilmore X-Ray Fluorescence Lab at UMass Amherst for sharing your extensive ITRAX expertise.

And a big thank you to Wesley Farnsworth and Håvard Toft Larsen for all the help during my fieldwork in Bødalen.

I would also like to thank Mike, Sylvia, Hannah, Emma, Julie and Leah for welcoming me to Maine and making my stay unforgettable.

Thank you to my “Svalbard family” for your encouragement. And the start of 2020 has been different for many and I will like to thank Lars for supplying me with an office. And friends and family for all your support.

TABLE OF CONTENTS

Chapter 1: Introduction	1
Chapter 2: Location and landscape	2
2.1 Study area.....	2
2.2 Catchment area.....	3
2.3 Bedrock geology	5
2.4 Periglacial geomorphology	7
2.4.1 Permafrost.....	9
2.5 Lacustrine Sediment.....	11
2.5.1 Annual rhythmic sedimentation and surge deposits	13
Chapter 3: Climate and hydrology	16
3.1 Glacial and climatic history.....	16
3.2 Ocean circulation and climate	17
3.3 Temperature	19
3.4 Precipitation	21
3.5 Hydrology	23
Chapter 4: Methods	25
4.1 Outline of the work	25
4.2 Fieldwork in 2019	27
4.3 Laboratory work of 2019.....	27
4.3.1 Thin sections	28
4.3.2 Grain Size.....	29
4.3.3 Magnetic Susceptibility.....	31
4.3.4 Dry Bulk density, water content and Loss-on-ignition.....	33
4.4.5 Geochemistry	36
4.4 Previous analysis.....	38
4.5 Validation of varve record.....	38
Chapter 5: Results	39
5.1 Visual Stratigraphy.....	39
5.2 Varve thickness and varve count.....	42
5.3 Physical parameters.....	44
5.5 Age determination.....	50
Chapter 6: Discussion	52
6.1 Identification of mass movement events in varved lake sediments.....	52
6.1.1 Varve chronology.....	52
6.1.2 Background sedimentation.....	53
6.1.3 Mass movement events	54
6.2 Interpretation of mass movement events	56

6.2.1 Avalanche and rain-on-snow events.....	57
6.2.2 Rainstorms and intense precipitation	58
6.3 Hydroclimatic influence on laminated lake sediments in Bødalsvatnet	60
6.4 Correlation with surface core and a precision core and implication in hydroclimate	65
Chapter 7: Conclusions	70
7.1 Further studies.....	70
References.....	71
Appendix A -Varve.....	79
Appendix B – Grain Size	82
Appendix C – Magnetic Susceptibility	84
Appendix D - Dry Bulk Density, Water content and Loss-On-Ignition.....	85
Appendix E – ITRAX	87

LIST OF FIGURES

FIGURE 2.1: GEOGRAPHICAL LOCATION OF SVALBARD IN THE NORTH ATLANTIC. B: SVALBARD ARCHIPELAGO WITH THE LARGEST ISLAND OF SPITSBERGEN WITH HIGHLIGHTED SECTION OF NORDENSKIÖLD LAND LOCATED IN CENTER. C: STUDY AREA IN BØDALEN (INDICATED IN RED) (MODIFIED FROM ECKERSTORFER & CHRISTIANSEN, 2011)	3
FIGURE 2.2: STUDY SITE OF BØDALSVATNET (MARKED IN RED) LOCATED IN THE EAST-WEST TRENDING VALLEY OF BØDALEN, NORDENSKIÖLD LAND, CENTRAL SPITSBERGEN (NORWEGIAN POLAR INSTITUTE, 2020).....	4
FIGURE 2.3: A: ADVENTDALEN GROUP LOCATED IN SPITSBERGEN MARKED IN BLACK (DALLMANN, 1999). B: ADVENTDALEN GROUP MARKED IN YELLOW AND THE UNDERLAYING VAN MIJENFJORDEN GROUP MARKED IN GREEN (DALLMANN, 2015).....	6
FIGURE 2.4: SCHEMATIC DIAGRAM OF PERMAFROST AND THE INFLUENCE OF VEGETATION AND SNOW COVER HAS ON PERMAFROST TEMPERATURES (SMITH & RISEBOROUGH 2002).	10
FIGURE 2.5: SCHEMATIC DIAGRAM OF HOW THE CLIMATE SHAPES LAKE SEDIMENT CHARACTERISTICS (MODIFIED FROM JANSSON, ROSQIST & SCHNEIDER, 2005).	11
FIGURE 2.6: PRINCIPAL INFLOW MIXING PATTERNS IN GLACIER-FED LAKES. A: ILLUSTRATION OF SEDIMENT TRANSPORTED INTO THE LAKE AS AN OVERFLOW, INTERFLOW AND UNDERFLOW WHERE THE LAKES DENSITY DETERMINES IF THE SEDIMENT FLOWS INTO THE LAKE MOVES AS AN UNDERFLOW, INTERFLOW, OR OVERFLOW. B: HOMOPHYCNAL INFLOW WATER IS OF EQUAL DENSITY OF THAT OF A NOON-STRATIFIED LAKE (MODIFIED FROM SMITH & ASHLEY, 1985).....	12
FIGURE 2.7: A SCHEMATIC COMPARISON OF THE DEPOSITIONAL RHYTHMITES IN A GALCIAL LAKE BASIN. A: SURGE RHYTHMITES DEPOSITED IN A SHORT TIME SUCH AS MINUTES. B: SEDIMENT DEPOSITED ANNUALLY WITH SUMMER AND WINTER SEASON; DEPTH DEPENDING ON FLOW PATTERN (MODIFIED FROM SMITH & ASHLEY, 1985).	14
FIGURE 3.1: THE WARM ATLANTIC GULF STREAM BECOMES THE NORWEGIAN ATLANTIC CURRENT (NAC) ALONG THE NORWEGIAN COAST. NAC SPLINTERS IN TO THREE DIRECTIONS ALONG THE NORTHERN NORWEGIAN COAST. ONE APPENDIX OF THE NAC IS THE WEST SPITSBERGEN CURRENT (WSC) THAT BRINGS WARM SALINE WATER FROM THE ATLANTIC (MAJEWSKII & ZAJACZKOWSKI, 2007).	18
FIGURE 3.2: ANNUAL AIR TEMPERATURE AT SVALBARD AIRPORT – LONGYEAR (LYR) SINCE 1911 (CHRISTIANSEN, HUMLUM & ECKERSTORFER, 2013).....	20
FIGURE 3.3: PRECIPITATION (MM) AT SVALBARD AIRPORT - LONGYEAR (LYR) WITH HIGH PRECIPITATION DURING SPRING AND AUTUMN – WINTER (HANSSEN-BAUER ET AL., 2019).	22
FIGURE 4.1: STRUCTURE OF THE WORK AND FINAL THESIS PROJECT	26
FIGURE 4.2: LEFT: THE BOATS ARE PRESSED DOWN INTO THE SEDIMENT ALONG WITH THE CORE IN AN ALTERNATING LEFT-RIGHT PATTERN WITH 1-2 CM OVERLAP. RIGHT: EPOXY-RESIN WAS POURED CAREFULLY IN THE CORNER OF THE PLASTIC BOX AND DID NOT COVER THE SUBSAMPLES.	29
FIGURE 4.3: SKETCH OF THE SIMPLIFIED ILLUSTRATION OF THE COULTER LASER PARTICLE SIZE ANALYSER BEHIND THE DETECTION OF GRAIN SIZE (LINDELOF, 2012).....	30
FIGURE 4.4: LEFT: THE SEDIMENT COLLECTED EVER 1CM WAS PLACED IN A CRUCIBLE. RIGHT: THE SEDIMENT SAMPLES IN THE CRUCIBLE WERE PLACED IN A DRYING OVEN.....	33
FIGURE 4.5: THE RELATIONSHIP BETWEEN BULK BENSITY AND WATER CONTENT BY TYPE OF SEDIMENT. TYPE OF SEDIMENT, DEGREE OF SORTED SEDIMENT, AND AMOUNT OF MINEROGENIC PARTICLES ARE ALL FACTORS THAT AFFECT BULK DENSITY (BAKKE ET AL., 2005).	34
FIGURE 4.6: DIAGRAM OF ITRAX CORE SCANNER (CROUDANCE, RINDBY AND ROTHWELL., 2006).....	37
FIGURE 5.1: STRATIGRAPHIC LOG BASED ON VISUAL INSPECTION AND VARVE COUNT OF CORE BSV– 2019 – 1, WITH RBG IMAGE TAKEN WITH ITRAX CORE SCANNER. THE SEDIMENT CORE IS DIVIDED IN TO UNIT A (GREEN), UNIT B (YELLOW) AND UNIT C (BLUE). LIGHT BROWN LAMINAЕ IN BLACK AND THICKER DARKER LAMINAЕ MARKED AS EVENT BEDS IN GREEN.....	40
FIGURE 5.2: A: AN EXAMPLE OF GRADED BED (MARKED BY AN ORANGE LINE). B: AN EXAMPLE OF VARVE COUPLETS WITH LIGHTER SUMMER LAYER FINING UPWARDS TO A DARKER WINTER LAYER. IN THE VARVE	

MARKED WITH AN ORANGE LINE, THE FINING UPWARDS SEQUENCE IS INTERRUPTED BY ONE OR MORE SEDIMENT PULSE.....	41
FIGURE 5.3: VARVE THICKNESS RECORDED AND CORRELATED TO VARVE COUNT GIVES AGE OF EACH SEDIMENTARY UNIT. THE SEDIMENT CORE RECORDS SEDIMENTARY UNITS FROM 2018 TO 1936. DISREGARDING POSSIBLE FURTHER VARVE COUNT UNDER GRADED BED OF 50,75 CM DEPTH.....	43
FIGURE 5.4: RBD IMAGE AND VARVE THICKNESS (CM) WITH PHYSICAL PARAMETERS GRAIN SIZE (μM), MAGNETIC SUSCEPTIBILITY (CGS $\times 10^{-6}$), DRY BULK DENSITY (G/CM 3), WATER CONTENT (%) AND LOSS-ON IGNITION (%). THE TRENDS OF THE SEDIMENT CORE ARE ENHANCED BY 10-POINT AVERAGE OF THE PHYSICAL PARAMETERS WITH GRAIN SIZE IN THE 90 TH PRESENTIAL. AND BASED ON THE TRENDS OF THE SEDIMENT CORE DIVIDED IN TO UNITS A, B AND C.....	46
FIGURE 5.5: ELEMENTS POTASSIUM (K), CALCIUM (Ca), MANGANESE (Mn), IRON (Fe), TITANIUM (Ti) AND ZIRCONIUM (Zr) NORMALIZED TO CPS WITH TREND BY 10-POINT RUNNING AVERAGE (APPENDIX E).....	49
FIGURE 5.6: RGB IMAGE AND STRATIGRAPHY OF 2019 SURFACE CORE (LEFT) WITH LINE SCAN IMAGE AND SCHEMATIC STRATIGRAPHY OF 2012 CORE (RIGHT). CORES WERE CROSS-CORELATED BY VARVE COUNT AND PLUTONIUM ($^{239+240}\text{Pu}$) MEASUREMENTS FROM 2012 SURFACE CORE.	51
FIGURE 6.1: A: YEARLY PRECIPITATION AND TEMPERATURE IN 1993 WITH NOVEMBER RAINSTORM. B: YEARLY PRECIPITATION AND TEMPERATURE IN 1983 AND MARCH RAINSTORM. C: YEARLY PRECIPITATION AND TEMPERATURE IN 1974 INTENSE PRECIPITATION EVENT (NORWEGIAN METROLOGICAL INSTITUTE, 2020)....	59
FIGURE 6.2: PERMAFROST DEPTH IN SPRING, SUMMER, AND THE AUTUMN WAS THE ACTIVE LAYER THAT HAS STARTED TO REFREEZE OR IS FULLY THAWED (MODIFIED FROM HUMLUM ET AL., 2016).....	60
FIGURE 6.3: WARMER TEMPERATURE PERIODS FROM 1936 TO 2019 WITH VARVE THICKNESS IN THE SURFACE CORE FROM 2019, SEPTEMBER, OCTOBER, NOVEMBER (SON) AND MARCH, APRIL, MAY (MAM) PRECIPITATION AND TEMPERATURE, ANNUAL PRECIPITATION, AND MEAN ANNUAL TEMPERATURE WITH THE NORMAL PERIOD (1961 – 1990) MARKED IN BLACK DOTTED AND STRAIGHT LINES (NORWEGIAN METROLOGICAL INSTITUTE, 2020).	63
FIGURE 6.4: CROSS-CORRELATION BY VARVE THICKNESS BETWEEN THE 2019 SURFACE CORE AND THE 2012 LONG CORE.....	66
FIGURE 6.5: LAMINATION THICKNESS FROM 2012 LONGER CORE, FROM BØDALSVATNET. (RETELLE, DOWEY & DULIN, 2013).....	67
FIGURE 6.6: COLDER TEMPERATURE REGIMES ACCORDING TO NORDLI ET AL., (2020) FROM 1840 TO 2018 WITH VARVE THICKNESS IN SURFACE CORE FROM 2019, SEPTEMBER, OCTOBER, NOVEMBER (SON) AND MARCH, APRIL, MAY (MAM) PRECIPITATION AND TEMPERATURE, ANNUAL PRECIPITATION AND MEAN ANNUAL TEMPERATURE WITH NORMAL PERIOD (1961 – 1990) MARKED IN BLACK DOTTED AND STRAIT LINES. SAME COMMENT ON THIS FIGURE. IT'S IMPORTANT AND TOO SMALL (NORWEGIAN METROLOGICAL INSTITUTE, 2020).	FEIL! BOKMERKE ER IKKE DEFINERT.

LIST OF TABLES

TABLE 5-0-1: EVENT BEDS BY NUMBER, DEPTH OF LOCATION IN CM, AND ASSOCIATED YEAR (AD). DEPTH, THICKNESS AND ASSOCIATED YEAR OF ALL SEDIMENTARY UNITS IS LOCATED IN APPENDIX A	42
TABLE 5-0-2: PHYSICAL PARAMETERS BY UNITS A, B AND C WITH RANGE OF RESULTS AND STANDARD DEVIATION (SD).....	45
TABLE 5-0-3: PHYSICAL PARAMETERS RANGE IN SEDIMENTARY UNITS MARKED AS GRADED BEDS.....	45
TABLE 5-4: XRF PARAMETERS BY UNITS A, B AND C WITH STANDARD DEVIATION (SD).....	48

CHAPTER 1: INTRODUCTION

The Arctic is warming faster than any other region on the globe, and Svalbard is at the forefront of the climatic changes that are taking place. Svalbard's location and presence of amplifying feedback loops result in Svalbard being particularly responsive to current climatic change (Hanssen - Bauer et al., 2019; Sereze et al., 2009; Humlum et al., 2009). Svalbard has experienced an increase in total annual precipitation and air temperature has affected Svalbard's environment, in particular the regional hydroclimate (Nowak & Hodson, 2013). An increase in heavy rainfall and extreme precipitation events may have an impact on the snow pack and permafrost (Hansen et al., 2014). Landslides, flooding and avalanches have been caused by heavy rainfall events that have occurred in and around the area of Longyearbyen (Hanssen-Bauer et al., 2019; Christiansen et al., 2016; Humlum et al., 2016; Larsson, 1982).

Laminated lake sediments are an excellent natural archive for past environmental and climate change allowing for a high-resolution multi-proxy record for reconstructing the past climate and environment (Zolitschka et al., 2015; Ojala et al., 2012; Kaufman et al., 2009). The research presented here aims to provide an annual paleoclimate record that indicates melt season processes and summer conditions in Bødalsvatnet, Nordenskiöld Land, Central Spitsbergen as part of a larger project. The project called "Arctic hydrological regime shifts in the warming climate" that looks at annually laminated lake sediments from lakes in Nordenskiöld Land, Central Spitsbergen. This master thesis investigates annually laminated sediments from Bødalsvatnet, Bødalen with a primary goal to present a more in-depth reconstruction, an understanding of the change in air temperature and hydroclimate in Bødalen, from approximately the last 150 years to the present. To achieve this the thesis will answer and substantiate the following research question;

Can mass movement events in the laminated lake sediment from Bødalsvatnet be linked to a recorded precipitation event or to a change in precipitation?

CHAPTER 2: LOCATION AND LANDSCAPE

As discussed in Chapter 1, Svalbard is at the forefront of climatic change, and Longyearbyen has the longest-running high latitude weather record in the Arctic (Humlum, 2003). This region thus offers a valuable opportunity to advance our understanding of elevated air temperatures, hydrology, and lacustrine sediments. This chapter introduces the study area and gives an overview of local geology and sedimentation.

2.1 STUDY AREA

The Svalbard archipelago lies in the Arctic region (Figure 2.1). The Arctic region is defined by the 10°C July isotherm or the region above 66° 32 °N. Svalbard is situated between latitude 74° and 81° north and 10° 35° east, halfway between Norway and the North Pole (Ingolfsson, 2004). It is located between the Norwegian Sea, the Barents Sea, the Greenland Sea, and the Arctic Ocean (Figure 2.1) (Svendsen & Mangerud, 1997). The largest and only inhabited island is Spitsbergen (37,637 km²) and the islands size is just slightly smaller than Holland.

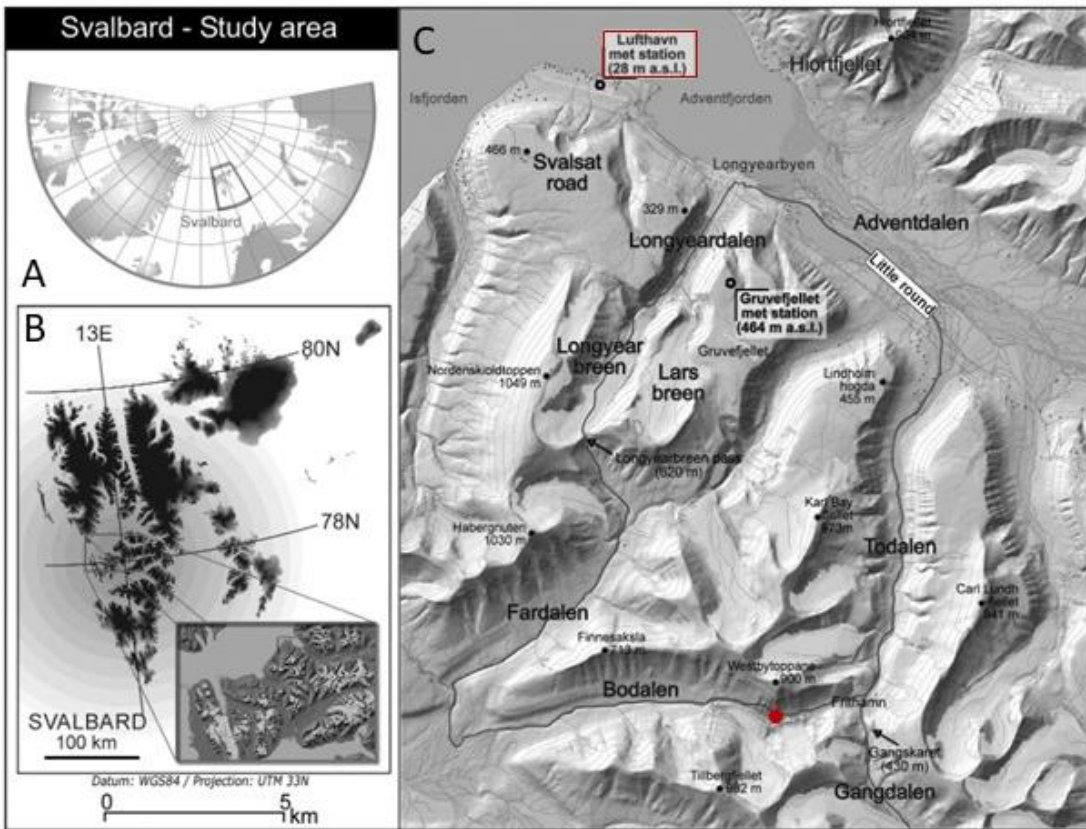


Figure 2.1: Geographical location of Svalbard in the North Atlantic. B: Svalbard archipelago with highlighted section of Nordenskiöld Land located in center. C: Study area in Bødalen (indicated in red) (modified from Eckerstorfer & Christiansen, 2011).

2.2 CATCHMENT AREA

Bødalen is located on the island of Spitsbergen. The name of Spitsbergen meaning spiky mountains and high relief. The high relief is pronounced along with the western coast of the island. The central part of Spitsbergen is predominantly plateau-style-mountains with flat tops, steep face walls, and flanks. Bødalen is an east-west trending previously glaciated valley located in central Spitsbergen (Figure 2.1). The valley has its outlet into the larger valley of Colsdalen. The Bødalen catchment contains an unnamed glacier and Bødalsbreen (Figure 2.2). The valley is situated approximately at 400-420 m.a.s.l and is 10 km long and is located between the mountain of Westbytappene at 898 m.a.s.l in the north and Tillbergfjellet at 981 m.a.s.l in the south.



Figure 2.2: Study site of Bødalsvatnet (marked in red) located in the east-west trending valley of Bødalen, Nordenskiöld Land, central Spitsbergen (Norwegian Polar Institute, 2020).

The proglacial lake of Bødalsvatnet is the largest lake in the valley and is located close to the head of the valley; the lake located furthest to the west at approximately 389 m.a.s.l (Johannesen, 2018). In the south the lake is bordering to the steep face of Westbytoppane. The sediment deposits surrounding the lake have a major impact on the sedimentation in Bødalsvatnet. The lake itself is estimated by Johannesen in 2018 to be about 0,0454km².

2.3 BEDROCK GEOLOGY

The archipelago of Svalbard is an exposure of the northwestern domain of the Eurasian continental plate, north-west corner of the Barents Sea. During the late Mesozoic and Cenozoic crustal activity, the Eurasian continental plate was uplifted (Worsley & Aga, 1986). According to Hjelle et al., (1986), Svalbard has a range of rocks recording back to the Precambrian era. During the Precambrian period, Svalbard was located close to what today is the south pole. During this period, Svalbard experienced several mountain-building events. The result of mountain-building events can be seen at Spitsbergen's west and north coast (Ingólfsson, Möller, & Lokrantz, 2008). During the island's during the pre-Devonian migration north, Paleomagnetic dating by Worsley and Aga, 1986 shows that the island was subequatorial.

At central Spitsbergen, the bedrock is mostly flat-lying sedimentary rock in the Paleogene and Neogene basin. Paleogene and Neogene bedrock in the Bødalen area mainly consists of the Van Mijenfjorden group (Dallmann, 1999) and its subgroup Adventdalen group (Figure 2.3). The Adventdalen group is a deep intertidal sequence of alternating sandstone, siltstone and shale-stone beds. From oldest to youngest, the tertiary bedrock consists of; Firkanten Formation (Fm), Basilika Fm, Sarkofagen Fm, Gilsonryggen Fm, Batterfjellet Fm and Aspelintoppen Fm (Major & Nagy, 1972).

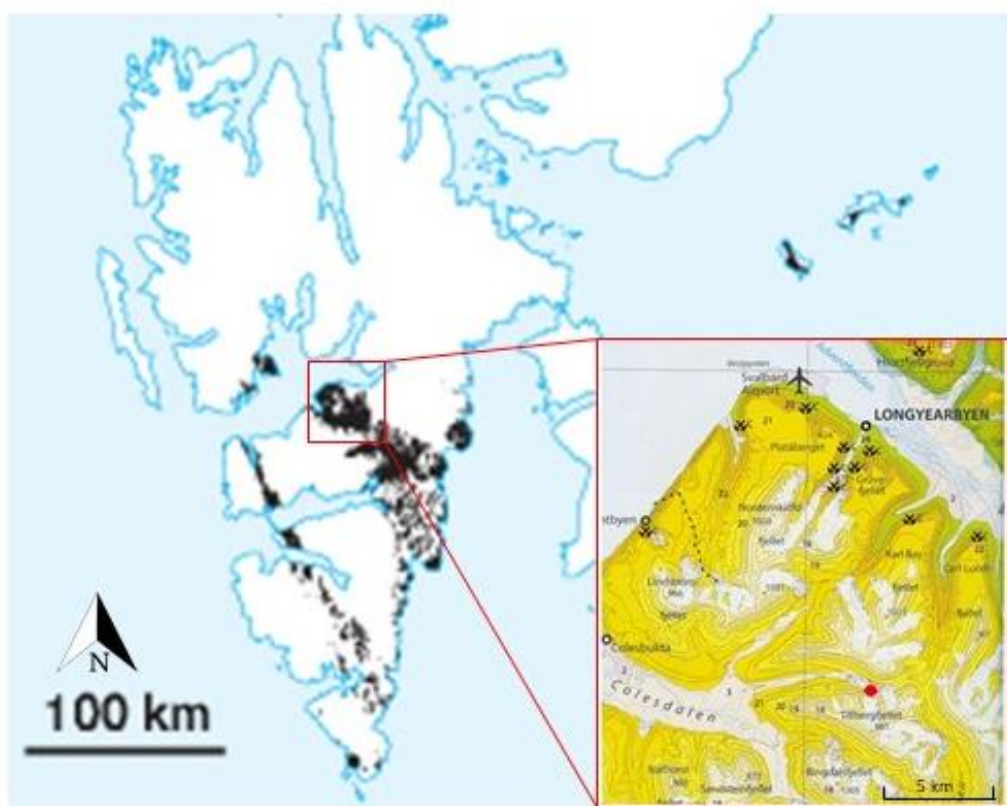


Figure 2.3: A: Adventdalen group located in Spitsbergen marked in black (Dallmann, 1999). B: Adventdalen group marked in yellow and the underlaying Van Mijenfjorden group marked in green (Dallmann, 2015).

2.4 PERIGLACIAL GEOMORPHOLOGY

Bødalen and Bødalsvatnet is proglacial, in front of a glacier or immediately beyond a glacier. The watershed in Bødalen is proglacial but also periglacial. The modern definition of periglacial is a range of cold climatic conditions where environments are dominated by processes caused by frost action (French, 2007). Mechanical weathering is the dominant form of weathering in Bødalen due to the climate. The weathering and bedrock are geomorphologically mapped in different shades of iliac around Bødalsvatnet in Figure 2.4. During the retreat of the last major ice sheet, the landscape was draped in till (marked in green in Figure 2.4). Till deposits which are a mixture of sediments that have been transported and eroded by glaciers. In Bødalen, till can be seen as a moraine formed by the small cirque glaciers during the Little Ice Age, LIA. Glaciofluvial deposits transported by water (yellow in Figure 2.4) are located east and west of Bødalsvatnet. In the mountainsides, slope deposits are marked in different shapes of red, deposited by gravitational processes including rockfall, avalanches or debris flow (Rubensdotter et al., 2015). The current geomorphic activity is controlled by precipitation and temperature (Humlum, 2002). From the northern side, the mountainside of Westbytoppen has high activity of mass movement that travels into the valley's largest and easternmost lake, Bødalsvatnet (Figure 2.4) (Eckersorfer & Christensen, 2012).

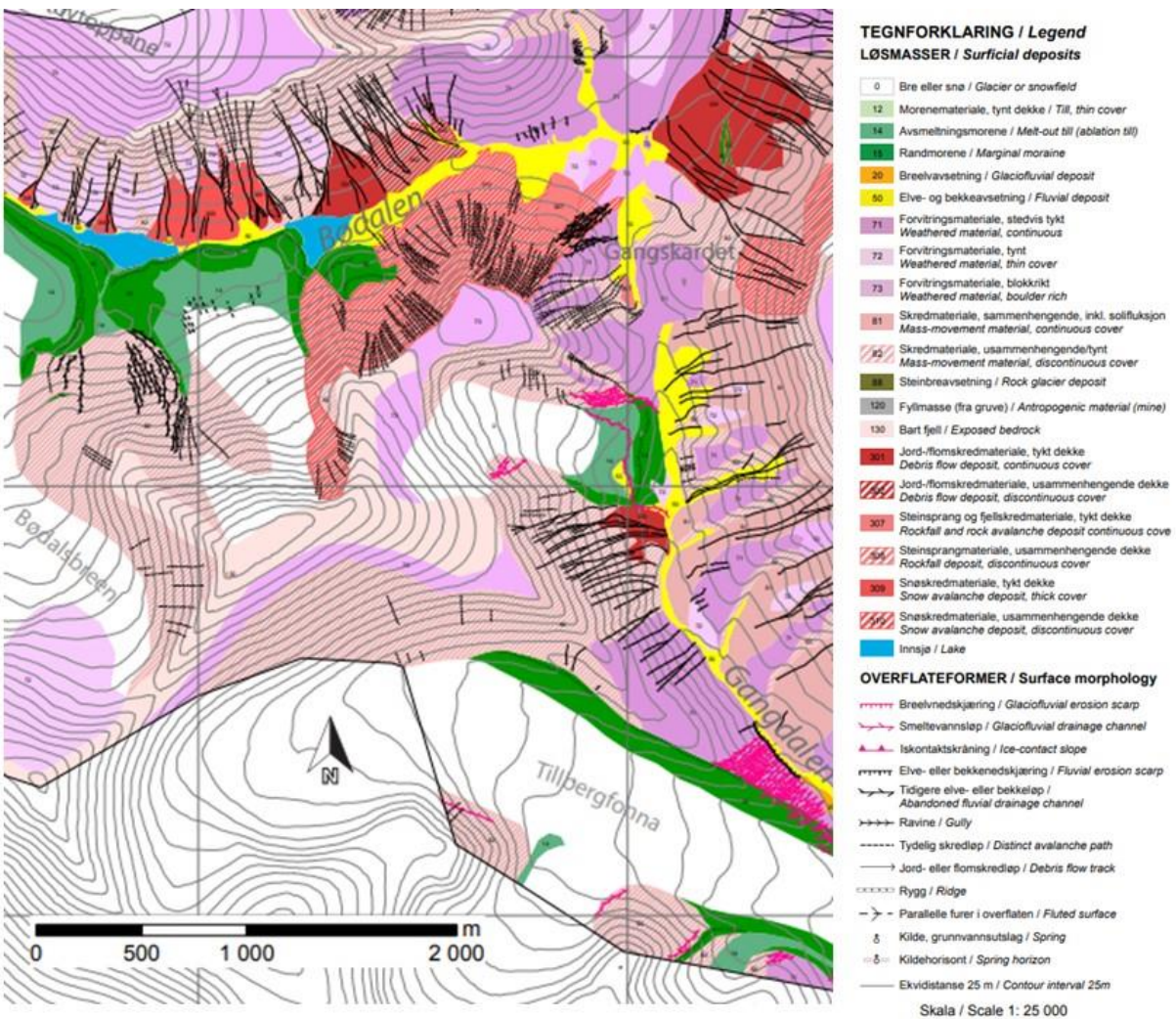


Figure 2.4: Map of landforms and sediments of Bødalen with Bødalsvatnet marked with a red circle (modified from Rubensdotter et al., 2015).

2.4.1 PERMAFROST

Permafrost is a prominent geomorphological feature in Bødalen. Permafrost is defined by French (2007) as ground material that remains at or below 0°C for two or more consecutive years. The Arctic region of Svalbard is characterized as near-continuous permafrost cover (Humlum, Instanes, & Sollid, 2003). The depth of the permafrost varies from 80-100m in coastal areas to 400-500m in mountainous areas (Humlum, 2005). Change in the Svalbard's climate is affecting the permafrost because permafrost is a ground thermal condition related to climate. Permafrost temperatures in the Arctic have as a response to the warming climate increased over the last century (Romanovsky et al., 2010; Burn & Zhang, 2009). These changes can be seen in the depth of the active layer in the permafrost. The upper permafrost zone near the surface thaws during the summer and is known as the active layer which is sensitive to changes in atmospheric temperature and ground temperature. The relation between the temperature in the atmosphere and the ground is determined by the ground thermal properties and ground cover. Ground cover can, for example, be snow or vegetation cover that results in surface offset. The amount of snow cover can make temperatures warmer or cooler, and the terrain surface is a critical boundary in the climate-permafrost relation. Therefore, it is possible that snow cover can influence the ground thermal regime. The ground thermal regime that largely controls periglacial landform dynamics. The thickness and seasonal distribution of vegetation and snow cover are seen in the difference between Mean Annual Ground Surface Temperature (MAGST) and Mean Annual Air Temperature (MAAT) (Figure 2.5) (Smith & Riseborough, 2002).

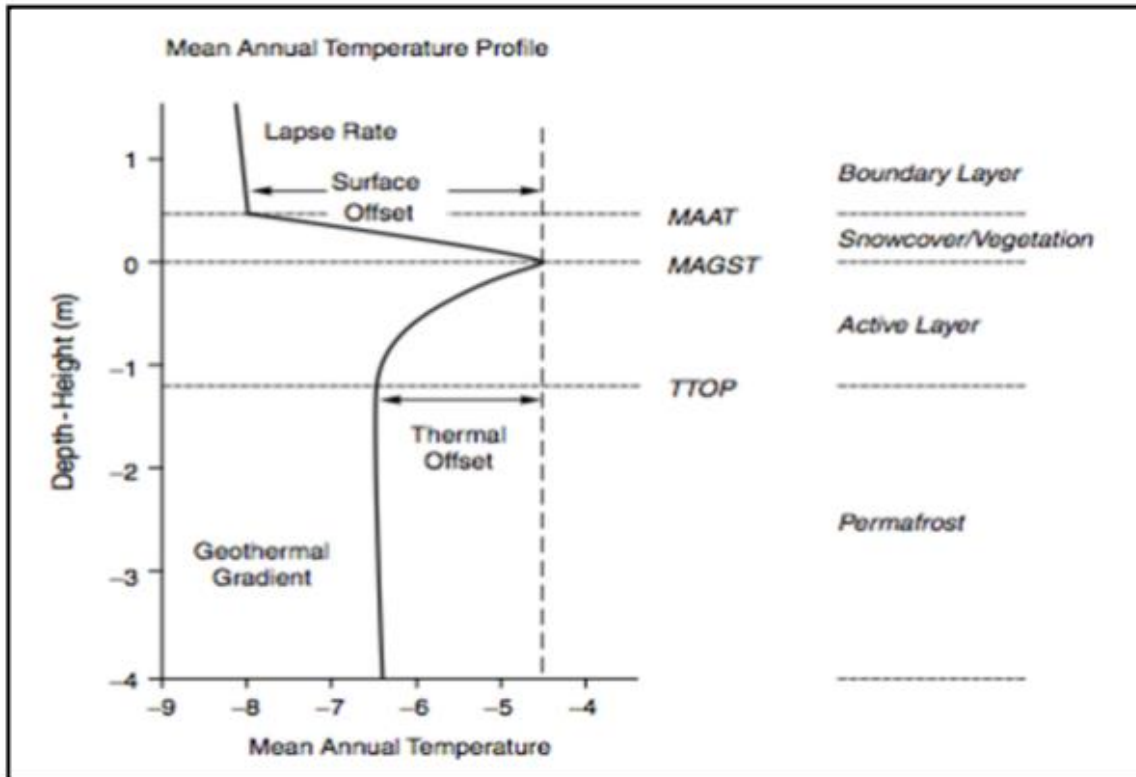


Figure 2.4: Schematic diagram of permafrost and the influence of vegetation and snow cover has on permafrost temperatures (Smith & Riseborough 2002).

Permafrost in Svalbard is increasingly sensitive to metrological variations due to the "one-sided, top-down" freezing of the active layer (Christiansen et al., 2010). The permafrost in Svalbard also influence the hydrology and sediment transport. Due to the active layer permafrost is not entirely impermeable and is considered an aquifer (Woo et al., 2008). The permafrost being an aquifer, permafrost is influencing basin hydrology (Hodson, 1994).

2.5 LACUSTRINE SEDIMENT

Geological, meteorological, and biological controls are factors that define a lacustrine ecosystem and are commonly divided into two categories, allochthonous and autochthonous processes and materials. Allochthonous processes and material are those related to transport to the lake while autochthonous material is within the water column e.g., organic material or inorganic precipitation (Bradley, 1999). Biological elements in the lake can stem from animals, vegetation and humans, and an example of a source of meteorological element is precipitation. But in a glacial lake, the geological elements and physical processes are often dominant. Geological materials are transported by mass movements, streams and rivers which can in turn be driven by seasonal meteorological processes, wind activity, temperature and precipitation. Hence, the elements are largely controlled by the climate (Figure 2.5) (Evans & Heller, 2003).

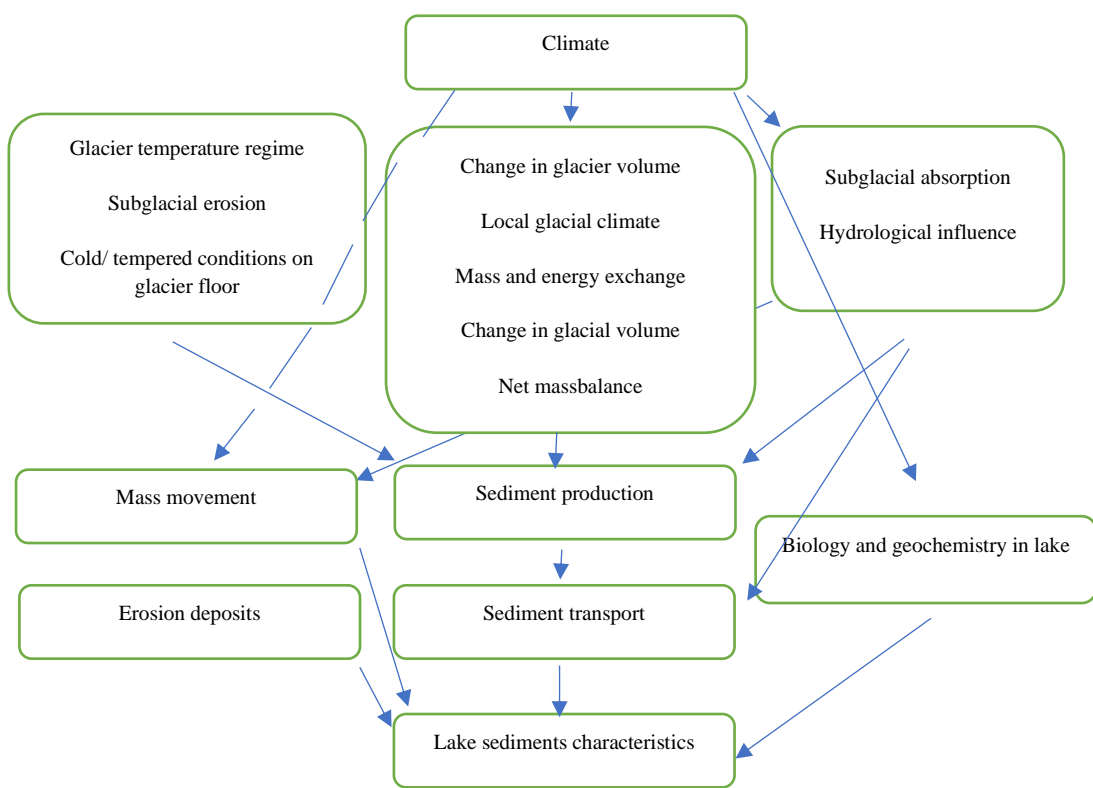


Figure 2-0-5: Schematic diagram of how the climate shapes lake sediment characteristics (modified from Jansson, Rosquist & Schneider, 2005).

According to Smith and Ashley (1985), the sedimentation in a proglacial lake such as Bødalsvatnet is dependent on multiple factors however meteorology and geomorphology are major controls on the annual sediment transfer. The annual sediment transfer is closely linked to the formation of sub annual sedimentation features and is driven by the amount of snowmelt runoff in a basin, glacier runoff in the melt season and rainfall (Schiefer, Menounous & Slaymaker, 2017). In winter fine-grained sediments form a clay cap over the coarser summer/melt season sediments because of the ice on lakes decreases mixing in the water column and allow for finer sediments to settle through the water column (Chutko & Lamoureux, 2008). The process of water column stratification and is a dominant influence on the distribution of sediments in a lake. Stratification happens through the three factors of salinity, density, and temperature (Smith & Ashley, 1985).

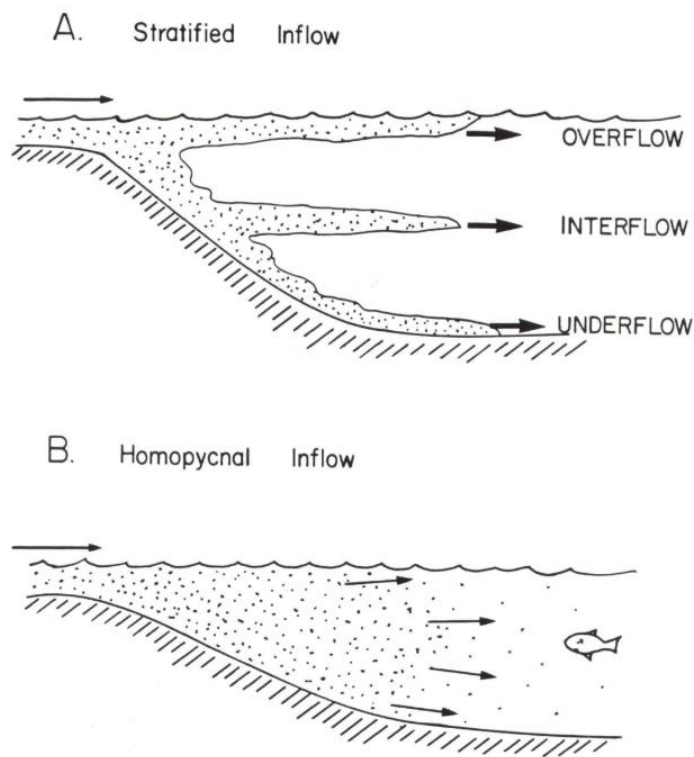


Figure 2.6: Principal inflow mixing patterns in glacier-fed lakes. A: Illustration of sediment transported into the lake as an overflow, interflow and underflow where the lake's density determines if the sediment flows into the lake moves as an underflow, interflow, or overflow. B: Homopycnal inflow water is of equal density of that of a noon-stratified lake (modified from Smith & Ashley, 1985).

Stratification due to density controls the sediment transportation and distribution in the lake (Carmack et al., 1979; Smith & Ashley, 1985). The lake's density determines if the sediment flows into the lake moves as an underflow, interflow, or overflow (Figure 2.7A). This is due to the relative density of the temperature stratified lake versus the inflowing river water whose density is controlled by temperature and suspended sediment concentration. If the river water and suspended sediment concentration (SSC) is denser than the lake water the sediment will go as an underflow. If the sediment is equal to the water density the sediment will go as an interflow and if the inflow has a lower density than the water in the lake the sediment will move through the water as an overflow. The sediment can also move through the water column as a homopycnal flow (Figure 2.7B) which occurs when the inflowing sediment consists of water that has the equal density of that of a non-stratified lake. The inflow of the sediment and the grain size distribution on the lake floor is linked. The sediment from a depositional event that settles first on the lake floor in delta proximal locations is generally coarser sand and silts and the clay particle remains suspended in the water column and can disperse through the basin (Smith & Ashley, 1985).

2.5.1 ANNUAL RHYTHMIC SEDIMENTATION AND SURGE DEPOSITS

The deposits of sediments on lake beds are dependent on the seasonal rhythm of the deposition which determines the sequence of the grain size in the deposit and is dependent on the time and processes used to deposit each rhythm. The two main rhythmite types in Bødalsvatnet are varves and surge deposits. The layering caused by overflow, interflow, and underflow in the summer and suspension settling during the winter takes a year to deposit. This annual layering of the sediment is called varve (Figure 2.8) (Ojala et al., 2012; Zolitschka et al., 2015). The glaciolacustrine varve is a couplet comprised of a coarser summer layer and finer grained winter layer. Hence, a varve has finer grain size upward through the varve. The sediment particle size in a varve generally transitions from silt to clay. A thick and often coarser interrupting layer can be that of a surge deposit.

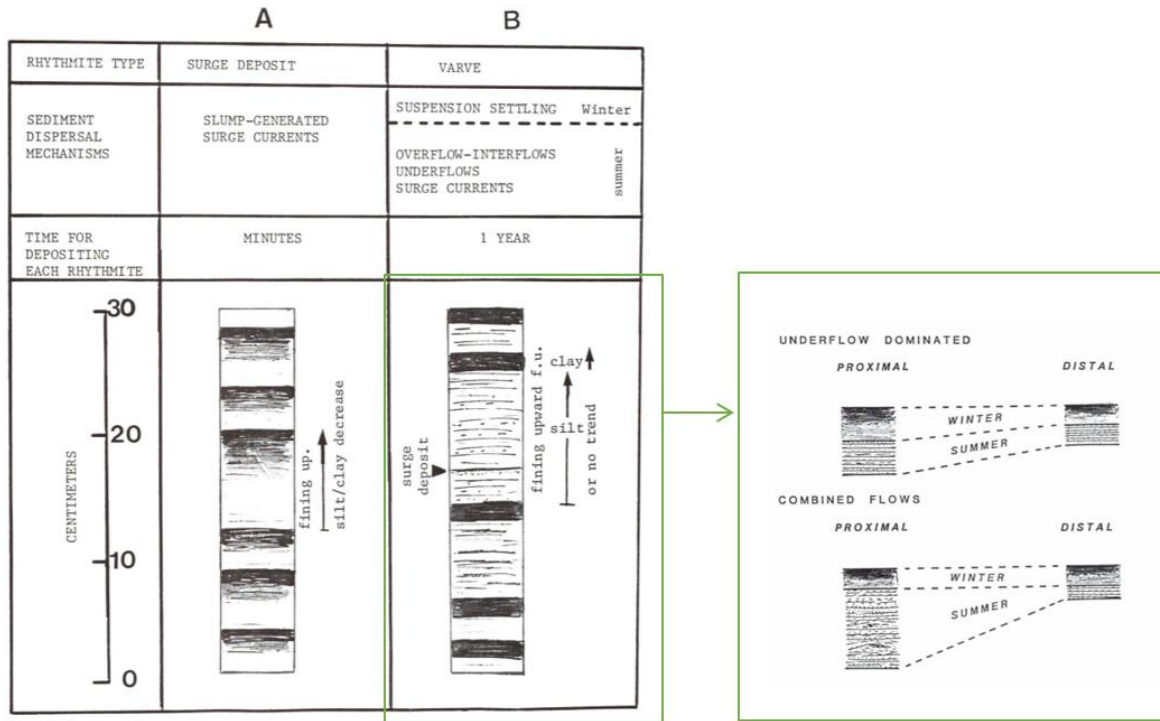


Figure 2.7: A schematic comparison of the depositional rhythmites in a glacial lake basin. A: Surge rhythmites deposited in a short time such as minutes. B: Sediment deposited annually with summer and winter season; depth depending on flow pattern (modified from Smith & Ashley, 1985).

Surge deposits are episodic and are generally not part of an annual lacustrine depositional cycle but instead are deposited by a surge of sediments over a short period of minutes. The surge deposits are deposited in the space of a few minutes and originates from slumps, avalanches and debris flows in the mountainside above the lake surface (Vasskog et al., 2011). Surge can also be triggered by slumping of lake margin sediments (Normandeau et al., 2016).

Turbidites are deposits form subaqueous mass movement that occur in water masses with increased density. A source of this subaqueous mass movement can be a terrestrial landslide or subaqueous landslides (Smith & Ashley, 1985). Terrestrial landslides bring with its material that contributes to incised sediment in suspension and, as a result, increased density in a restricted area of the lake. Subaqueous sedimentary streams can be divided into concentrated- and hyper-concentrated streams (Mulder & Alexander, 2001; Hansen, 1962). The difference between the streams can be seen in grain size (coarse silt, sand, and gravel) while concentrated streams have normal grading, and hyper-concentrated streams have little grading. According to

(Rubensdotter & Rosquist, 2009), turbidites are minerogenic layers with high density and shape transition to the underlying layer.

A surge can interrupt the sequence of the annually formed varves. They can also occur repeatedly with no clear varves present (Figure 2.8). Episodic slump generated surge deposits and varve (seasonally rhythmic deposits) both may occur due to overflow – interflow, quasi-continues interflows and surge currents. Table 2.1 compare characteristics of the annual rhythmites and surge deposits.

Table 2.1: Annual and surge rhythmite in lacustrine sediments (modified from Ashley & Smith, 1985).

Annual rhythmite	Surge rhythmite
<ol style="list-style-type: none"> 1. The silt layer thickness varies, and the clay layer is constant throughout the lake basin. 2. Breaks can occur within the annual rhythmite. 3. Lebenssspuren can occur in the annual rhythmite. 4. An annual rhythmite occurs as a couplet. Silt layer has an inverse or normal grading or no trend in the grain size with the clay layers fines upwards in the sediment deposit. 	<ol style="list-style-type: none"> 1. The clay and silt layers thicknesses in proportion. 2. There is no break within the deposits. 3. There is no occurrence of <i>lebenssspuren</i> within the rhythmite. 4. The surge sediments are fining upwards and have a gradual decrease in the silt and clay ratio.

The annual rhythmicity of a varve chronology provides a record of sediment deposition by calendar year (Ojala et al., 2012). Thus, varves provide a chronological tool for reconstructing high-resolution climate variability over the last centuries (Snyder, Werner & Miller, 2000).

CHAPTER 3: CLIMATE AND HYDROLOGY

The significance of investigating the varved lacustrine sediment record of Bødalsvatnet within the framework of climatic change was established in Chapter 2. To place this discussion in context, the following chapter will present Holocene glacial change and discuss the impact of ocean currents, regional climate, temperature, precipitation, and hydrology. Current knowledge of changes in climate that will impact the lacustrine sediment will be reviewed.

3.1 GLACIAL AND CLIMATIC HISTORY

The landscape of Svalbard is largely modified by Quaternary glaciations; mountains, fjords, cirques, and valleys. The last glacial cycle had two or three major glaciations in the period 115,000-10,000 years B.P. During the major glaciations, Svalbard was covered by the Barents Sea Ice sheet (Ingolfsson, 2004). In the Late Weichselian, the last of the ice advances covered the Barents Sea up to Svalbard and northern Europe (Hughes et al., 2016). The glaciation was followed by major deglaciation from 14,000-10,000 BP, thus ending the Last Glacial Maximum (LGM). As the deglaciation occurred, the sea level rose by approximately 80-70 m due to isostatic depression (Mangerud & Svendsen, 1990). During the cooler Younger Dryas (12,800-11,500 BP), Svalbard apparently had little relative re-advance in contrast to North America and Northern Europe that had significant re-advances during this time period (Svendsen & Mangerud, 1997; Svendsen & Mangerud, 1990), however Farnsworth et al, (2018) note that radiances did occur in some areas of Svalbard during the early Holocene.

During the late Holocene, the Arctic experienced a cooling trend (approximately 0-1900 AD), followed by a rapid warming (D'Andrea et al., 2012; Kaufman, 2009). The cooling and following warming trend are only interrupted by two anomaly periods; the Medieval Warm Period (MWP) and the Little Ice Age (LIA).

The MWP lasted from approximately 950-1250 AD and in places exhibits warmth equal to today's temperatures and even at some locations exceeds it. But there are no indications that these temperatures experienced in the Arctic reached a global scale (Mann et al., 2009). The timing of MWP on a global scale is more contested than the timing of the LIA. In the Arctic,

the LIA lasted approximately from 1400-1850 AD (Moore et al., 2001; Humlum, 2002). On Svalbard, the glaciers reached their late Holocene maximum during the Little Ice Age (LIA) (Snyder, Werner & Miller, 2000; Svendsen & Mangerud, 1997). Since the LIA, the glaciers of Svalbard have retreated, and their new margins are located behind their LIA moraines (Ingolfsson, 2004). The LIA is generally known for being a cool period with cool temperatures, but D'Andrea et al., (2012) found that western Spitsbergen may be an exception. The late Holocene cooling was likely caused by a combination of factors including; decreased heat transport to the arctic because of a decrease in Gulf Stream density, orbital, volcanic and solar forcing, and lower summer insolation in the Northern atmosphere (Miller et al., 2012).

3.2 OCEAN CIRCULATION AND CLIMATE

Norway, Svalbard, and the North Atlantic region is influenced largely by the Gulf Stream which moves warm saline water to the Arctic basin and Svalbard by the Gulf Stream appendix; the West Spitsbergen Current (WSC) (Figure 3.1). The currents strength is determined by the pressure gradient between the Azores High in the subtropics and the Icelandic low in the North Atlantic (Majewski & Zajaczkowski, 2007). Spitsbergen's position at 78°N and the WSC gives Spitsbergen ice free winter conditions and the environment distinctively sensitive to slight changes in climate (Førland et al., 1997).

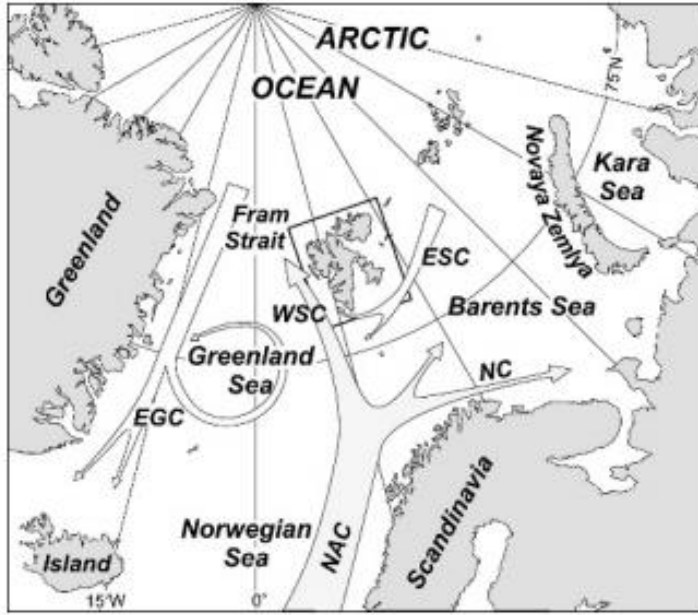


Figure 3.1: The warm Atlantic Gulf Stream becomes the Norwegian Atlantic Current (NAC) along the Norwegian coast. NAC splinters in to three directions along the northern Norwegian coast. One appendix of the NAC is the West Spitsbergen Current (WSC) that brings warm saline water from the Atlantic (Majewskii & Zajaczkowski, 2007).

Svalbard is located at the boundary of air masses and distinct ocean currents, as a result producing a highly sensitive climate (Spielhagen et al., 2011; Hald et al., 2007). The interaction of air masses, winter sea ice extent, and water masses of different thermal regimes controls the local climate. The regional climate is controlled by interactions between the Siberian High-pressure systems and the Icelandic Low. The North Atlantic cyclone drives warm temperatures over the Svalbard archipelago (Hanssen-Bauer et al., 1990). Winter cyclones deliver large air temperature variations on a weekly and daily time scale. As a result, Svalbard has mid-winter thaws, heavy snowstorms, snow- and rain events (Wickström et al., 2019). The climate of Svalbard is largely influenced by the North Atlantic Oscillation (NAO) which undergoes large scale variations in both decadal and seasonal time scales (Dickson et al., 2000; White et al., 1996). The NAO index positively correlates with winter precipitation, temperature and glacier mass in Svalbard and Western Spitsbergen (Nesje, Lie & Dahl, 2000).

Svalbard's climate is categorized as a High Arctic climate and a High Arctic desert (Ingolfsson, 2004). And the interaction between meteorological and oceanic conditions classifies Svalbard as a marine high arctic marine climate (Eckerstorfer & Christiansen, 2011), a climate that is cold and wet (Ingolfsson, 2004) due to its location at the boundary between the warm North Atlantic air and the cold polar front. The outcome is that Svalbard has a milder climate than

other regions at similar latitudes (Eckerstoffer & Christiansen, 2011). The effect is that Svalbard can experience both snow and rain during all seasons. As an effect, any season in Svalbard has greater degrees of inter-annual variability (Førland et al., 1997). As a result, the High Arctic climate in Svalbard has periglacial conditions; warm continuous permafrost and extreme winter temperatures (Christiansen et al., 2010; French, 2007).

3.3 TEMPERATURE

The regional climate is controlled by two different air pressure systems, the Icelandic Low and Siberian high-pressure system with warm air following the NAO cyclone pattern north to Svalbard. The interaction of water and air masses, and winter sea ice extent largely controls the local climate (Hanssen-Bauer et al., 1990). The weather in Svalbard and the Arctic is characterized by a fluctuating pattern of low- and high-pressure systems (Hanssen-Bauer et al., 2019). The pattern is strong in the winter but weaker during the summer. This is a result of daily and seasonal air temperature (Dickson et al., 2000). The percent mean annual temperature in Svalbard varies from -6°C to -15°C in the high mountains. During the 20th century, the air temperature in Svalbard has risen with temperatures exceeding the temperatures of MWP with 2-2,5°C increase in the period of 1987-2000 (D'Andrea et al., 2012). The rise in air temperature is linked to the strong flux of warm water and associated warm air from the Atlantic Ocean. The largest settlement and the closest to Bødalen is Longyearbyen. Here the temperature is coldest in February with a temperature around -15,2°C, and the warmest month is July with a temperature around 5,8°C. The temperature is an average temperature measured in the city between 1975 and the year 2000 (Ingolfsson, 2004). The summer inter-annual variations in temperature are on a scale of 0,2°C-0,6°C and during winter season variability is on a scale of 3-6°C (Humlum et al., 2002). The winter variability has a large impact on the stability of the snow and its stability.

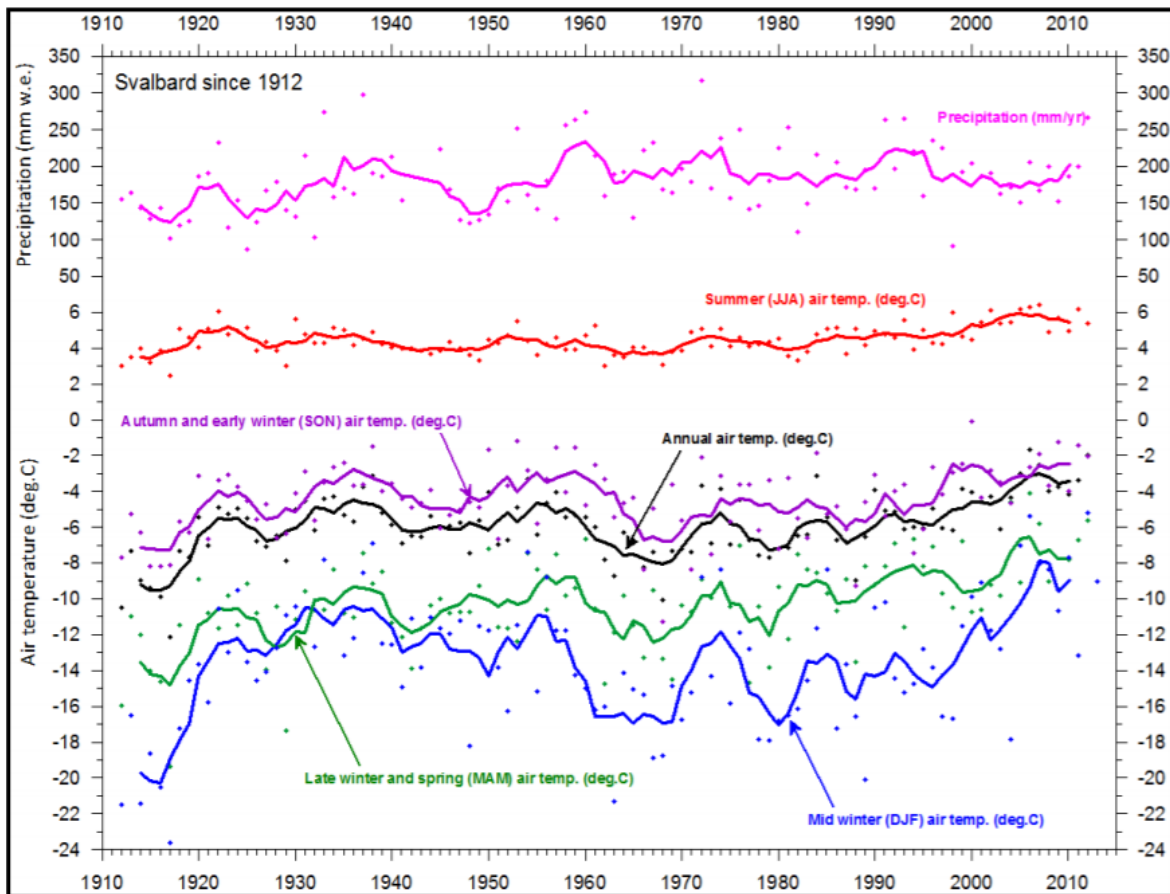


Figure 3.2: Annual air temperature at Svalbard airport – Longyear (LYR) since 1911 (Christiansen, Humlum & Eckerstorfer, 2013).

The temperature measured at LYR shows an increase in temperature by 5,6°C degrees since 1961, within the normal period 1961-1990 (Figure 3.2) with some locations in Svalbard experiencing an increase in temperature with 12-14 degrees over the normal. In comparison, the temperature in Oslo has increased by 2°C, and the global average increased by 0,9°C. In other words, the increase in temperature in Svalbard has approximately increased three times that of Oslo and six times by the global average. The temperature increase in Svalbard causes the permafrost active layer to thaw and increase. As a result, there stability instability in the mountainsides (Hanssen-Bauer et al., 2019).

Svalbard's low land and coastal regions are generally warmer than the highland region in Svalbard (Humlum, 2002). The air masses are usually unstable; hence temperature inversions do occur but are generally short-lived (Christiansen, Humlum & Eckerstorfer, 2013). The warmer climate will increase the river and stream discharge, sediment supply of the rivers, and

the erosion intensity. The increase in sediment transported in the rivers may increase channel splitting and expose other slopes for erosion (Hanssen-Bauer et al., 2019).

3.4 PRECIPITATION

Each decade since meteorological measurements started in 1910, the precipitation has increased by 3-4%. The normal annual precipitation for the normal period 1961 – 1990 was 190 – 440mm (Humlum, Instanes, & Sollid, 2003). Today the region around Longyearbyen is very dry with annual precipitation of 196 mm, with the highest amount of precipitation in Longyearbyen in autumn (Figure 3.3) (Hanssen-Bauer et al., 2019). The region around Longyearbyen is the driest part of Svalbard (Førland et al., 1997). The precipitation trends from 1971 – 2017 in Svalbard is in a large degree, governed by atmospheric circulation patterns, more so than for temperature. Temperature can only partly be explained by the atmospheric circulation patterns (Nordli et al., 2020; Hanssen-Bauer et al., 2019).

Precipitation events can correlate with low-pressure systems with heavy precipitation during winter (Figure 3.3) (Hanssen-Bauer et al., 2019; Wickström et al., 2019) with the dominant form of precipitation being snow, and rain and snow events occur mid-winter regardless of mean monthly temperature. The snow season has decreased by approximately 20 days in the period 1958-2017 (Hanssen-Bauer et al., 2019). Higher winter temperatures increase the possibility that precipitation will fall as rain and not snow (Førland & Hanssen-Bauer et al., 2000; Bintanja & Andry, 2017). More recently there has been a steady increase in precipitation since the year 2000, with the largest seasonal increase during autumn (Figure 3.3) where 25% of all annual precipitation occurring during one precipitation event. The events happen during mid-winter and are causing slush avalanches, debris flows, and flooding of which 40% occurs in December-February, and 28% occurs between September to November (Hanssen-Bauer et al., 2019). With measurements from November-April 1995-96, 2009-10, 2011-12, and 2016-

17 indicates that more than 50% of the precipitation is rain (Hansen et al., 2014; Vikhamar-Schuler et al., 2016).

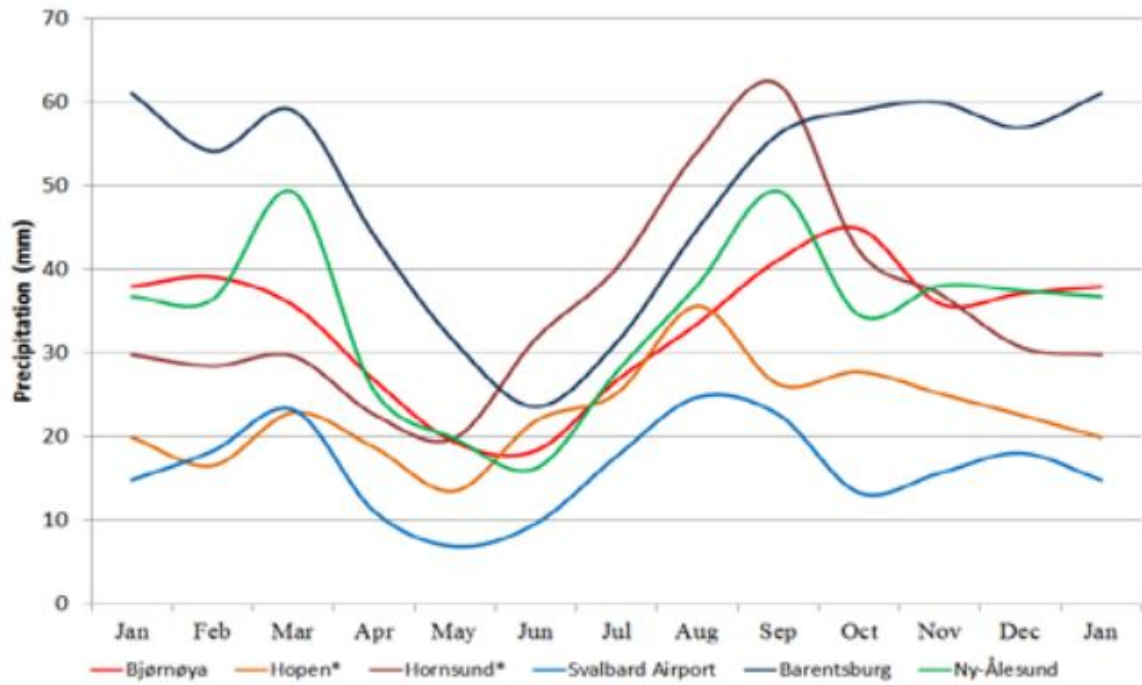


Figure 3.3: Precipitation (mm) at Svalbard airport - Longyear (LYR) with high precipitation during spring and autumn – winter (Hanssen-Bauer et al., 2019).

In the winter, the rain on snow (ROS) events cause an ice crust to form on the existing snow surface. The crust on the top layer of the snow will eventually cause more unstable layers in the snowpack with implications for avalanches (Wickström et al., 2019; Bintanja & Andry, 2017). An increase in rainfall and warmer permafrost will speed up processes such as solifluction and detachment of rockslides. Because the rising temperatures may lead to more freeze-thaw events, this will lead to increased rockfall events. Furthermore, an increase in the permafrost temperature will lead to greater slope instability and more slope processes. The increase in permafrost temperature combined with a higher amount of precipitation and more heavy rainfall on sloping terrain will lead to an increase in soil slides. The increased rainfall combined with warmer air temperature will likely increase the frequency of most landslides and avalanches. Due to a rise in temperatures, a decrease in maximum annual snow precipitation and shorter snow season is predicted to lead to fewer dry snow avalanches. More heavy rain- and snowfall will increase the occurrence of wet avalanches such as slushflows (Hanssen-Bauer et al., 2019).

3.5 HYDROLOGY

The hydrology in glacial environments is unique due to being heavily influenced by the glacier's thermal regime (Hodgkins, 1997). Most of the glaciers in Svalbard are classified as polythermal ice and referred to as sub-polar glaciers (Hagen et al., 1993). Where the ice has a cold-based thermal regime act as an aquiclude. This restricts runoff drainage to incised surface channels. In addition, the glacier bed can be at the melting point, and an unfrozen area within the permafrost, a thawed subglacial talik can form. According to Hagen et al., (2003), a subglacial talik can connect the glacier to the underlying groundwater.

Hydrological systems in the arctic are complex. The contentious permafrost dictates the structure of the watersheds and spring snowmelt is often the dominant feature in the annual hydrology. The combination of permafrost, snow accumulation, and cold winters causes precipitation to be stored until the melt season (Hanssen-Bauer et al., 2019). According to Nowak and Hodson (2013), the majority of melt-driven discharge occurs from June to August in northern Svalbard two “shoulder seasons” occur on either side of the spring/ summer melt season. In the shoulder seasons, discharge is present but variable. Sporadic discharge can also occur from November to May. This is due to the volatility of wintertime temperatures (Humlum, 2002; Førland et al., 1997).

Precipitation has increased by 14 %, and the last 4-5 decades air temperature in Svalbard has risen by approximately 2.-3°C. A further increase in precipitation by 40% with an increase in air temperature by 2-8°C will have consequences for understanding the hydrological processes and water budget. In the high Arctic consequences of increased temperature and precipitation will be:

1. Prolonged melt season (Sherp & Wolken, 2010 cited by Nowak & Hodson, 2013).
2. Within a hydrological year (1 October to 30 September) the formation of ground icings can occur (Nowak & Hodson, 2013)
3. Thawing of the permafrost (Boike, 2009; Christiansen et al., 2010) and, as a result deepening of the active layer (Åkerman, 2005).
4. Change in snow cover, glacier mass balance, erosion, and sediment transport. This will influence river flow and increased precipitation will lead to increased weathering of soil and rock (Hanssen-Bauer et al., 2019)

5. Slush avalanches, thaw on snow, and thaw-refreeze events (Eckerstofer & Christiansen, 2012).

Thawing of the permafrost and prolonged meltwater season can produce more meltwater from ground ice and glacial ice, acting as a water source. And the increasing of the active layer and formation of ground icing over a year can prolong the transfer of meltwater over time, acting as a water store. The formation of ground icing during a hydrological year can also interact with the glacial mass balance. This is due to the redistribution of snow across the landscape and change of the insolation, e.g., firn, ice layers, densification, and the creation of superimposed ice layers (Nowak & Hodson, 2013).

During the runoff season in a glacial catchment, the runoff is expected to decrease through the runoff season. But a cold-based glacier does not typically let go of the sediment supply during the melt season. This is due to the lack of subglacial drainage systems (Hodkins, 1997). Glacier melt between 1980-2015 is calculated to have contributed to an annual runoff increase by 35% (Hanssen-Bauer et al., 2019).

During winter when precipitation is stored as snow and streams and rivers in Svalbard have little to no discharge flow. From June through September, highest discharge occurs due to meltwater from snow and glaciers, but also precipitation, particularly if rain occurs during melt season when large floods can occur. The Norwegian Water Resources and Energy Directorate (NVE) has, from the 1990s through today, conducted a study in De Geerdalen that shows a connection between anomaly high temperatures that lead to increased meltwater and rainfall (Hanssen-Bauer et al., 2019).

According to Killingtveit, Petterson and Sand (2003), there is no change in the storage capacity of a catchment in a permafrost environment. Newer studies by Rutter et al. (2011) and Nowak and Hodson (2013) disagree. This is due to the last decade's hydrological shift in Svalbard where an increase in the water budget has occurred due to the melting of glaciers and ground ice. In addition, a longer melting season has occurred (Nowak and Hodson, 2013).

CHAPTER 4: METHODS

This chapter reviews the methods used to address the research aims and is divided into five sections. Subsection one focuses on the structure of the thesis and gives an outline of the following sections. The second section describes the fieldwork, and the third section describes the laboratory methods of 2019. The fourth section describes previous (2012) laboratory methods and the final section describes the comparison between 2012 and 2019 surface cores and validation of varve count. The methods used are selected to answer the thesis aims.

4.1 OUTLINE OF THE WORK

The thesis has been structured according to figure 4.1. The thesis work was carried out with the notion of contributing to the larger research project "Arctic hydrological regime shifts in a warming climate." The plan was to take one surface core and one long percussion core. Two surface cores were recovered during field work and one was used for this study. The long percussion core was lost; as a result, unpublished data from a long percussion core from 2012 is utilized. The results from the surface core from 2019 will be compared to the varve count and plutonium measurements done on a surface core from 2012, with the aim to validate the varve count from the 2019 surface core. The validated varve count from 2019 will be compared to the long core from 2012, and the combined varve count and thickness will be compared to temperature and precipitation record and other regional environmental data in the discussion. Furthermore, rainfall events will be identified and associated with event beds to identify mass movement events in the 2019 sediment core. The findings are presented in conclusions and additional data in the appendix.

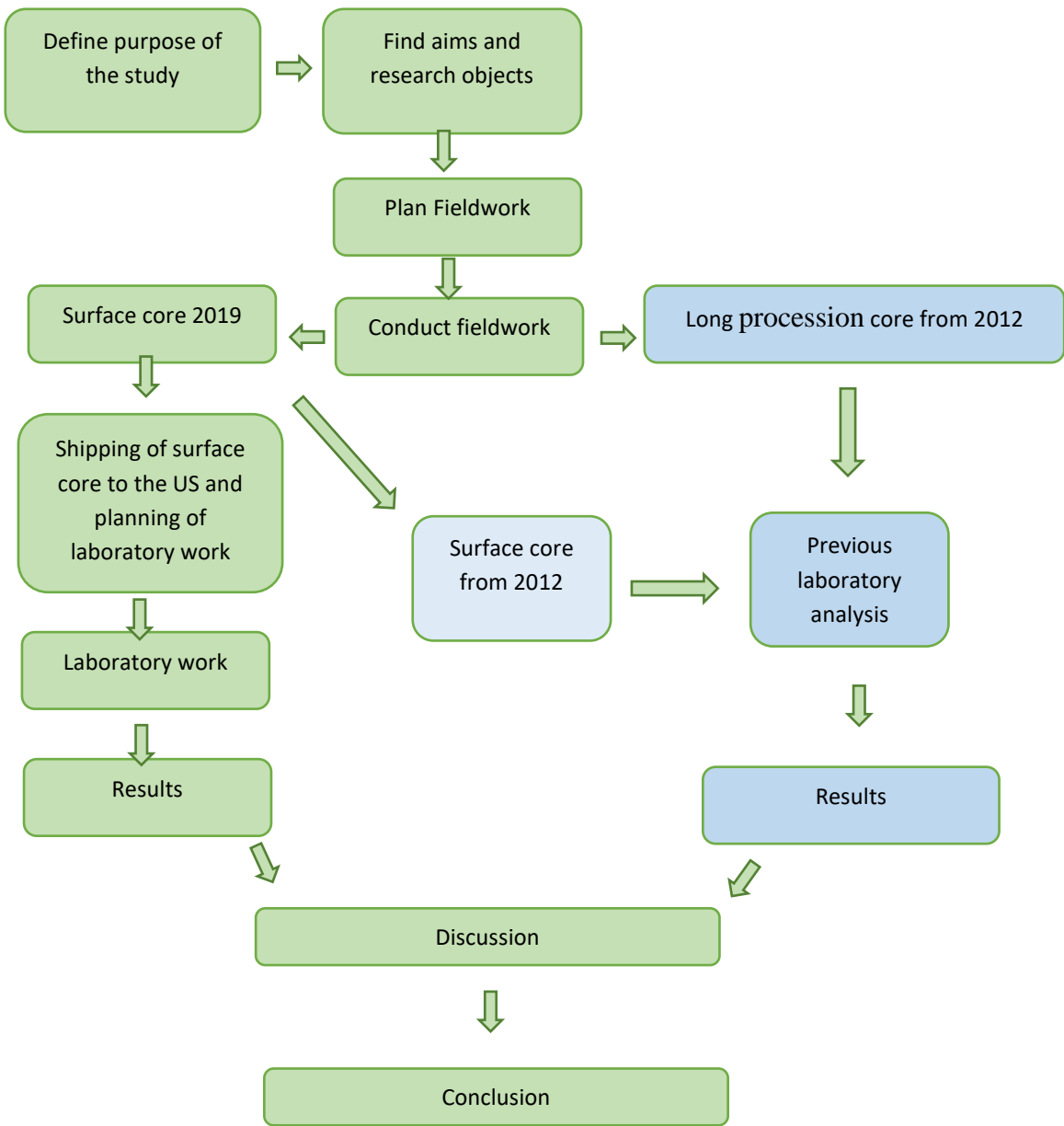


Figure 4.1: Structure of the work and final thesis project.

4.2 FIELDWORK IN 2019

The surface sediment core (BSV-2019-1) of approximately 52cm was collected from 78° 05.750' N 015° 40.687' E, Bødalsvatnet 26th of April 2019. The location is located at approximately the same locations where the previous surface sediment core was taken in with a length of approximately 40 cm in 2012. The core collected by drilling a hole in the ice and using a K-B universal corer in a clear plastic tube with an interior diameter of 6,6 cm. The device uses a one-way valve to ensure that the sediment is not lost or disturbed while it is pulled through the water column. BSV-2019-1 was collected, and floral foam was added to suck up the water and preserve the top layers of the surface sediment core. A second sediment core (BSV-2019-2) was taken, but gel absorbent as used, and the top layers were disturbed by water during transport. Therefore, BSV-2019-1 was used in this study.

In April 2019, an attempt to core a long percussion core with a modified Nesje percussion coring device. The device uses a piston to collect the sediment cores in an aluminum tubing; as a result, the top centimeters of the sediment core can be disturbed. The long core of 2019 is still in the sediment of Bødalsvatnet; as a result, the long percussion core from 2012 of the length 1,4 meter will be used in this study.

After the cores were collected, they were transported for storage at UNIS before being transported to Bates College, Maine, and UMass, Amherst, Massachusetts in the U.S., where the sediment core was stored vertically in a refrigerated core storage at 4°C before laboratory work could take place.

4.3 LABORATORY WORK OF 2019

The surface core BSV-2019-1 was processed in the Bates College sedimentology lab. The sediment core was split in two by using a table saw and a Dremel tool. The core was split lengthwise, and a fishing line was used to divide the two halves, thus creating a working half and an archive half.

4.3.1 THIN SECTIONS

Thin sections were created by subsampling the length of the core. The subsampling was done by making nine "boats" of aluminum; 1 cm deep, 2 cm wide and 7 cm length. Each boat has holes drilled inn to them approximately 2-3 millimeters apart. The holes in the boats are made because this makes it easier for the epoxy to penetrate the sediment in the boat. The finished subsamples are pressed completely into the sediment along with the core length with 1-2 cm overlap between each subsample. When all the nine subsamples were pressed down the length of the core (Figure 4.2), the subsamples with the sediment was collected. For collecting the subsamples, a fishing tool and a U-shaped cutting tool were pressed underneath each subsample separating them from the rest of the sediment in the core. The excess sediment was cleaned of by the usage of a fishing line and wipes. The subsamples were placed in two plastic boxes.

The subsamples were then freeze dried. In preparation for freeze-drying, the boats were exposed to liquid nitrogen. The liquid nitrogen was poured into a styrofoam box. Each subsamples were slowly immersed in the liquid nitrogen in the syrofoam box to prevent cracks and bubbles. Subsamples were the freeze dried in the Lasbconoco band Freeze Dry System. The subsamples were placed back into the plastic boxes and placed on top of each other with space in between them in the freeze-drying system with pressure of 5-10 μ g Hg. When the subsamples were properly frozen, low viscosity epoxy-resin carefully poured around the samples (Figure 4.2). The epoxy-resin is comprised of cyclohexyl carboxylate (ERL4221), diglycerol ether polypropylene glycol (DER, nonyl succinic anhydride (NSA) and dimethylaminoethanol (DMAE). The mass ration between these substances was ERL: DER: NSA: DMAE. The boxes with the subsamples were placed on top of each other with a space between them in a vacuum chamber. The epoxy-resin is sucked up through the sediment.

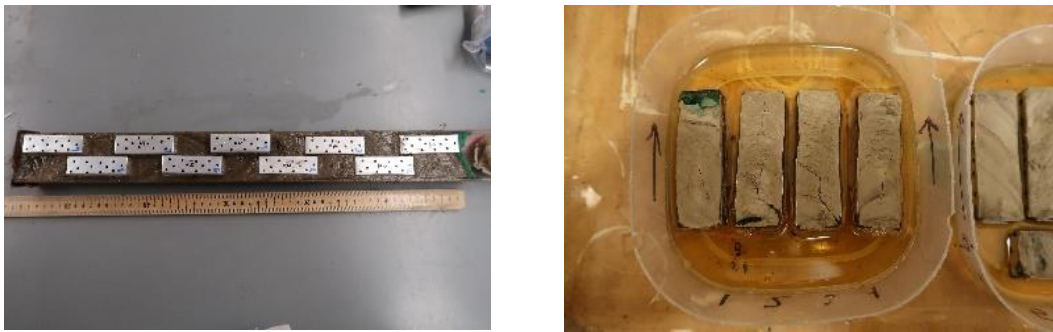


Figure 4.2: Left: the boats are pressed down into the sediment along with the core in an alternating left-right pattern with 1-2 cm overlap. Right: Epoxy-resin was poured carefully in the corner of the plastic box and did not cover the subsamples.

When the epoxy-resin was sucked up through the sediment, the boxes with the subsamples were placed in a warm cabinet (50°C), and the sediment and epoxy hardened. Later the subsamples were taken out of the “boats” and trimmed with a saw band. The sediment slabs were then sent to Quality Thin Section in Tucson, Arizona where they were cut, polished, and mounted on slides. The finished slides were sent to Bates College, scanned at 2400 dpi, and sent digitally to Norway for analysis.

4.3.2 GRAIN SIZE

Grain size analysis was done using Coulter Laser Particle Size Analyser. The Coulter LPSA calculates the grain size distribution of the sample by using diffracted laser light. Particle size is measured by the direction and strength of the light that passes through the particles in the sample (Figure 4.3). Due to the increased efficiency of the sonic dismembrator in breaking up particle aggregates or flocs, the third samples run is often used for measuring the grain size.

The working half of the BSV – 2019 - 1 surface core was continuously sampled for grain size analysis at a 1 cm interval. The samples were collected and prepared following Dowey (2013). Each sample contained approximately 0,25 cm² sediment. The sample was transferred to a 47 mL Oak Ridge centrifuge tube. Hydrogen peroxide (H₂O₂) was added to the sediment in the tube, just enough to cover the sediment. The sample tubes were then capped and stored overnight to oxidize any organic matter. After 12 hours, 17 mL of dispersant (0,7g/L sodium metaphosphate) and 20mL deionized water was added to each sample tube. For one minute, the

sample tube was shaken by Vortex-Genie and sonicated with the Fisher Science Sonic Dismembrator 60 for 1 minute. A prepared sample in the sample tube was then loaded into the Coulter Laser Size Analyser for grain size analysis. Each sample is run three times and recorded by mean, median, 50th, 10th, and 90th percentile values. For this thesis, grain size values for mean, median, and 90th percentile is used to illustrate the grain size value of each sample. The values given by Coulter LPSA represent the different types of grain size

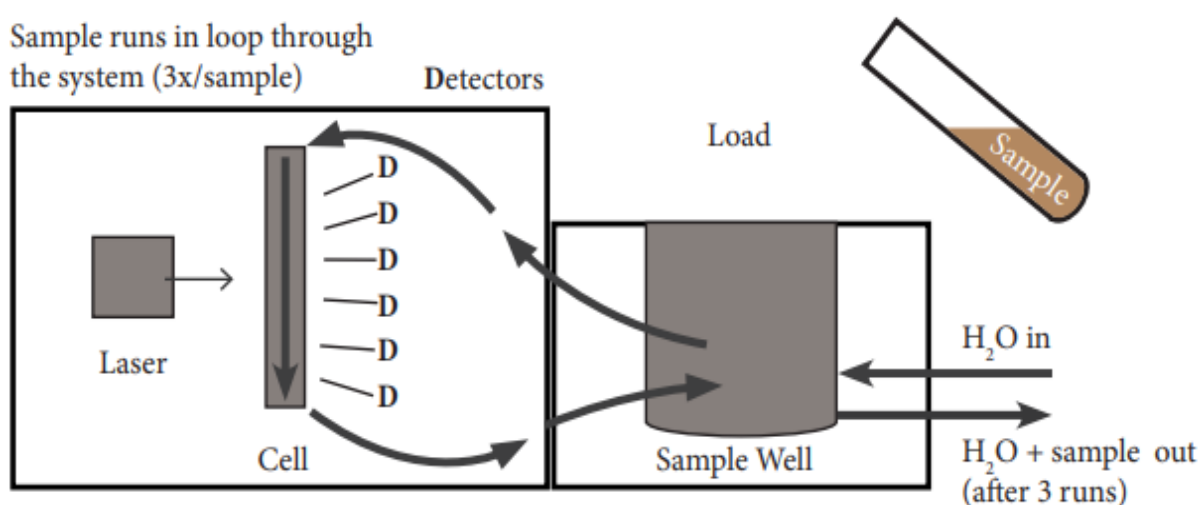


Figure 4.3: Sketch of the simplified illustration of the Coulter Laser Particle Size Analyser behind the detection of grain size (Lindelof, 2012).

Sorting of the grain size in sediment cores from proglacial lakes has the potential to give a continuous glacier history. The amount of medium silt (16µm – 31µm) in the sediments can be an indicator of the size of the glacier. The grain size of medium silt does not consistently indicate glacial size for every bedrock or area. This is a method that needs interpretation regarding the depositional environment and catchment area topography (Lie et al., 2004; Matthews et al., 2000).

The sorting of the sediment and mean grain size can point to mass-movement events documented in the sediment. Where increased flow in the water column results in increasing grain size and fluvial sorting, an indication of mass movement deposition can be bad sooting with a high average of grain size (Arnaud et al., 2002).

4.3.3 MAGNETIC SUSCEPTIBILITY

Magnetic susceptibility (M.S.) is a nondimensional parameter (Dearing, 1994). M.S. is a measurement of the ability of the material to become magnetized, a property related to the lithology of the sediment (Dearing, et al., 1996). The MS method measures the value of the concentration of magnetic minerals in the test sample by:

The low frequency of mass-specific susceptibility (lf) (m^3kg^{-1}):

$$Klf = \frac{K}{P}$$

Where M.K. is the volume of susceptibility, p is the sample bulk density (kg m^{-3}), and the specific mass susceptibility is expressed Si units by the most common $10^{-6}\text{m}^3\text{kg}^{-1}$.

M.S. is a conventional analysis that is used to examine sediment cores (Røthe et al., 2015; van der Bilt et al., 2015; Rubensdotter & Rosenquist, 2009). At Lake Baikal MSE2 has been used to identify turbidities, and in Greenland, the measurement technique has been used to identify mineral characteristics of laminated sediment (Dearing, 1994). On the BSV-2019-1 surface core M.S. measurements were taken every 1 cm on the archive half using a Barington MSE2 sensor set to 0,1 SI units and recorded in the Mulitus Software. The sensor was re-zeroed every five measurements, and therefore, the measurements were corrected for drift.

Sediment can, as described in table 4.1, be divided into five groups: ferromagnetic (strongly positive), ferrimagnetic (strongly positive), antiferromagnetic (moderate positive values), paramagnetic (weak positive) and diamagnetic (negative) (Dearing, 1994). The scale is due to the relationship between the non-magnetic and the magnetic minerals in the sediment. Diamagnetic sediment is approximately a hundred times weaker than paramagnetic minerals, and a thousand times weaker than ferromagnetic minerals. Examples of diamagnetic minerals are often disregarded. An example of diamagnetic minerals is feldspar and quartz, minerals that are often found in lacustrine sediments. Paramagnetic sediments such as sulfate, sodium, and carbonate can be found in lacustrine sediments. Paramagnetic and diamagnetic sediments have the opposite charge of each other and will often zero each other out. If ferromagnetic minerals such as magnetite are present in the lacustrine sediments, they will be the dominant magnetic force in the sample. This is due to the ferromagnetic minerals being associated with iron minerals and other natural minerals natural to lakes (Dearing, 1994).

Table 4.1: Simplified classification of magnetic susceptibility (Gunn & Best, 1998; Dearing, 1994). The values in the table indicates that the materials magnetic susceptibility value increases with the ability of magnetization.

Material	Example	Magnetic Susceptibility χ , $10^8 \text{m}^3/\text{kg}$
Diamagnetic	Organic matter & plastics	Weak negative susceptibility
	Quarts (SiO_2)	-0,62
	Calcite (CaCO_3)	-0,49
	Water (H_2O)	-0,90
Paramagnetic		Weak positive susceptibility
	Montmorillonite (clay)	13
	Nontronite (iron rich clay)	65
	Biotite (silica)	79
	Siderite (carbonate)	100
	Pyrite (sulfide)	30
Antiferromagnetic	FeS_2 , Fe_2O , TiO_2 , MnSO_4 , FeCO_3	Moderate positive values
Ferrimagnetic	MnFe_2O_4 , NiFe_2O_4 , MgFe_2O_4	Strong positive susceptibility
Ferromagnetic	Fe, Ni, Co	Strong positive susceptibility

4.3.4 DRY BULK DENSITY, WATER CONTENT AND LOSS-ON-IGNITION

Dry bulk density is the relationship between the volume of the sediment and the dry material. In preparation for calculating dry bulk density, a sediment sample (1cm^3) was collected at 1 cm intervals with an open-ended aluminum cube ($1\text{cm} \times 1\text{cm} \times 1\text{cm}$) that was pressed into the sediment and removed with a spatula. The cube with the sediment was then placed in a crucible for drying and roasting (Figure 4.4). Dry Bulk Density (DBD) is defined as the relationship between the dry sediment and volume of the sample shown in equation 2:

1. Bulk density (g(cm³)):
$$\frac{\text{Dry weight} - \text{Weight crucible}}{1}$$
2. Dry bulk density (g(cm³)):
$$\frac{\text{Bulk Density} - \text{Weight crucible}}{1}$$



Figure 4.4: Left: The sediment collected every 1cm was placed in a crucible. Right: The sediment samples in the crucible were placed in a drying oven.

Dry bulk density indicates how well the sediment is packed (Figure 4.5) and measures the porosity of the sediment (Blake & Hartge, 1986, cited in Bakke et al. (2005)). Fine-grained and badly sorted minerogenic sediments give high-value DBD in contrast to organic sediments that give low DBD values (Bakke et al., 2005). DBD is closely linked to the mineralogic composition of the sediment (Nesse, 2000). The water content and especially large water content in the sample is largely linked to low DBD values. And in organic material, water is part of the matrix. In minerogenic sediments the water fills up the sediment pores. A study by Bakke et al, (2005) implicates change in glacier equilibrium line and DBD in proglacial lake sediments.

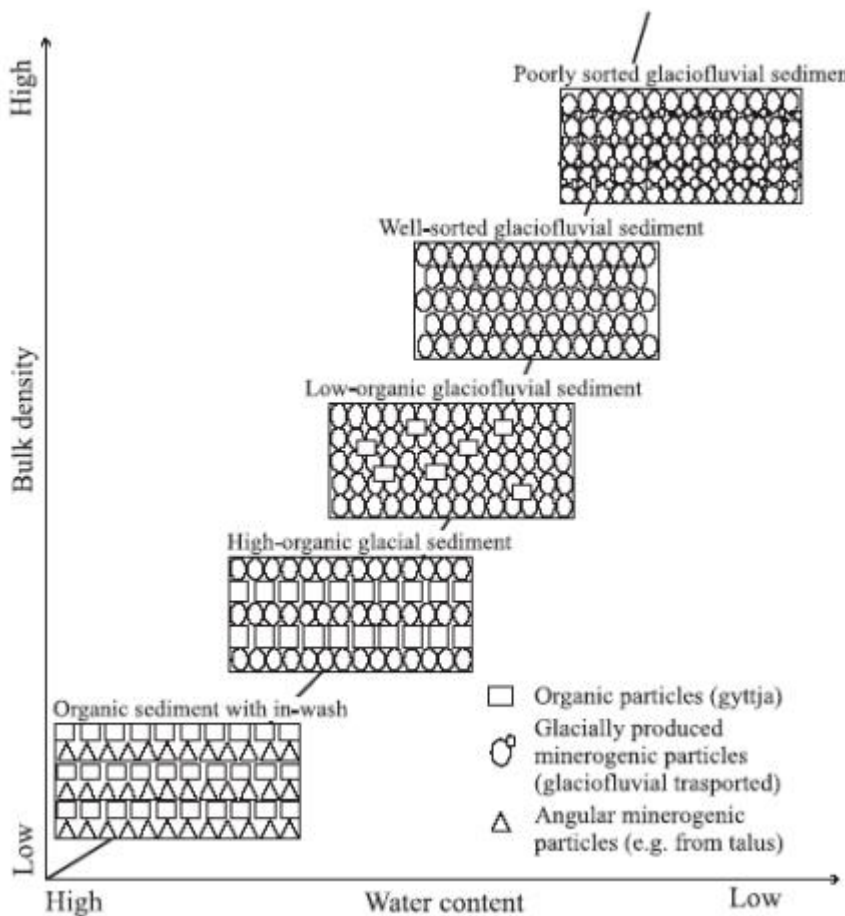


Figure 4.5: The relationship between bulk density and water content by type of sediment. Type of sediment, degree of sorted sediment, and amount of minerogenic particles are all factors that affect bulk density (Bakke et al., 2005).

Organic sediments have a low DBD, but elements that consist of badly sorted, fine grains minerogenic sediment gives high DBD values (Bakke et al. 2005). All sediment pores in lake sediments will be filled with water. Hence, dry bulk density indicates the water content in the sediments. Water content can also be calculated by the weight of the sediment in the crucible before and overnight drying in the drying oven (Figure 4.4B) at 100°C as described in equation 3:

$$3. \text{ Water content (wc%)}: \left(\frac{\text{Wet Bulk Density} - \text{Dry Bulk Density}}{\text{Wet Bulk Density}} \right) * 100$$

Loss-on-ignition is a widely used method for calculating the sediments of the amount of organic material and carbon in sediments. The relationship between the organic material and carbon content is linear (Santisteban et al., 2004; Heiri, Lotter & Lemcke, 2001; Snowball & Sandgren, 1996). The samples were then placed in the furnace with 550°C for 1 hour. Loss-on-ignition was calculated using the data from the weighing of the crucible before and after the furnace, as described in equation 4:

4. Loss-on-ignition (%LOI):

$$\frac{(Bulk\ Density - Weight\ Crucible\ furnace\ (500\ degrees\ celsius))}{(Bulk\ Density - Weight\ crucible)} * 100$$

The organic material in the sediment is not directly measured by Loss-on-ignition, but by weight loss. Weight loss is not only connected to organic material but can also be other materials that are burned away in the furnace, such as Loss of salts and clay minerals. According to Heiri, Lotter and Lemcke (2001), the Loss of organic material can be minimized by accurate following the recommended furnace time. In contrast, Nesje et al. (2001) conclude that time in the furnace does not have an effect on the factor of error in the loss-on-ignition procedure. Another issue with the Loss-on-ignition method is that sediments with <5% organic material can give unreliable values. Such sediments can be proglacial sediments (Snowball & Sandgren, 1996). Due to this issue, Sandtisteban et al. (2004) concluded that such sediments should be interpretive with consideration to each sediment samples of mineral properties.

4.4.5 GEOCHEMISTRY

The geochemical structure of the sediment core was examined through X-ray Fluorescence (XRF) analysis. XRF is used to determine the relative abundance of elements in the sediment core. The atoms are bombarded with X-rays and an electron or more will be ejected. Hence, the atom becomes unstable, and the ejected electron(s) place is filled by electron(s) with higher energy. As a result, a photon (discrete packet of energy) is ejected and measured by the XRF. Each element in the sediment core has its own photon energy level, and the energy measured by the XRF detector can be classified as a specific element. This non-destructive semi-quantitative high-resolution analysis is useful for paleoenvironmental studies (de Wet, 2013; Cuven et al., 2010; Croudace, Rindby & Rothwell, 2006). The changes in downcore elemental profiles reflect changing environmental parameters including redox conditions in the water column (Naehler et al., 2013), paleoproductivity in lakes (Johnson, Brown & Shi 2011), and changes in a sediment source (de Wet, 2013). This technique is particularly useful in varved lacustrine sediment cores with high temporal paleoclimatological and paleohydrological signals (Cuven et al., 2015; Van der Bilt et al., 2015).

For the analysis, the archive half of the surface sediment core (BSV-2019-1) was transported to the Ronald B. Gilmore XRF Laboratory at the University of Massachusetts, Amherst. At the laboratory, a Cox ITRAX XRF Core scanner was used to determine the geochemical (elemental) structure of the surface sediment core. ITRAX scanner can obtain non-destructive sub-millimeter precision; geochemical data has made it an excellent choice for studies of lacustrine sediment provenance (Culven et al., 2015).

The surface core was loaded into the ITRAX with the flat surface of the sediment facing upwards in the machine. For processing the sample, the ITRAX makes two scans (Croudace, Rindby & Rothwell, 2006). The first scan gives an RGB (Red Green Blue) image, a radiograph, and a laser triangulated topographic surface profile. When the scan was done, a plastic film was placed on top of the sediment core to protect the sediment core from drying out during the longer XRF scan.

The XRF analysis was done every 1mm with 10 seconds exposure time. The analysis was done with a molybdenum (Mo) tube that produces X-rays with a current of 55mA and a voltage of 30kW. With the topographical RGB image and scan used to obtain the correct distance to the sediment (Figure 4.6) (Croudace et al., 2006). The finished result of the geochemical data is

semi-quantitative due to the results that can vary because of the difference of water content a bulk density in the sediment (Rothwell et al., 2006). The analysis was done for 30 elements with elements at the low end of the sensitivity range of the Mo tube being noisy.

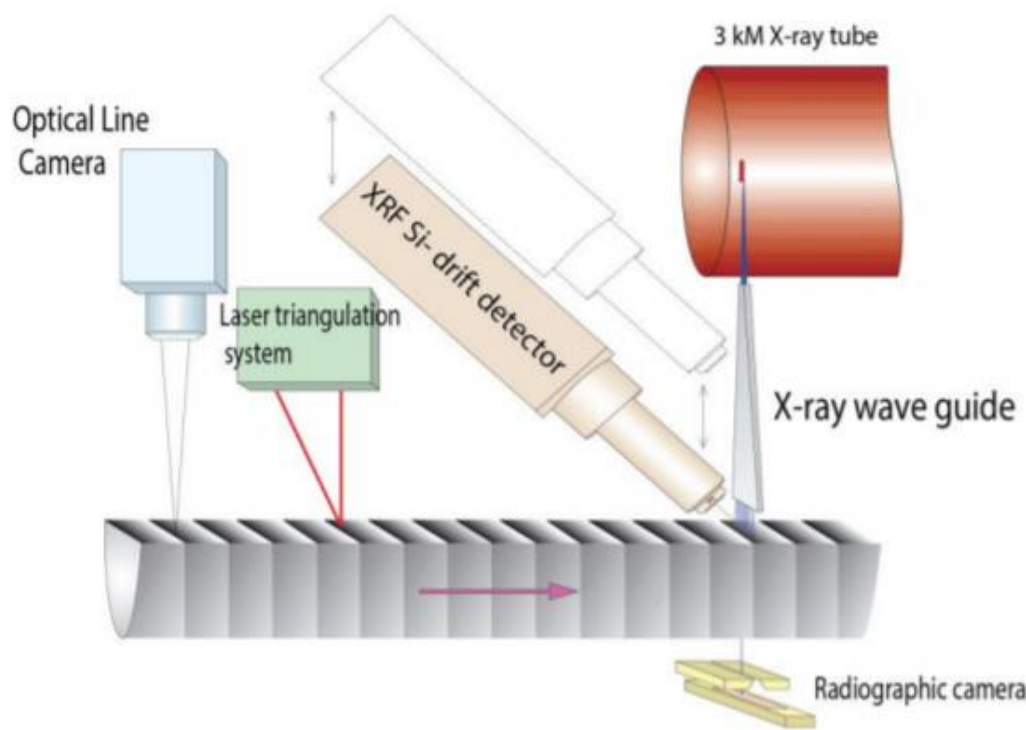


Figure 4.6: Diagram of ITRAX core scanner (Croudance, Rindby and Rothwell., 2006).

According to Croudance, Rindby and Rothwell (2006) element profiles from XRF core scanner should be cautiously interpreted because of the core scanner being affected by physical sediment properties. Hence, the XRF profiles only, include elements that had a high sensitivity to Mo tubing. The exclusions include Aluminum (Al) and Silicon (Si) which are sensitive to scattering (Tjallingii et al., 2007). Furthermore, elements with a low signal-to-noise ratio in counts-per-second (cps) were excluded. SNR is defined as;

$$SNR = \frac{Mean \mu}{Standard deviation (SD)}$$

The elements Potassium (K), Calcium (Ca), Aluminum (Al), Manganese (Mn), Iron (Fe), Titanium (Ti) and Zirconium (Zr) was chosen. Zirconium, Potassium, and Calcium and indicate terrestrial erosion. And a difference in the relationship between elements Iron and Titanium indicates a change in erosion in the catchment area (Croudance, Rindby & Rothwell., 2006) while according to Bakke et al., (2009), titanium can indicate a link to glacial erosion. The relationship between the elements can be used to identify sediment sources in the lake sediments (Croudance, Rindby & Rothwell., 2006; Rotwell et al., 2006).

4.4 PREVIOUS ANALYSIS

Previous laboratory work has been conducted on precision core and surface cores from 2012. High resolution image from Geotek Multi-Sensor Core Scanner was taken at the University of Massachusetts, Amherst – UMass Hartshorn Quaternary Laboratory. Visual stratigraphy, varve count and varve thickness were done (Retelle, Dowey & Dulin, 2013). On surface core from 2012 plutonium ($^{239+240}\text{Pu}$) was measured every centimeter from 1 cm to 39 cm, and sent for analysis at Northern Arizona University. Plutonium analysis was done to locate the maximum deposition date of 1963 (Ketterer, 2013).

4.5 VALIDATION OF VARVE RECORD

To validate the varve count in the 2019 surface core, the sediment core was cross-correlated to a 2012 sediment core taken in close proximity. Correlation was done by comparing varve count and marker beds. The comparison was then correlated whit the plutonium ($^{239+240}\text{Pu}$) measurements done on the 2012 surface core. By correlating the stratigraphic log of both cores to the plutonium measurements the maximum $^{239+240}\text{Pu}$ from 1963 was located and associated lamina was identified by depth.

CHAPTER 5: RESULTS

The chapter is divided into five sections. First four section presents visual stratigraphy, varve thickness and varve count, physical- and geochemical results obtained from the surface core (BVS-2019-1) from 2019. The fifth section validates the yearly record of the surface core from 2019 by correlating it to the surface core from 2012 by plutonium measurement.

5.1 VISUAL STRATIGRAPHY

The surface core sediment from 2019 (BVS – 2019 -1) is divided in to three units; A, B and C based on varve count and physical parameters (chapter 5.3). The sediments are laminated and has several shades of brown. Unit A (0 – 20 cm) is visible deformed and can be identified by small visible color changes within the grayish brown color (Figure 5.1). Unit B (20- 44 cm) is characterized by thicker darker brown laminae identified in figure 5.1 with its darker brown color. Unit C (44 – 52 cm), the unit consists of lighter brown laminae and a thick drake brown lamina. The thicker darker brown laminae in unit B and C have sharp distinctive boundaries to the overlaying and underlaying laminae and is identified as event beds.

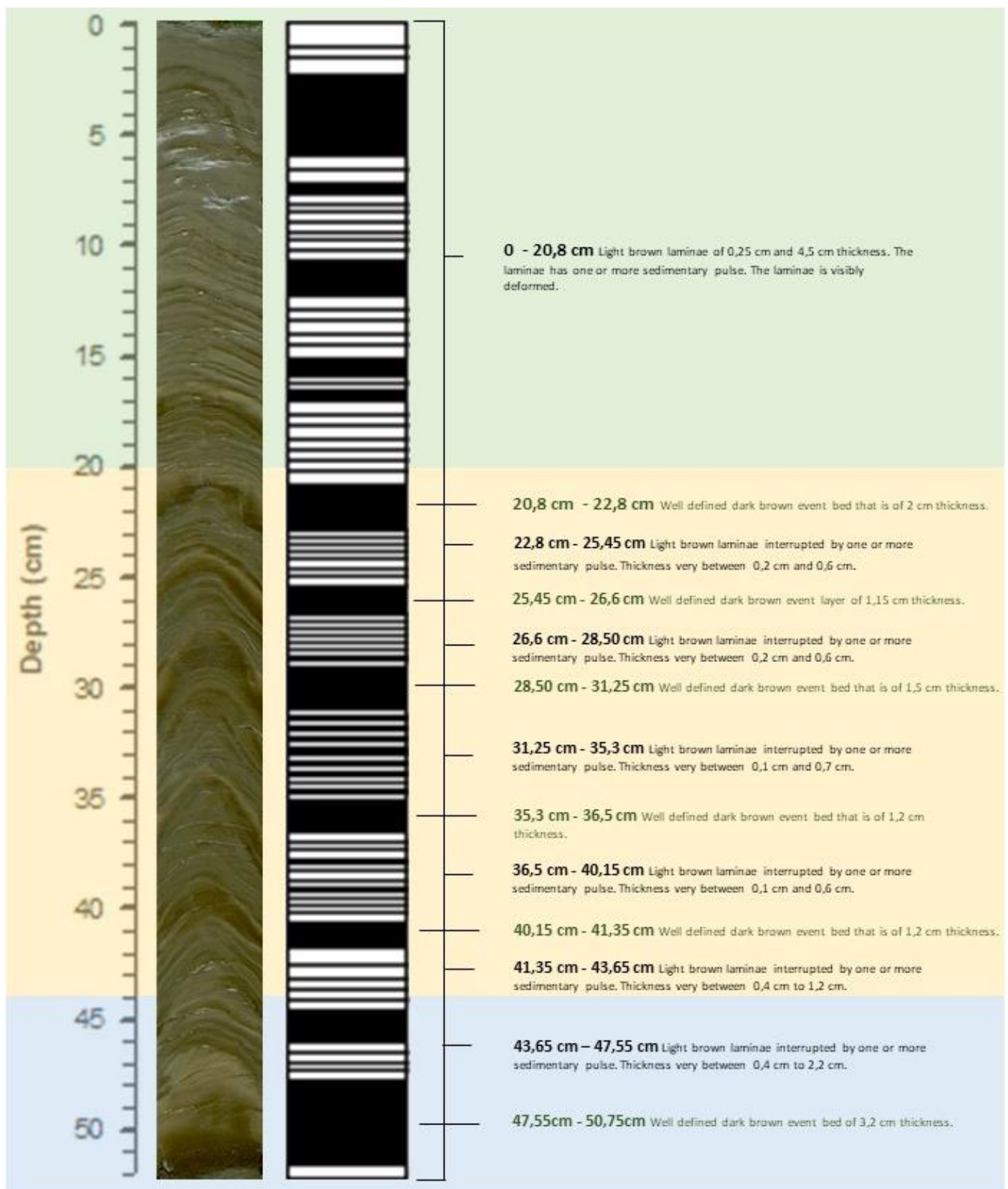


Figure 5.1: Stratigraphic log based on visual inspection and varve count of core BSV– 2019 – 1, with RBG image taken with ITRAX core scanner. The sediment core is divided in to unit A (green), unit B (yellow) and unit C (blue). Light brown laminae in black and thicker darker laminae marked as event beds in green.

The details of darker brown event beds identified in figure 5.1 are better observed in the nine thin sections. Figure 5.2A illustrates a thick darker lamina is observed in the sediment core. Thickness of the “laminae A” is marked in orange and is characterized by a thick lamina with coarse grained “summer sediment” that is a fining upward layer. The sequence ends in a thick clay cap with a clear boundary to the overlaying laminae. This lamina is identified as a graded bed. A thinner “lamina B” is observed in figure 5.2 B and marked in orange. The lamina is characterized by coarser grained summer sediment. The laminae have a fining upward sequence that is interrupted by one or more sediment pulse. The lamina ends in a darker winter layer. Both “lamina A” and “lamina B” has color differences in lighter summer and darker winter sediment overserved in figure 5.2 but is not clearly identified in image of sediment core in figure 5.1.

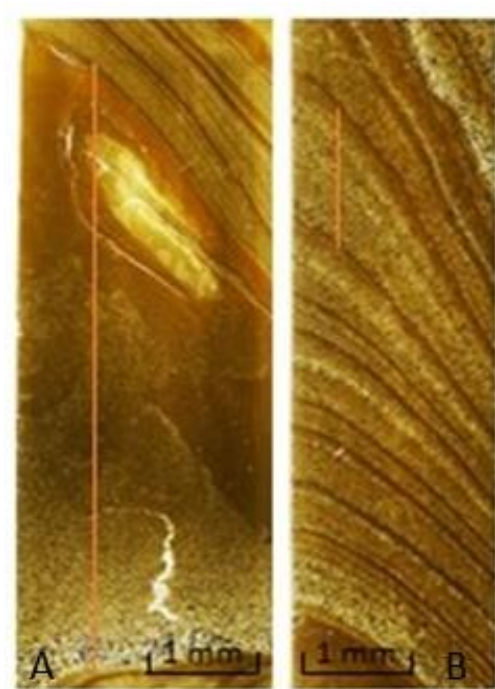


Figure 5.2: A: An example of graded bed (marked by an orange line). B: An example of varve couplets with lighter summer layer fining upwards to a darker winter layer. In the varve marked with an orange line, the fining upwards sequence is interrupted by one or more sediment pulse.

5.2 VARVE THICKNESS AND VARVE COUNT

Thin sections were overlapped according to distinctive marker beds (Appendix A). A total of 83 sedimentary units was observed. Sedimentary units identified as varve couplets has a variation in thickness between 0,1 cm and 4,5 cm, with a mean varve thickness of 0,52 cm. The thicker darker graded beds identified as event beds in unit B and C have a thickness between 1,15 cm – 3,2 cm. Event beds by year is noted in table 5.1 and varve thickness by year is illustrated in figure 5.3.

Table 5.1: Event beds by number, depth of location in cm, and associated year (AD). Depth, thickness and associated year of all sedimentary units is located in appendix A.

<i>Graded bed by number</i>	<i>Depth of bottom of the graded bed (cm)</i>	<i>Thickness of graded bed (cm)</i>	<i>Year (AD)</i>
E6	22,8	2,0	1993
E5	26,6	1,15	1983
E4	31,25	2,6	1974
E3	36,5	1,2	1957
E2	41,35	1,2	1945
E1	50,75	3,2	1936

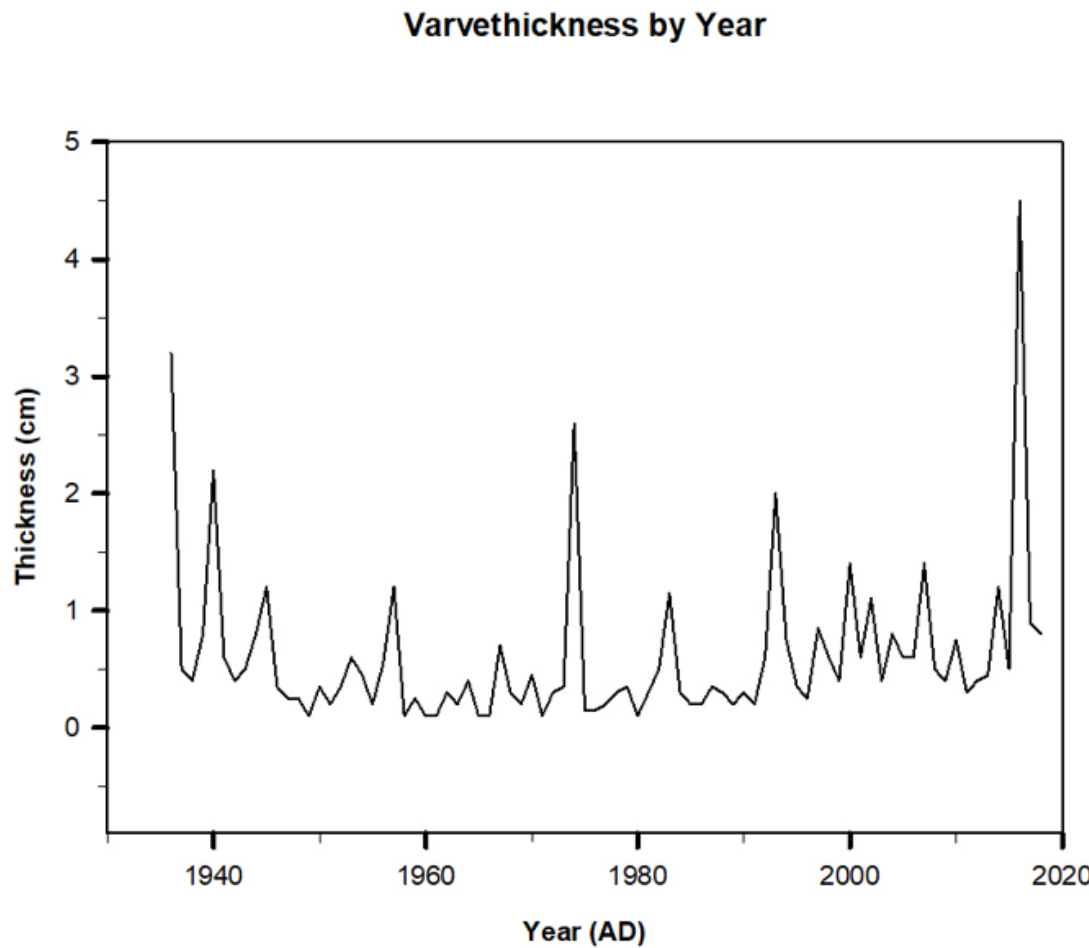


Figure 5.3: Varve thickness recorded and correlated to varve count gives age of each sedimentary unit. The sediment core records sedimentary units from 2018 to 1936. Disregarding possible further varve count under graded bed of 50,75 cm depth.

5.3 PHYSICAL PARAMETERS

Though the sediment core measured grain size varies from 3,1 μm to 52,3 μm . Observations also noted; coarse gravel of 2 cm length occurs in an event bed at 35,5 cm, black coarser grained sediment at 26 cm and sand at event bed is located at 50,75 (Appendix B). Magnetic susceptibility ($\text{cgs} \times 10^{-6}$) varies from 8,4 to 13,6 (appendix C), Dry Bulk Density (DBD) varies from 0,8 (g/cm^3) to 1,6 (g/cm^3), water content (%WC) varies from 22,3% to 36,8% and Loss-on-ignition (%LOI) varies from 3,7% to 8,4% (appendix D).

Unit C (45-52 cm)

The unit encompasses the bottom 8 cm of the surface core and comprises one thick event bed (E1). The unit has the overall largest differences in physical parameters of the three units. Grain size initially decrease towards the boundary to unit B with a total range of 52,3 – 4,0 μm . A decrease is also observed in dry bulk density (1,5 – 1,0 (g/cm^3)) and loss-on-ignition (8,4 – 3,7%). In contrast magnetic susceptibility and water content has an increasing trend towards unit B (Table 5.2). Overall unit C is characterized by the rapid changes in the parameters associated with graded bed E1 (table 5.3). The event bed is associated with a spike in grain size, magnetic susceptibility, dry bulk density and loss-on-ignition (Figure 5.4).

Unit B (20 – 44 cm)

Unit B is the middle section of the sediment core and is distinctive with its five graded beds (E2 – E6). The unit has overall smaller changes in physical parameters compared to unit C, but (Figure 5.4) both magnetic sustainability and grain size are increasing towards the middle of the unit and then decrease again. The coarsest grain size measured is at E5 (Table 5.3) where large black grains were observed (Appendix B) and a gravel fragment of 2 cm length was observed at E3. Unit E4 has the maximum magnetic sustainability recorded at 13,6 ($\text{cgs} \times 10^{-6}$).

Unit A (1 – 19 cm)

The unit consists of the first half of the sediment core and figure 5.4 shows that the unit differs significantly from the underlying units B and C. Grain size and loss-on-ignition showing no distinctive trend compared to water content, dry bulk density and magnetic susceptibility (Figure 5.4) where the latter two have a decreasing trend throughout the unit. Water content

has an opposite trend of magnetic susceptibility and dry bulk density increases towards the core surface with the highest range of water content recorded (27,2 – 36,8%) of the units.

The unit consists of the upper half of the sediment core and figure 5.4 shows that the unit differs significantly from the underlying units B and C. Grain size and loss-on-ignition shows no distinctive trend compared to water content, dry bulk density and magnetic susceptibility (Figure 5.4) where the latter two have a decreasing trend throughout the unit. Water content has an opposite trend of magnetic susceptibility and dry bulk density increases towards the core surface with the highest range of water content recorded (27,2 – 36,8%) of the units.

Table 5.2: Physical parameters by units A, B and C with range of results and standard deviation (SD).

<i>Physical parameter</i>	<i>Section A</i>		<i>Section B</i>		<i>Section C</i>	
	Range	SD	Range	SD	Range	SD
<i>Grain Size (µm)</i>	3,1 – 12,6	2,35	4,5 – 30,9	6,24	4,0 – 52,3	14,35
<i>Magnetic Susceptibility (cgs x 10⁻⁶)</i>	8,8 – 11,1	0,69	11,0 – 13,6	0,74	8,4 – 12,0	1,30
<i>Dry Bulk Density (g/cm³)</i>	0,9 – 1,6	0,17	1,0 – 1,4	0,11	1,0 – 1,5	0,17
<i>Water content (%)</i>	27,2 – 36,8	2,21	25,4 – 31,1	1,48	22,3 – 34,8	4,17
<i>Loss-On-Ignition (%)</i>	4,4 – 5,5	0,22	4,1 – 5,7	0,41	3,7 – 8,4	1,59

Table 5.3: Physical parameters range in sedimentary units marked as graded beds.

<i>Graded bed</i>	<i>Grain Size (µm)</i>	<i>Magnetic Susceptibility (cgs x 10⁻⁶)</i>	<i>Dry Bulk Density (g/cm³)</i>	<i>Water content (%)</i>	<i>Loss-On-Ignition (%)</i>
<i>E6</i>	4,5 – 10,1	11 – 12,1	1,2 – 1,3	28,6 – 31,1	4,6 - 5,6
<i>E5</i>	5,1 – 30,9	12,7 – 13,1	1,3 – 1,4	28,0 – 28,6	4,4 - 4,6
<i>E4</i>	5,8 – 21,3	12,2 – 13,6	1,0 – 1,4	27,0 – 30,6	4,7 - 4,9
<i>E3</i>	6,2 – 20,0	13,0 – 13,4	1,0 – 1,2	27,1 – 29,9	4,5 - 5,7
<i>E2</i>	5,9 – 28,4	11,9 – 13,0	1,2 – 1,3	27,7 – 29,9	4,0 - 4,7
<i>E1</i>	4,0 – 52,3	8,4 – 11,9	1,4 – 1,5	22,3 – 27,3	4,0 - 8,4

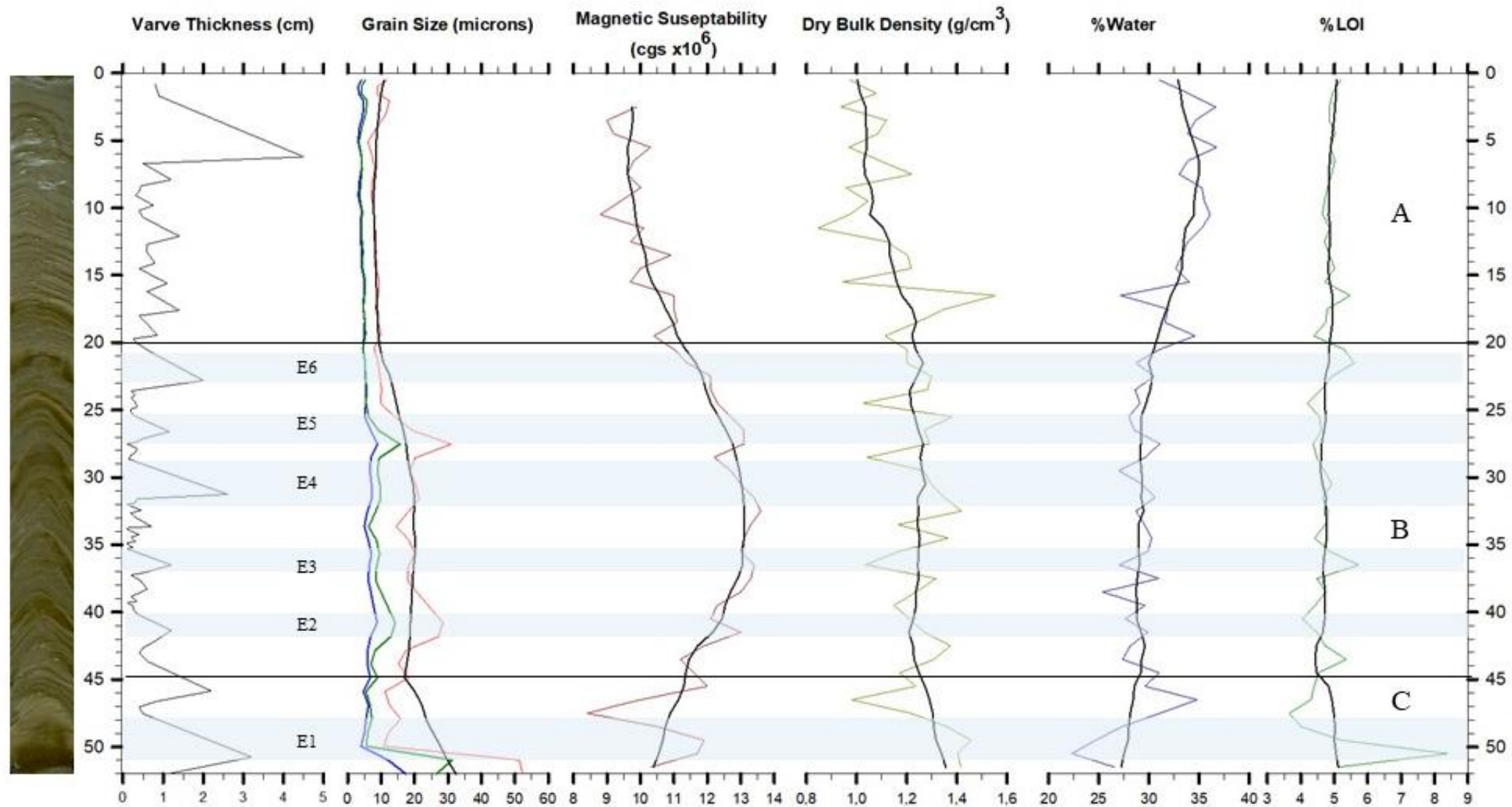


Figure 5.4: RBD image and varve thickness (cm) with physical parameters grain size (μm), magnetic susceptibility ($\text{cgs} \times 10^{-6}$), dry bulk density (g/cm^3), water content (%) and loss-on ignition (%). The trends of the sediment core are enhanced by 10-point average of the physical parameters with grain size in the 90th presentiel. And based on the trends of the sediment core divided in to units A, B and C.

5.4 GEOCHEMISTRY

The geochemical XRF analysis by ITRAX was done in the center of the sediment core and physical parameters were sampled off center. Hence, the depth between the physical and geochemical parameters do not exactly align in unit B. Following the previously described selection criteria of normalization (Chapter 4.3.6) the elements Potassium (K), Calcium (Ca), Manganese (Mn), Iron (Fe), Titanium (Ti) and Zirconium (Zr) (appendix E) were chosen to detect interruptions in the varve rhythmites by surge deposits that result from mass movement events. Descriptions of the elements are described under in unit C, B and A.

Unit C (45 – 52 cm)

Unit C shows distinct trend with increase in Potassium (0,07 – 0,14 kcps) and Iron (1,86 – 2,31 kcps) and a decrease in Calcium, Manganese, Titanium and Zirconium towards unit B (figure 5.5). The sharp increase in K and F in combination to the decrease in Ca, Mn, Ti and Zr occurs in E1.

Unit B (20 – 44 cm)

All event beds in the unit are indicated by decreasing levels of Potassium (figure 5.5), located approximately at 40 cm, 35 cm, 29cm, 25 cm and 21 cm depth. The decreasing levels of Potassium deviate from the stable base line seen through the unit. Calcium shows the opposite trend of Potassium. Iron decreases markedly at 29 cm and 40 cm. Both Titanium and Zirconium have a linear trend through the unit but is elevated at 40 cm, 29 cm and 21 cm.

Unit A (1 – 19 cm)

The unit is characterized by the smallest changes overall in the parameters (Table 5.4). Figure 5.5 shows Potassium increases but deviates from the trend towards the top of the sediment core. Calcium, Manganese, Iron and Titanium all have a decreasing trend through the unit. As Potassium, Manganese and Iron deviates from the trend towards the top of the sediment core. Zirconium is stable (Figure 5.5).

Table 5.4: XRF parameters by units A, B and C with standard deviation (SD).

<i>Element (kcps)</i>	<i>Section A</i>		<i>Section B</i>		<i>Section C</i>		<i>Total</i>	
	Range	SD	Range	SD	Range	SD	Range	SD
<i>Potassium (K)</i>	0,09 –	0,008	0,07 –	0,009	0,07 –	0,012	0,07 –	0,012
	0,14		0,12		0,12		0,14	
<i>Calcium (Ca)</i>	0,10 –	0,002	0,01 –	0,007	0,01 –	0,003	0,01 –	0,002
	0,02		0,02		0,02		0,02	
<i>Manganese (Mn)</i>	0,01 –	0,002	0,02 –	0,002	0,02 –	0,002	0,01 –	0,003
	0,02		0,03		0,03		0,03	
<i>Iron (Fe)</i>	1,86 –	0,050	1,92 –	0,052	1,9 –	0,075	1,86 –	0,070
	2,14		2,31		2,24		2,31	
<i>Titanium (Ti)</i>	0,06 –	0,004	0,07 –	0,004	0,05 –	0,007	0,05 –	0,005
	0,08		0,09		0,09		0,09	
<i>Zirconium (Zr)</i>	0,01 –	0,003	0,01 –	0,004	0,01 –	0,006	0,01 –	0,004
	0,02		0,04		0,04		0,04	

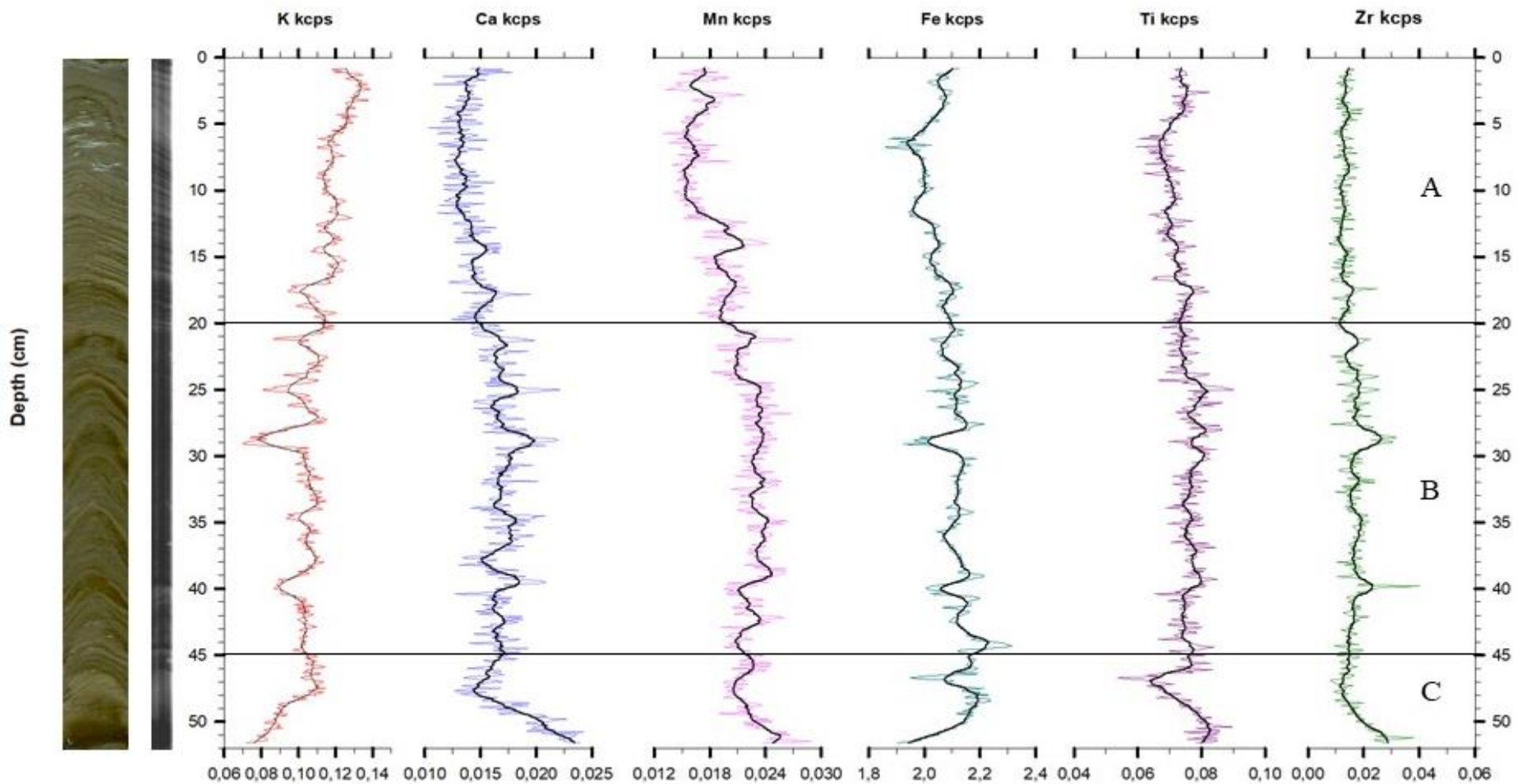


Figure 5.5: Elements potassium (K), calcium (Ca), manganese (Mn), iron (Fe), titanium (Ti) and zirconium (Zr) normalized to cps with trend by 10-point running average (Appendix E).

5.5 AGE DETERMINATION

For age determination the 2019 surface core were cross-correlated to a surface core from 2012 (Figure 5,6). The maximum of 3,220 Bq/kg $^{239+240}\text{Pu}$ was measured at approximately 34 cm depth in the 2012 surface core. By varve count the plutonium depth correlates to the 1963 lamina at 34,45 cm depth in the 2019 sediment core. Older marker beds of 1945 and 1957 correlate to marker beds in the 2012 sediment core. In contrast, the younger marker beds in the 2019 surface core do not correlate that well to the 2012 core and this is likely linked to an error in counting of the varves in the 2012 sediment core.

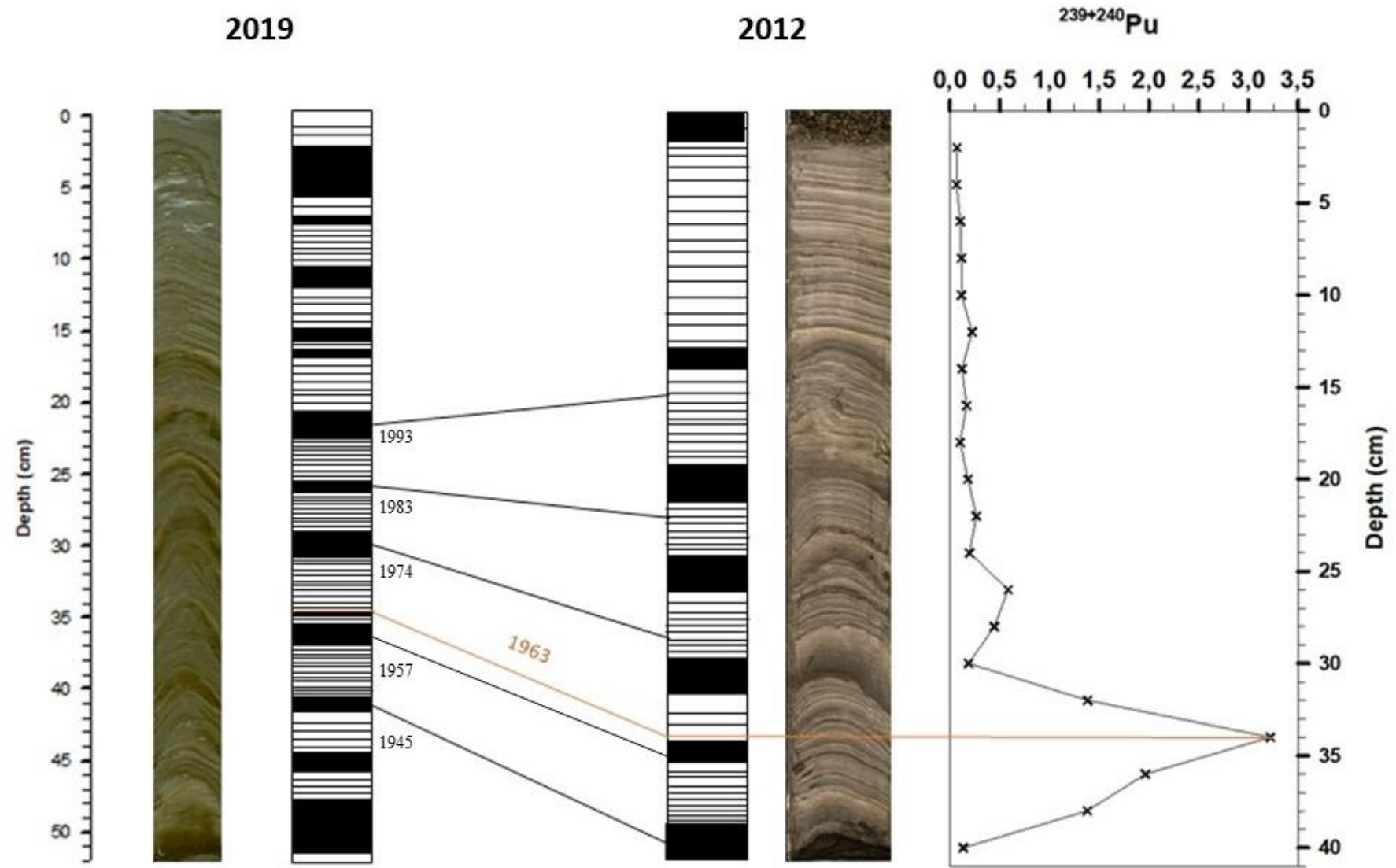


Figure 5.6: RGB image and stratigraphy of 2019 surface core (left) with line scan image and schematic stratigraphy of 2012 core (right). Cores were cross-correlated by varve count and plutonium ($^{239+240}\text{Pu}$) measurements from 2012 surface core.

CHAPTER 6: DISCUSSION

The main objective of this thesis has been to identify mass movement events in the laminated sediment record in Bødalsvatnet. Below mass movement events are identified and interpreted on a decadal scale, and finally, placed into a longer-term context of the late Holocene hydroclimate.

6.1 IDENTIFICATION OF MASS MOVEMENT EVENTS IN VARVED LAKE SEDIMENTS

6.1.1 VARVE CHRONOLOGY

Glaciolacustrine varve structures reflect the annual cycle of meltwater sediment deposition in Bødalsvatnet (Sturm, 1979). The varve count of these laminated lake sediments in the proglacial lake gives high resolution climatological, limnological, biological, and hydrological processes. To count the annually laminated sediments, thin sections were utilized, and varve count is dependent on the manual determination of varve boundaries. According to Ojala et al., (2012) the typical varve count has an estimated error estimation of $1 \pm 1 - 4\%$. Systematical errors in the varve count in the sediment of Bødalsvatnet can be attributed to changes in sedimentation rates and poor preservation of varve sections in the core (Zolitzckha, 2007). Systematic errors cannot be avoided and can also go undetected during the varve count and the following analysis; therefore, it is vital to cross-check the varve depth calculations with an independent varve dating method (Ojala et al., 2012; O`Sullivan, 1983). The study utilizes cross-correlation with a sediment core from 2012; however, there are errors associated with cross-correlation of sediment cores, e.g., varves can be falsely identified, or extra varves can be counted, varves can be missed in one or both cores. Additionally, varve structures can be complex, indistinct, and very thin varves and the inexperience of the operators sampling and measurement technique can be inconsistent (Ojala et al., 2012). As previously mentioned, cross-checking of the varved sediment sequence is essential to validate the dating of the varves, and this study utilized the independent dating method bomb test of Plutonium measurements which has a peak in 1963 (Cook et al., 2008) and therefore is an excellent dating method for the sediment in Bødalsvatnet. The varve count is taken directly from the lake surface sediment and

therfore the surface varve chronologies that can represent absolute calendar year scale, but errors associated with cross correlation of sediment cores is associated with the plutonium measurements being utilized on the 2012 sediment core and not the 2019 sediment core (Ojala et al., 2012). The correlation of the sediment cores is also made more difficult by the deformation of the sediment cores, especially in the 2019 surface core.

6.1.2 BACKGROUND SEDIMENTATION

Past environmental changes produced variation in sediment structure (Ojala et al., 2012) in the Bødalsvatnet sediment. The lake sediment consists of typical laminae characterized by a fining upward melt season sequence with a clay cap formed during winter when the lake is covered by ice, as described by Cook et al., (2008), Zolitschka (2007) and Sturm (1979). The sediment, for the most part, consists of silt and clay. Hence, the sediment is indicative of a classic description of clastic varves that, according to Sturm (1979) and Zolitschka (2007), and are typical of a cold glacigenic environment with lake ice cover during winter (Strum, 1979). The formation of the sediment is controlled by high seasonal variability in precipitation, temperature, and inflow from the catchment area (e.g., Paret et al., 2020; Kastner et al., 2010).

The changes in inflow to the lake during the melt season result in multi-laminae in the summer part of the varve that reflect meltwater runoff pulses from the glacier responding to the local climate signal (Kastner et al., 2010). Changes in inflow to the lake can also result from heavy precipitation events that can trigger sediment loaded streams due to snowmelt, meltwater from Bødalsbreen and the other unnamed glacier in the catchment area, or debris flows from the steep slope in the north of the lake. The interruption of varve sedimentation by strong meltwater pulses or mass flows causes a coarser intra-varve formation in the lake sediments.

In units, B and C, the sediment rhythmites (varve couplets of an average size of ca 0,52 cm thickness) are interrupted by surge deposits or abnormally thicker layers up to 3,2 cm thick that are overlain by a clay cap. Cook et al., (2008) point out that high energy transport is difficult to assess but Francus et al., (2008) indicate that such high energy deposits can be a result of turbid underflow that is a result of steam flow or high energy rainfall events.

6.1.3 MASS MOVEMENT EVENTS

Rain events and elevated streamflow events that result in turbid underflow are both dependent on metrological and lake sedimentation conditions (Cook et al., 2008). Rainfall events in Svalbard are known to trigger mass movement events, e.g., landslides, mudflows, debris flows and avalanches (Larsson, 1982). These gravity driven mass flows that causes density currents in lakes that have a higher density than the ambient lake water resulting in an underflow or hyperpycnal flow that penetrates through a lake's stratification and produces turbidites. The turbidites have a thick homogeneous coarser and erosive basal sub-layer and a fining upward sequence and they occur six times in the studied sediments. The deposits vary in size from 1,2 to 3,2 cm with a general thickness of 1,9 cm compared to a varve couplet average size of 0,52 cm. Thin sections were used to measure varve thickness distribution, and objectively identified turbidities were distinguished from the background varve sedimentation (Praet et al., 2020).

Physical analysis of the sediments (bulk density, grain size and magnetic susceptibility and the modern scanning technique of ITRAX micro x-ray fluorescence (XRF) geochemical analysis were utilized to substantially increase the resolution of the sediment record. ITRAX XRF is a valuable tool for identifying turbidites (Rothwell, 2006), and in this study, the elements K, Ca, Mn, Fe, Ti, and Zr are used for identifying the coarser mass flow deposits. XRF gives semi-quantitative results (Rothwell, 2006), and errors may be related to changes in porosity, compaction, weak peaks in the X-ray spectra related to grain size or shape and low counts related to cracks in the sediment (Rothwell, 2006). There are also errors associated with elemental profiles from ITRAX due to the placement of subsamples and resolution but also because the technique is sensitive to the sediment LOI, WC, DBD and grain size (Tjallingii et al., 2007; Rothwell et al., 2006). The element Mn has the atomic number of 25; therefore, it is thought that Mn is not influenced by physical changes. Heavier elements such as K, Ca, Ti, Fe, and Zr do not react to the sediment water content and organic material the same way as lighter elements such as Aluminum (Tjallingii et al., 2007) which was excluded from this study due to high signal to noise ratio.

In the sediment, the event beds were identified in the thin sections, and by a general grain size distribution (Cook et al., 2008). However, due to the sampling resolution of the physical parameters, they are not measured for each individual varve. However, grain size variability is

well reflected in XRF profiles, seen in changes especially in the elements Zr and Ti, and are enhanced in turbidite bases since Zr is associated with resistant minerals which are carried with fine sand and very coarser silt (Vrasskog et al., 2011; Cuven et al., 2010; Rothwell, 2006). Simultaneous increases in Ti and Ca records allochthonous input (Kastner et al., 2010) where Ca by itself, according to Evans et al., (2019) is associated with autochthonous precipitation of calcium carbonate or an allochthonous source. Increases in Mn is often associated with spring sedimentation and oxygenation (Naeer et al., 2013). Fe/Ti, can indicate clay-rich units and corresponds to clay in structures marked as turbidities (Cuven et al., 2010; Rothwell, 2006) where Fe/Ti indicates the clay on top of the turbidite in the same way K/Ti does (Cuven et al., 2010). The indicators of clay-size fractions are seen in all the event beds. In general, K can also be associated with fine particles and higher water content enhanced in turbidite mud (Rothwell et al., 2006).

Ti can also indicate clay minerals or clay size particles, in relationship with iron (Fe/Ti), can indicate clay-rich units and corresponds to clay in structures marked as turbidites (Cuven et al., 2010; Rothwell, 2006) where Fe/Ti indicates the clay on top of the turbidite in the same way K/Ti does (Cuven et al., 2010). The indicators of clay-size fractions are seen in all the event beds. In general, K can also be associated with higher water content enhanced in turbidite mud (Rothwell, 2006).

6.2 INTERPRETATION OF MASS MOVEMENT EVENTS

The turbidites are linked to precipitation events and therefore compared to weather data from the nearest weather station at LYR. Precipitation events or rainfall events in Longyearbyen are associated with documented mass movement events (e.g., Christiansen et al., 2016; Humlum et al., 2016; Larsson, 1982). Before the mass movement event of 1972 described in Larsson (1982), reports of the mass movement in the area was scarce. The recorded mass movement events in the surrounding area of Longyearbyen are not associated with prolonged precipitation. Instead Larsson (1982) specified that the mass movements events are triggered by intense rainfall with an hourly intensity of 2,5 mm. The recorded events in the sediment can be correlated to the weather record and, one can use similarities with historical counterparts to infer environmental conditions (Praet et al., 2020) during the pre-instrumental events in the sediment record.

In this study, an annually resolved reconstruction of the mass movement events in Bødalsvatnet was developed comparing the visual stratigraphy, physical parameters, and geochemical parameters to weather data from the nearest weather station at Svalbard Airport at Longyearbyen (LYR) (Figure 6.1, 6.3 and 6.6). The weather record also referred to as the Svalbard temperature series is reconstructed, or “homogenized” from measurements taken at the old weather station in Longyearbyen (including Advent Bay and the old Hospital) and smaller surrounding weather stations; Green Harbour and Barentsburg (Nordli et al., 2020; Nordli et al., 2014; Nordli et al., 1996). The old weather station 4 km from LYR started observations in 1916 and ended in 1977, but the location varied, and the observations were scarce with a long portion of the weather record missing. Temperature data in the figures are based upon a composite of measurements made at LYR from 1975. The series also used data from smaller local stations, and to ensure data comparability to the principal series, the local data was quality checked and homogenized before being adjusted (Nordli et al., 2020). In 2017 and 2018, old weather data (1916 – 1939) from the old weather station in Longyearbyen was found giving new insight to temperatures in this period, compared to old mean monthly temperature calculations (Nordli et al., 2020). The precipitation and temperature record from 1942 – 1944 during the second world war (WW2), is interrupted (Nordli et al., 1996). As pointed out by Nordli et al., (2020), even with the limitations of the weather data, the Svalbard temperature series is widely used in studies; e.g., Gjelten et al., (2016) and Isaksen et al., (2016)

6.2.1 AVALANCHE AND RAIN-ON-SNOW EVENTS

The 1957 turbidite (E3) contains coarser grain size, up to 2 mm gravel, which could have been transported on to the lake and frozen within the lake ice, thereafter rafted into a deeper part of Bødalsvatnet. Coarser particles of >1 mm is not common in the sediment and are not in the background sedimentation; therefore, the coarser particle is interpreted to be connected to a mass-wasting event (Vasskog et al., 2011; Nesje et al., 2007). Vasskog et al. (2011), note that avalanches are a common probable mechanism for delivering coarse-grained sediment in. During the spring, when the ice cover melts away, the debris will be rafted along the will be deposited when the ice melts away. If the lake ice is not present, there is a likelihood that the large particles will be deposited closer to the lakeshore. The presence of particles >1 mm can, point to a snow avalanche deposition, but the lack of >1 mm cannot in itself be evidence of the lack of avalanches (Vasskog et al., 2011). Hence gravel of 2 mm in length can indicate that the E3 mass movement is a result of an avalanche.

The possible avalanche event at E3 can be associated with a temperature above 0°C and whet precipitation of 1 mm or more on snow cover and is referred to as rain – on – snow event (ROS) (Wickström et al., 2019). ROS events in Svalbard are mostly associated with the months April and March, which are the driest months; hence a precipitation event can have a significant impact on the landscape or the snowpack (Wickström et al., 2019). ROS events cause an increase in permafrost temperatures, e.g., a recorded ROS event in Svalbard in January 2012 caused an increase in the permafrost temperature approximately up to 5 m and the event resulting in the occurrence of slush avalanches (Hansen et al., 2014). ROS events are related mostly related to south-west cyclones but also to southerly cyclones and south-westerly anticyclones (Wickström et al., 2019).

6.2.2 RAINSTORMS AND INTENSE PRECIPITATION

During 1993 two precipitation events occurred, one in March and one in November. The one in March is contributed to snow due to the cold temperature at approximately - 9°C (Norwegian Metrological Institute, 2020). But Dobler et al., (2019) recorded rainstorms that can be linked to the 1993 event and the 1983 event. Recorded rainstorms on the 2nd of March 1983 (E5), and the 30th of November 1993 (E6) both contributed to increased temperature and moist air associated with a south-westerly cyclone. Both rainstorms increased in temperature during the storm and had recorded precipitation of 13 mm and 11,8 mm during a 12-hour period respectively shown in figure 6.1A, and B (Norwegian Metrological Institute, 2020). E4 is not connected to a rainstorm by Dobler et al., (2019) but is contributed to an increase in precipitation on the 5th of March 1974 34mm in 12 hours (figure 6.1 C) with normal total precipitation for March being 24 mm (Norwegian Metrological Institute, 2020). But it is important to note that Wickström et al., (2019) pointed out that working with mean daily temperature does not guarantee rainfall and above freezing temperature occurring at the same time.

The precipitation record connected to event beds E5 (1983) and E6 (1993) likely occurred on either side of the summer season. Hence the impact of precipitation events has a different side indicates that it is plausible that intense precipitation events may have occurred in the spring and in the fall. An important factor to consider in the development of mass flows is the timing of the precipitation event in combination with the thickness of the permafrost active layer. If a precipitation event occurs during the spring, the debris flows are usually small because of the shallow depth of the permafrost active layer that is thawed, as illustrated in figure 6.2. But if a precipitation event occurs during fall as E6 does, where the active layer is thawed to a greater depth, the mass movement event can be more significant as was the case during the October rainstorm of 2016 (Christiansen et al., 2016; Humlum et al., 2016). The active layer in Longyearbyen usually starts freezing in September and October, and during the November 2016 rainstorm, the mass movement events were smaller than during the October rainstorm even though the November rainstorm had 46 mm precipitation and the October rainstorm had 18 mm (Humlum et al., 2016). None of the event beds (E4 to E6) contains dropstones, but as mentioned in chapter 6.2.1, this does not exclude a possible presence of an avalanche (Vasskog et al., 2011; Nesje et al., 2007).

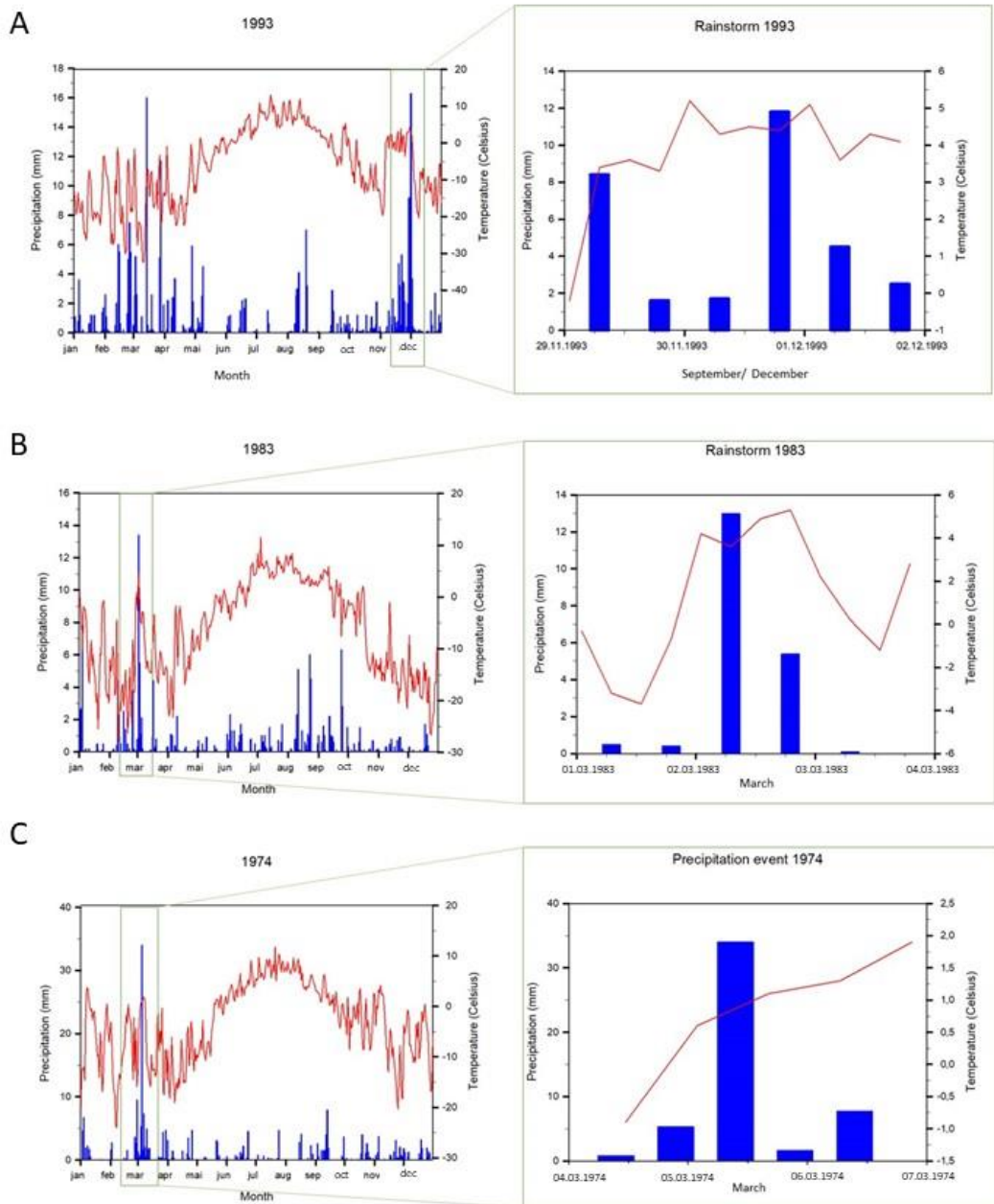


Figure 6.1: A: Yearly precipitation and temperature in 1993 with November rainstorm. B: Yearly precipitation and temperature in 1983 and March rainstorm. C: Yearly intense precipitation event (Norwegian Metrological Institute, 2020).

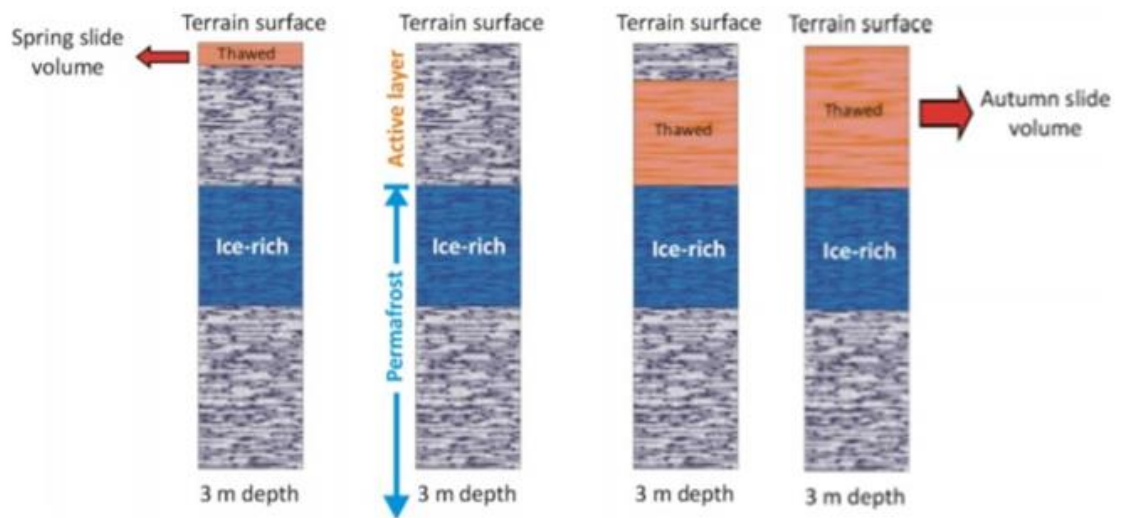


Figure 6.2: Permafrost depth in spring, summer, and the autumn was the active layer that has started to refreeze or is fully thawed (Modified from Humlum et al., 2016).

6.3 HYDROCLIMATIC INFLUENCE ON LAMINATED LAKE SEDIMENTS IN BØDALSVATNET

The recorded turbidites in Bødalsvatnet provide a record of extreme rainfall during parts of the 1900s at an annual scale. By correlating the sedimentary record to weather data from LYR, a change in precipitation is noted, and the period 1936 to 2018 is divided into four warm periods following the example of Nordli et al. (2020).

There are noted mass movement events in 1936, 1945, 1957, 1974, 1983, and 1993 that are linked to increases in precipitation. However, the correlation is somewhat limited by the available meteorological records, in that, precipitation intensity was not measured, and precipitation was only measured daily or twice in the hydrological day (7 am and 7 pm) (Metrological Institute, 2020). Hence in this study, mass movement events are correlated to increases in precipitation during the spring shoulder months March, April, and May (MAM) and after summer, September, October, and November (SON).

The series starts off with what Nordli et al., (2020) have indicated as a warm period at LYR wherein lies E1. The period is followed by the colder 1940s, which had a decreasing precipitation event with the exception of 1945, which had a notable increase in SON temperature (Norwegian Metrological Institute, 2020). The 1940s were followed by the warmer period of the 1950s, a period identified in figure 6.3 by the largest changes in SON precipitation in the series, giving a plausible explanation of the accorded avalanche in E3. The warm period of the 1950s is followed by the cold period of the 1960s, a decrease in with 1960 having no recorded ROS events (Nordli et al., 2020). This lone period stands out as the only period from the 1930s to the 1990s without a recorded mass movement event. Since that cold period, precipitation has had a linear increase in precipitation by 2 %, whereas from the previous period of 1946 to 1965 had an increase in precipitation by 1% (Hanssen – Bauer et al., 2019). The cold period of the 1960s is followed by the warmer 1970s with a peak in MAM precipitation and hereby E4. E4 is linked to a March precipitation event and correlates to a maximum measured MAM precipitation and large amplitudes in annual precipitation (Norwegian Metrological Institute, 2020). The warm period is followed by a colder period of the 1980s to 1999 (Nordli et al., 2020). Within this period, mean annual temperature increased steadily while MAM precipitation fluctuates through the period, and E5 is connected to the first of three peaks in MAM precipitation. E5 to E4 and E3 to increase in precipitation during spring. In comparison, SON precipitation is stable through the 1980 and 1990s but increases towards the millennia. E6 is connected to an event during SON; the increase in MAM is associated with snow with recorded sub-zero temperatures (Norwegian Metrological Institute, 2020).

The colder period ends in 1999 with a recorded decadal shift in annual temperature that is related to the increase of warm Atlantic water in the Svalbard archipelago (Nordli et al., 2020). An increase in precipitation coincides with the decadal shift in winter temperature responded to the increase in Atlantic water noted by Nordli et al., (2020). Due to the increase in overall temperature and precipitation, three times more ROS events have been recorded during the 21st century (Hanssen-Bauer et al., 2019; Isaksen et al., 2007; Hansen et al., 2014). With a predicted increase in slush avalanches (Hanssen-Bauer et al., 2019) the study expected to see an elevated frequency in mass movement events during the 21st century. And within the 2019 sediment cores unit A. This study has not been able to distinguish between the background sedimentation and possible mass movement events due to the deformation in the uppermost part of the sediment core.

The colder period ends in 1999 with a recorded decadal shift in annual temperature that is of the related to warm Atlantic water in the Svalbard archipelago (Nordli et al., 2020). An increase in precipitation coincides with the decadal shift in winter temperature responded to the increase in Atlantic water noted by Nordli et al., (2020). Due to the increase in overall temperature and precipitation three times more ROS events have been recorded during the 21st century, and within (Hanssen-Bauer et al., 2019; Isaksen et al., 2007; Hansen et al., 2014). With a predicted increase in slush avalanches (Hanssen-Bauer et al., 2019) the study expected to see an elevated frequency in mass movement events during the 21st century and the 2019 sediment cores unit A. This study has not been able to distinguish between the background sedimentation and possible mass movement events due to the deformation in the uppermost part of the sediment core.

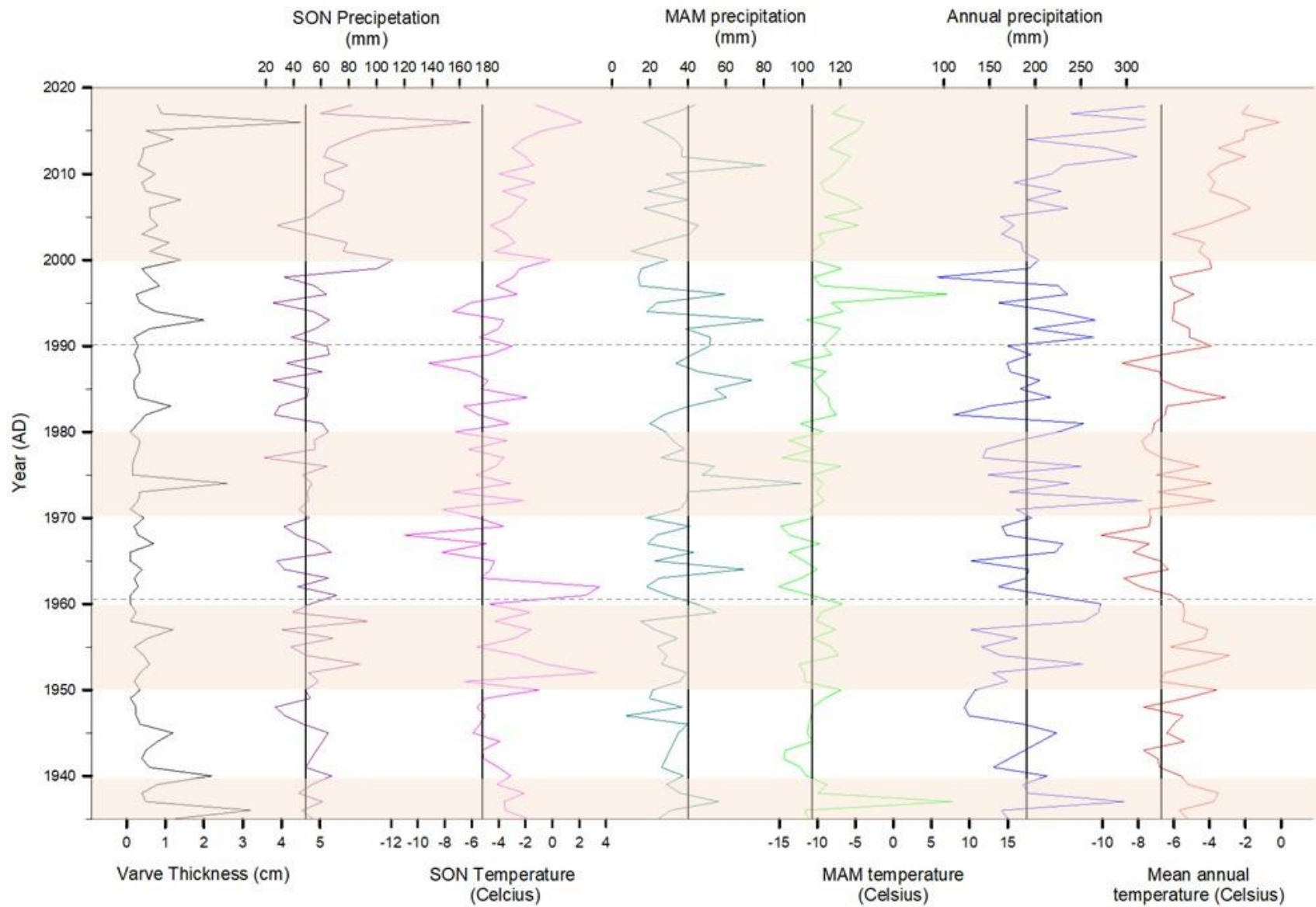


Figure 6.3: Warmer temperature periods from 1936 to 2019 with varve thickness in the surface core from 2019, September, October, November (SON) and March, April, May (MAM) precipitation and temperature, annual precipitation, and mean annual temperature with the normal period (1961 – 1990) marked in black dotted and straight lines (Norwegian Metrological Institute, 2020).

Though the resolution of the 2019 sediment core is not used for identification and interpretation of the most recent mass movement events(e.g. the October 2016 event) , the sediment core can be cross-correlated and compared to unpublished data from a longer percussion core from 2012 (Retelle, 2013) taken in close proximity to the 2019 core (figure 6.4).

At the end of LIA, a temperature increase occurred with SON precipitation increasing but is interrupted by the cold period of the 1940s (Norwegian Meteorological Institute, 2020; Nordli et al., 2020). In contrast, the MAM precipitation thus not experience the same increase and is, in general, stable beneath the boundary of the normal period precipitation (Norwegian Metrological Institute, 2020). The warm regime is interrupted by the second cold regime is from 1962 through to 1998, the regime is 1°C warmer than the first cold regime (Nordli et al., 2020). The cold period is relieved by the present warm regime that is 1,7°C warmer than the first (Nordli et al., 2020). With increasing SON precipitation and temperature in contrast to MAM temperature that has a small increase. The change in mean annual temperature, annual precipitation and in SON indicates a current change in the climate as multipole climatic models have implicated (Hanssen-Bauer et al., 2019), e.g., 37 CMIP5 (Bintanja & Andry, 2017) and Arctic CORDEX results (Hanssen-Bauer et al., 2019). The climate models indicate an increase in temperature and precipitation and that more of the future precipitation is going to fall as rainfall and not snow (Hanssen-Bauer et al., 2019). With an increase in the occurrence of ROS events (Hansen et al., 2014) that are related to a south-westerly cyclone (Wicstrøm et al., 2019). The same weather pattern that Dobler et al., (2017) connected to 13 rainstorms over Longyearbyen and the same weather pattern that is associated with the precipitation events that have resulted in mass movement events E4, E5 and E6.

6.4 CORRELATION WITH SURFACE CORE AND A PRECISION CORE AND IMPLICATION IN HYDROCLIMATE

Though the resolution of the 2019 sediment core is not used for identification and interpretation of mass movement events in the 21st century, the sediment core can be cross-correlated and compared to unpublished data from a longer percussion core from 2012 (Retelle et al., 2013) taken in close proximity to the 2019 core (figure 6.4).

A composite varve chronology was constructed by overlapping the long core with the surface core from 2012 (mentioned in chapter 5.5). Marker beds were identified and correlated to the surface core marker beds and plutonium ($^{239+240}\text{Pu}$) measurements (Ketterer et al., 2004) with the aim of distinguishing between intra—annual deposits and thinner varve couplets. As a result, a varve and turbidite record from 1844 to 2011 was established (figure 6.5). Based on lamination thickness in the sediment core, the record can be divided into three sections; 1844 – 1920, 1920 – 1990 and 1990 – 2011.

In the first half of the sediment core (1844 – 1920) has the varve couplets have an average thickness of 0,9 cm. The second half (1920 – 1990) is characterized by thicker layers with coarser fining upward beds occurring within a background sediment of thinner varve couplets with an average thickness of 0,35 cm. The upper most half of the sediment core (1990 – 2011) varve thickness increases to between 0,5 cm and 0,8 cm (Retelle, Dowey & Dulin, 2013).

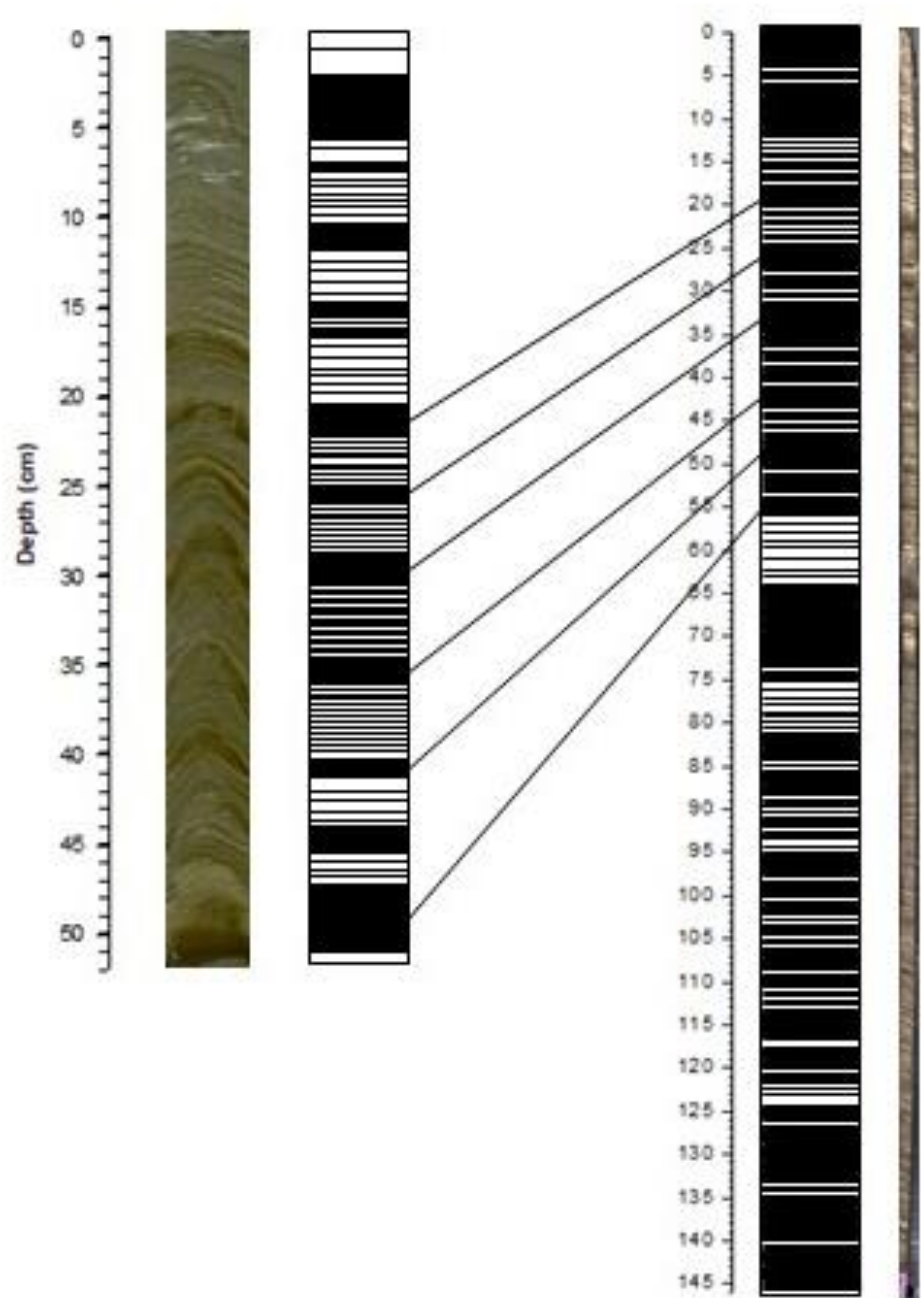


Figure 6.4: Cross-correlation by varve thickness between the 2019 surface core and the 2012 long core.

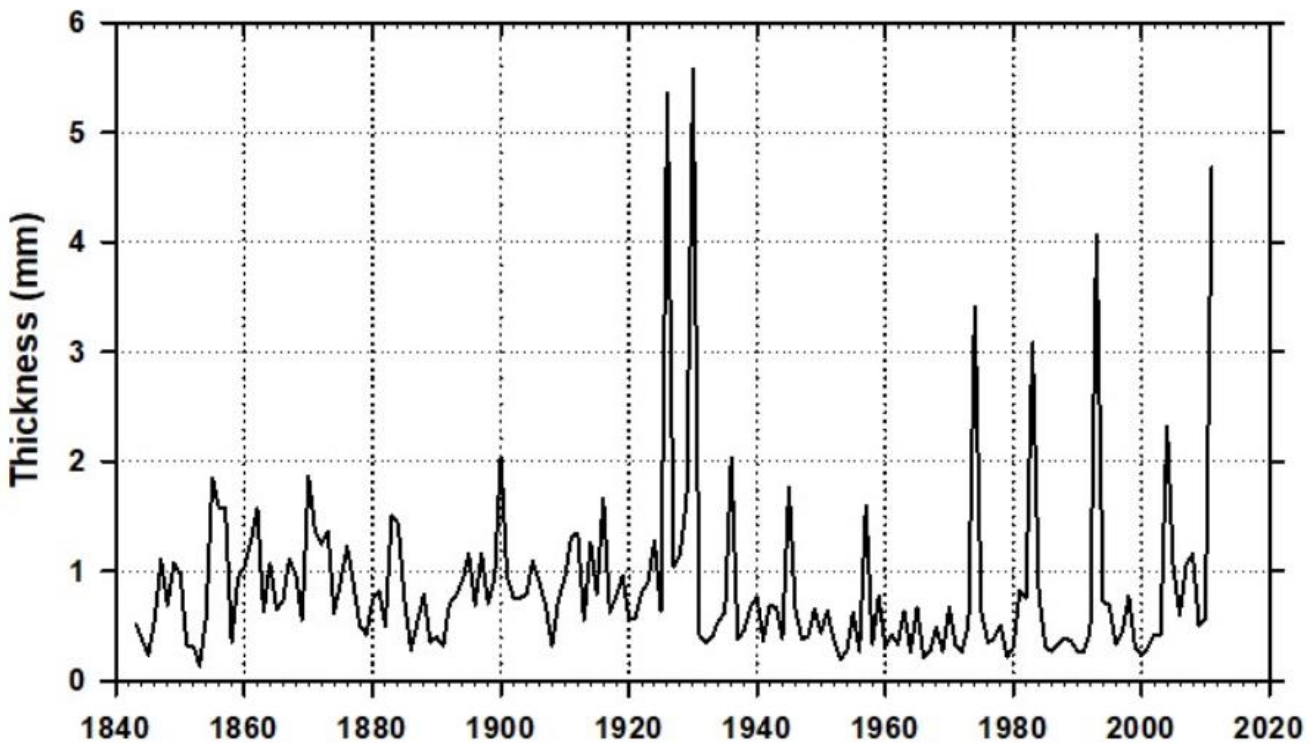


Figure 6.5: Lamination thickness from 2012 longer core, from Bødalsvatnet. (Retelle, Dowey & Dulin, 2013).

The composite sediment core of 2012 starts in a cold period, the LIA. During this period the temperature was gradually increasing (Figure 6.6). But the period was still cold and the maximum extent of Bødalsbreen was likely at or near its maximum extent (D'Andrea et al., 2012) and LIA superseded by a warmer temperature regime starting in 1930 (Nordli et al., 2020). But the period was still cold and Bødalsbreen's maximum extent is thought to have been in 1936 (D'Andrea et al., 2012; Retelle, Dowey & Dulin, 2013). The glacier maximum of Bødalsbreen is related to low summer temperature and increased winter precipitation led on by changes in NAO. The temperature increase was gradual through to the 1890s where it accelerated (D'Andrea et al., 2012). The LIA superseded by a warmer temperature regime starting in 1930 (Nordli et al., 2020). During this accelerated temperature increase turbidites are observed in both the 2012 and the 2019 sediment cores (Figure 6.6) where the turbidites interrupt the thinner varve couplets (D'Andrea et al., 2012). The turbidites are interpreted to be deposited from increases in rainfall events, and surge deposits related to increased melting, episodic slumps or avalanches related to a warming of the permafrost active layer (Retelle, Dowey & Dulin, 2013).

Following the end of the LIA, a temperature increase occurred with SON precipitation increasing but was interrupted by the cold period of the 1940s (Norwegian Meteorological Institute, 2020; Nordli et al., 2020). In contrast, the MAM precipitation thus not experience the same increase and is, in general, stable beneath the boundary of the normal period precipitation (Norwegian Metrological Institute, 2020). During the sediment cores time span the climate undergone changes and is identified by Nordli et al., (2020) as two cold regimes 1899 – 1929 and 1962 – 1998) and two warmer regimes (1930 – 1961 and 1999 – 2018). Where the second cold regime was 1 °C warmer than the first and the current warm regime is 1,7°C warmer than the first. With increasing SON precipitation and temperature in contrast to MAM temperature that has a small increase. The change in mean annual temperature, annual precipitation and in SON indicates a current change in the climate as multipole climatic models have implicated (Hanssen-Bauer et al., 2019), e.g., 37 CMIP5 (Bintanja & Andry, 2017) and Arctic CORDEX results (Hanssen-Bauer et al., 2019). The climate models indicate an increase in temperature and precipitation and that more of the future precipitation is going to fall as rainfall and not snow (Hanssen-Bauer et al., 2019). With an increase in the occurrence of ROS events (Hansen et al., 2014) that are related to a south-westerly cyclone (Wickström et al., 2019). The same weather pattern that Dobler et al., (2017) connected to 13 rainstorms over Longyearbyen and the same weather pattern that is associated with the precipitation events that have resulted in mass movement events E4, E5 and E6. The current increase in temperature and precipitation events is linked to a positive NAO and increase in warm Atlantic water and laminae interrupted by thicker turbidites, the same as the end of LIA and the associated regime shift.

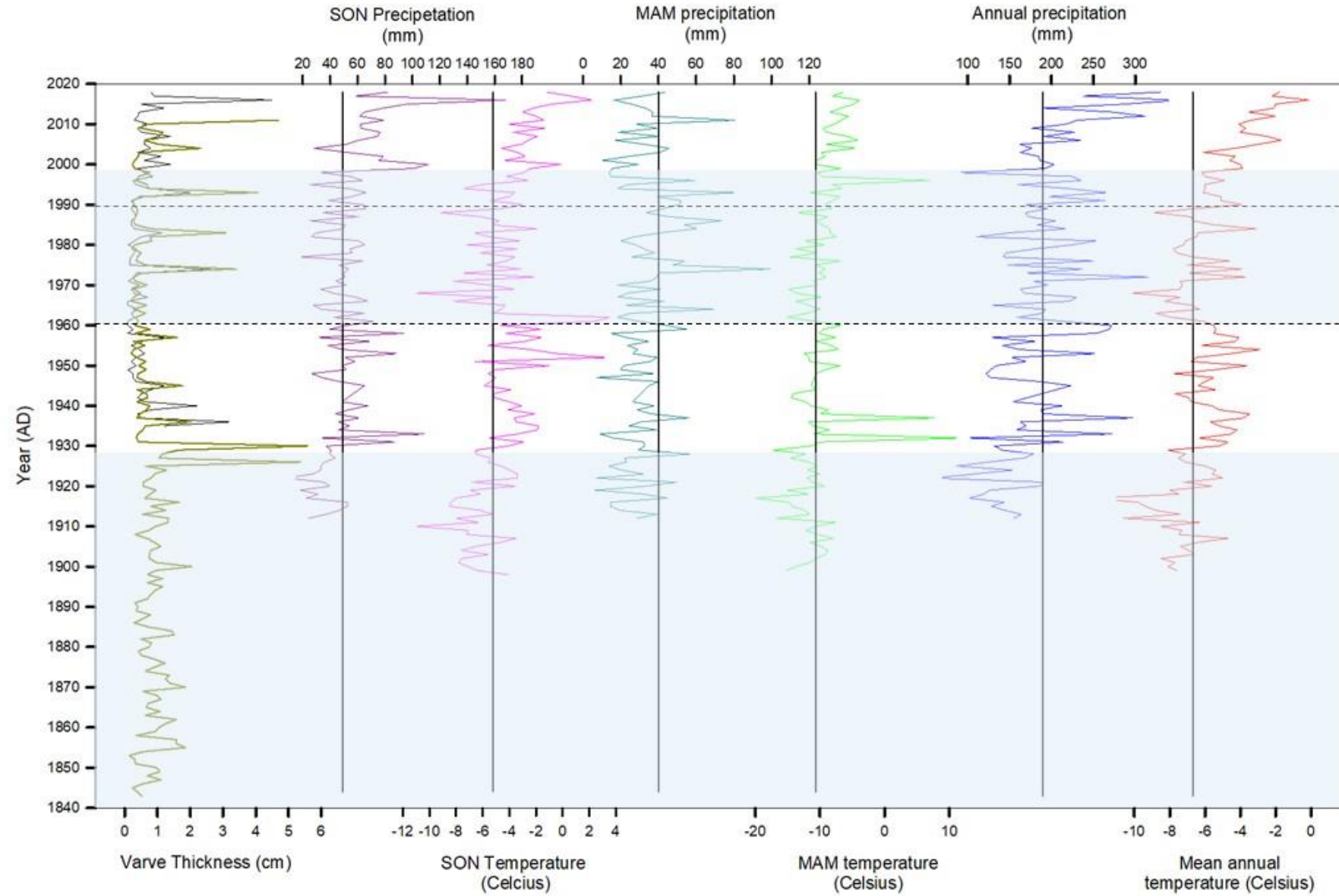


Figure 6.6: Colder temperature regimes according to Nordli et al., (2020) from 1840 to 2018 with varve thickness in surface core from 2019, September, October, November (SON) and March, April, May (MAM) precipitation and temperature, annual precipitation and mean annual temperature with normal period (1961 – 1990) marked in black dotted and strait line (Norwegian Metrological Institute, 2020).

CHAPTER 7: CONCLUSIONS

By identification of mass movement events through varve count, physical- and geochemical parameters and interpretation of annual laminated sediment in Bødalsvatnet, mass movement events been connected to wet precipitation events and shifts in the precipitation pattern since the end of the Little Ice Age (LIA). The following results have been concluded:

1. Mass movement events are dated to 1936, 1945, 1957, 1974, 1983 and 1993.
 - a. The 1957 mass movement (E3) event is likely related to a snow avalanche.
 - b. E4 is related to an intense precipitation event with measured 34 mm precipitation during a 12 – hour period.
 - c. E5 is related to the rain storm the 2nd of March 1983 that had a measured precipitation of 13 mm within a 12-hour period.
 - d. E6 is related to the rain storm of 30th of November 1993 that had a measured precipitation of 11,8 mm within a 12 – hour period.
2. The paleoclimate described indicates an increase in laminae size caused by a change in temperature and precipitation during the end of LIA and points in the direction of a current change in the hydroclimate that needs further investigation.

7.1 FURTHER STUDIES

The analysis of the 2019 sediment core has allowed for the interpretation off mass movement events as relating to rainfall events and rainstorms for identifying a new hydrological and reconstruct the long-term history of rainfall related mass movement event we recommend to collect a new short sediment core from Bødalsvatnet. And use the same multiproxy analysis as in this study to identify possible mass movement events resulting from the thought hydrological shift in the 21th century. Thereafter connect the result form the multiproxy analysis and interpretation to the longer varved sedimentary record from the other location for the project, Kapp Linne.

REFERENCES

- Arnaud, F., Lignier, V., Revel, M., Desmet, M., Beck, C., Pourchet, M., Charlet, F., Trentesaux, A. and Tribouillard, N., 2002. Flood and earthquake disturbance of ^{210}Pb geochronology (Lake Anterne, NW Alps). *Terra Nova*, 14(4), pp.225-232.
- Bakke, J., Lie, Ø., Heegaard, E., Dokken, T., Haug, G.H., Birks, H.H., Dulski, P. and Nilsen, T., 2009, April. Rapid oceanic and atmospheric changes at the end of the Younger Dryas cold period. In *EGU General Assembly Conference Abstracts* (Vol. 11, p. 14016).
- Bakke, J., Lie, Ø., Nesje, A., Dahl, S.O. and Paasche, Ø., 2005. Utilizing physical sediment variability in glacier-fed lakes for continuous glacier reconstructions during the Holocene, northern Folgefonna, western Norway. *The Holocene*, 15(2), pp.161-176. Available at: <https://pdfs.semanticscholar.org/14ab/7687a1ac13b6a65e982bde746240b8ea5e01.pdf> (Accessed: 24.12.2020)
- Bintanja, R. and Andry, O., 2017. Towards a rain-dominated Arctic. *Nature Climate Change*, 7(4), pp.263-267.
- Boike, J., 2012. SPARC and disappearing permafrost* a story from Bayelva in Svalbard. Accessed on the internet at <http://ssf.npolar.no/pages/news318.htm> on, 1.
- Bradley, R.S., 1999. *Paleoclimatology: reconstructing climates of the Quaternary*. Elsevier. Available at: https://crudata.uea.ac.uk/cru/people/briffa/bradley1999_chapter10.pdf (Accessed: 04.02.2020).
- Burn, C.R. and Zhang, Y., 2009. Permafrost and climate change at Herschel Island (Qikiqtaruk), Yukon Territory, Canada. *Journal of Geophysical Research: Earth Surface*, 114(F2). Available at: <https://agupubs.onlinelibrary.wiley.com/doi/pdf/10.1029/2008JF001087> (Accessed: 20.10.2019).
- Carmack, E.C., Gray, C.B., Pharo, C.H. and Daley, R.J., 1979. Importance of lake-river interaction on seasonal patterns in the general circulation of Kamloops Lake, British Columbia. *Limnology and Oceanography*, 24(4), pp.634-644. Available at: <https://aslopubs.onlinelibrary.wiley.com/doi/pdf/10.4319/lo.1979.24.4.0634> (Accessed: 5.04.2020).
- Christiansen, H.H., Etzelmüller, B., Isaksen, K., Juliussen, H., Farbrot, H., Humlum, O., Johansson, M., Ingeman-Nielsen, T., Kristensen, L., Hjort, J. and Holmlund, P., 2010. The thermal state of permafrost in the nordic area during the international polar year 2007–2009. *Permafrost and Periglacial Processes*, 21(2), pp.156-181. Available at: <https://onlinelibrary.wiley.com/doi/pdf/10.1002/ppp.687> (Accessed: 20.10.2019).
- Christiansen, H. H., Farnsworth, W., Gilbert, G., Hancock, H., Humlum, O., O'Neill, B., Prokop, A., Strand, S. (2016) Report on the 14-15 October 2016 mass movement event in the Longyearbyen area. The University Centre in Svalbard, UNIS, Arctic Geology Department, vers. 2 from 24 October 2016
- Christiansen, H.H., Humlum, O. and Eckerstorfer, M., 2013. Central Svalbard 2000–2011 meteorological dynamics and periglacial landscape response. *Arctic, antarctic, and alpine research*, 45(1), pp.6-18. Available at: <https://www.tandfonline.com/doi/pdf/10.1657/1938-4246-45.16> (Accessed: 21.03.2020).
- Chutko, K.J. and Lamoureux, S.F., 2008. Identification of coherent links between interannual sedimentary structures and daily meteorological observations in Arctic proglacial lacustrine varves: potentials and limitations. *Canadian Journal of Earth Sciences*, 45(1), pp.1-13.
- Cook, T.L., Bradley, R.S., Stoner, J.S. and Francus, P., 2009. Five thousand years of sediment transfer in a high arctic watershed recorded in annually laminated sediments from Lower Murray Lake, Ellesmere Island, Nunavut, Canada. *Journal of Paleolimnology*, 41(1), p.77.
- Croudace, I.W., Rindby, A. and Rothwell, R.G., 2006. ITRAX: description and evaluation of a new multi-function X-ray core scanner. *Geological Society, London, Special Publications*, 267(1), pp.51-63.

Cuven, S., Francus, P., Crémer, J.F. and Bérubé, F., 2015. Optimization of Itrax core scanner protocols for the micro X-ray fluorescence analysis of finely laminated sediment: A case study of lacustrine varved sediment from the high arctic. In *Micro-XRF Studies of Sediment Cores* (pp. 279-303). Springer, Dordrecht. Available at: https://www.researchgate.net/profile/Pierre_Francus/publication/299848396_Optimization_of_Itrax_Core_Scaner_Proocols_for_the_Micro_X-Ray_Fluorescence_Analysis_of_Finely_Laminated_Sediment_A_Case_Study_of_Lacustrine_Varved_Sediment_from_the_High_Arctic/links/575094c508ae1c34b39c2ce0/Optimization-of-Itrax-Core-Scanner-Protocols-for-the-Micro-X-Ray-Fluorescence-Analysis-of-Finely-Laminated-Sediment-A-Case-Study-of-Lacustrine-Varved-Sediment-from-the-High-Arctic.pdf (Accessed: 04.04.2020).

Cuven, S., Francus, P. and Lamoureux, S.F., 2010. Estimation of grain size variability with micro X-ray fluorescence in laminated lacustrine sediments, Cape Bounty, Canadian High Arctic. *Journal of Paleolimnology*, 44(3), pp.803-817. Available at: https://www.researchgate.net/profile/Stephanie_Cuven/publication/259481917_Cuven-al-2010/links/0c96052c1c57a38450000000.pdf (Accessed: 06.03.2020).

Dallmann, W.K., 2015. *Geoscience atlas of Svalbard*. Norsk polarinstitutt.

Dallmann, W.K., (ed) 1999. *Lithostratigraphic lexicon of Svalbard*. Norwegian Polar Institute. Available at: <http://www.nhm2.uio.no/norges/litho/svalbard/adven.htm> (Accessed: 14.07.2020).

D'Andrea, W.J., Vaillencourt, D.A., Balascio, N.L., Werner, A., Roof, S.R., Retelle, M. and Bradley, R.S., 2012. Mild Little Ice Age and unprecedented recent warmth in an 1800 year lake sediment record from Svalbard. *Geology*, 40(11), pp.1007-1010. Available at: https://www.ideo.columbia.edu/~dandrea/index/Publications_files/D'Andrea%20et%20al%202012.pdf (Accessed 15.03.2020).

Dearing, J.A., 1994. *Environmental magnetic susceptibility: using the Bartington MS2 system*. Chi Pub..

Dearing, J.A., Dann, R.J.L., Hay, K., Lees, J.A., Loveland, P.J., Maher, B.A. and O'grady, K., 1996. Frequency-dependent susceptibility measurements of environmental materials. *Geophysical Journal International*, 124(1), pp.228-240.

De Wet, G.A., 2013. Holocene Paleo-environmental Variability Reconstructed from a Lake Sediment Record from Southeast Greenland. Available at: <https://scholarworks.umass.edu/cgi/viewcontent.cgi?article=2192&context=theses> (Accessed: 08.07.2020).

Dickson, R.R., Osborn, T.J., Hurrell, J.W., Meincke, J., Blindheim, J., Adlandsvik, B., Vinje, T., Alekseev, G. and Maslowski, W., 2000. The Arctic ocean response to the North Atlantic oscillation. *Journal of Climate*, 13(15), pp.2671-2696. Available at: <https://journals.ametsoc.org/jcli/article/13/15/2671/105284> (Accessed : 14.02.2020).

Dobler, A., Førland, E.J. and Isaksen, K., 2019. Present and future heavy rainfall statistics for Svalbard-Background report for Climate in Svalbard 2100.

Dowey, C.W. and Retelle, M.J., 2013. 600 Years of Late Holocene Climate Variability Inferred from a Varved Proglacial Sediment Record Linnévatnet, Svalbard, Norway.

Eckerstorfer, M. and Christiansen, H.H., 2012. Meteorology, topography and snowpack conditions causing two extreme mid-winter slush and wet slab avalanche periods in High Arctic Maritime Svalbard. *Permafrost and Periglacial Processes*, 23(1), pp.15-25. Available at: https://d1wqxts1xzle7.cloudfront.net/45316594/Meteorology_Topography_and_Snowpack_Cond20160503-53089-ellyja.pdf?1462292203=&response-content-disposition=inline%3B+filename%3DMeteorology_Topography_and_Snowpack_Cond.pdf&Expires=1594734601&Signature=T6AYpDpBsPRcauf6PwXx9cUfYYRRnYcSq2o6xdA8TOWUUPoAADykzds1mnDupFFPk~FzI8p2uIIgPGSh9Fa82pcM6-LK6m0iLnHzpYOyAug-bJaRpc3l26ie2-W-s60iD602FGgiyXv2dV~F1ugdg3IGYqfyM06cB~KCPOQu~EJNvkjW9Dz41avtifoIS5xDR4Bj0BqbJicqMifIdVce1NKWRiR89Y3ERAU9oOImk2i81fpAD7TmgdXZOTEyiC4M9KwNozKjcxNXzL3D0eQSOerHd5ekYzBRd61dIsC-K6KXnHM4ULcKqphbS2C89LF-ZnejPE42vLCGsBg2k8sYg_&Key-Pair-Id=APKAJLOHF5GGSLRBV4ZA (Accessed: 12.05.2020).

Eckerstorfer, Markus, and Hanne H. Christiansen. "The "High Arctic maritime snow climate" in central Svalbard." *Arctic, Antarctic, and Alpine Research* 43, no. 1 (2011): 11-21. Available at: <https://www.tandfonline.com/doi/pdf/10.1657/1938-4246-43.1.11> (Accessed:04.11.2020).

Evans, G., Augustinus, P., Gadd, P., Zawadzki, A. and Ditchfield, A., 2019. A multi-proxy μ -XRF inferred lake sediment record of environmental change spanning the last ca. 2230 years from Lake Kanono, Northland, New Zealand. *Quaternary Science Reviews*, 225, p.106000.

Evans, M. and Heller, F., 2003. *Environmental magnetism: principles and applications of enviromagnetics*. Elsevier.

Farnsworth, W.R., Ingólfsson, Ó., Retelle, M., Allaart, L., Håkansson, L.M. and Schomacker, A., 2018. Svalbard glaciers re-advanced during the Pleistocene–Holocene transition. *Boreas*, 47(4), pp.1022-1032.

French, M.H. 2007. The Periglacial Environment: Third Edition: Wiley & Sons. Pp. 458

Førland, E.J. and Hanssen-Bauer, I., 2000. Increased precipitation in the Norwegian Arctic: true or false?. *Climatic change*, 46(4), pp.485-509. Available at: https://www.researchgate.net/profile/Inger_Hanssen-Bauer/publication/226099788_Increased_Precipitation_in_the_Norwegian_Arctic_True_or_False/links/0a85e534252b302f3d000000/Increased-Precipitation-in-the-Norwegian-Arctic-True-or-False.pdf (Accessed:15.01.2020).

Førland, E.J., Hanssen-Bauer, I. and Nordli, P.Ø., 1997. Climate statistics and longterm series of temperature and precipitation at Svalbard and Jan Mayen. *Det Norske Meteorologiske Institutt Klima Report*, 21, p.97.

Gjelten, H.M., Nordli, Ø., Isaksen, K., Førland, E.J., Sviashchennikov, P.N., Wyszynski, P., Prokhorova, U.V., Przybylak, R., Ivanov, B.V. and Urazgildeeva, A.V., 2016. Air temperature variations and gradients along the coast and fjords of western Spitsbergen. *Polar Research*, 35(1), p.29878.

Gunn, D.E. and Best, A.I., 1998. A new automated nondestructive system for high resolution multi-sensor core logging of open sediment cores. *Geo-Marine Letters*, 18(1), pp.70-77.

Hagen, J.O., Liestøl, O., Roland, E.R.I.K. and Jørgensen, T., 1993. *Glacier atlas of svalbard and jan mayen* (Vol. 129, p. 141). Oslo: Norsk polarinstitutt. Available at: <https://core.ac.uk/download/pdf/30910443.pdf> (Accessed 19.11.2019).

Hagen, J.O., Melvold, K., Pinglot, F. and Dowdeswell, J.A., 2003. On the net mass balance of the glaciers and ice caps in Svalbard, Norwegian Arctic. *Arctic, Antarctic, and Alpine Research*, 35(2), pp.264-270. Available at: <https://www.tandfonline.com/doi/pdf/10.1657/1523-0430%282003%29035%5B0264%3AOTNMBO%5D2.0.CO%3B2> (Accessed: 15.01. 2020).

Hald, M., Andersson, C., Ebbesen, H., Jansen, E., Klitgaard-Kristensen, D., Risebrobakken, B., Salomonsen, G.R., Sarnthein, M., Sejrup, H.P. and Telford, R.J., 2007. Variations in temperature and extent of Atlantic Water in the northern North Atlantic during the Holocene. *Quaternary Science Reviews*, 26(25-28), pp.3423-3440. Available at: https://d1wqxts1xzle7.cloudfront.net/44502176/Variations_in_temperature_and_extent_of_20160407-9640-urgbp8.pdf?1460022414=&response-content-disposition=inline%3B+filename%3DVariations_in_temperature_and_extent_of.pdf&Expires=1594890900&Signature=OF9zLvWzPZIq-ULv3kORExGjAOYWYrznmYblF6oD4X5-u0yfr3F8VNuEQ56JzYbKg6ceIZKtHjj4vugn~I5U7Ys2oiZbrQtHWJZWJ0yRBwUf9DbtUTkfdQ~00Pya8LM6vdLaK7aDi2b1irkSrhi~MQEF1lw3FCLp-ouXxAjMDr9Mw8csHlbOekpEDrnr3QYcrpZJ5vnCXAhMv5NT6dla4pxoqbGJ-KbwA3JzN7rpx-HHuMg6U0wNnzABxcg1vdJtkvkJcEhpQNj2NW~AZGjcUSTuM8gZuf0K6D3TzfMREUptT2JYLubVWu1xPBuIxQ~5rifNhC0DQCVN~wBVC-2MA &Key-Pair-Id=APKAJLOHF5GGSLRBV4ZA (Accessed: 01.05.2019).

Hanssen-Bauer, M., 1990. The climate of Spitsbergen. *Klima, Den Norske Meteorologiske Institutt Rapport*, 39, pp.1-40.

Hanssen-Bauer, I., E. J. Førland, H. Hisdal, S. Mayer, A. B. Sandø and A. Sorteberg (eds.), 2019. Climate in Svalbard 2100 - a knowledge base for climate adaptation. NCCS report 1/2019

Hansen, K., 1962. A.H. Bouma: Sedimentology of Some Flysch Deposits. A graphic approach to facies interpretation. Elsevier Publishing Company. Amsterdam, New York 1962. 168 sider, 31 fig., 8 pi. og 3 løse bilag. 17x25 cm. Hfl. 32,—. *Geografisk Tidsskrift*, 61.

Hansen, B.B., Isaksen, K., Benestad, R.E., Kohler, J., Pedersen, Å.Ø., Loe, L.E., Coulson, S.J., Larsen, J.O. and Varpe, Ø., 2014. Warmer and wetter winters: characteristics and implications of an extreme weather event in the High Arctic. *Environmental Research Letters*, 9(11), p.114021. Available at: <https://iopscience.iop.org/article/10.1088/1748-9326/9/11/114021/pdf> (Accessed. 03.03.2020).

Heiri, O., Lotter, A.F. and Lemcke, G., 2001. Loss on ignition as a method for estimating organic and carbonate content in sediments: reproducibility and comparability of results. *Journal of paleolimnology*, 25(1), pp.101-110.

Hjelle, A., Lauritzen, O., Salvigsen, O. and Winsnes, T.S., 1986. *Geological Map of Svalbard 1: 100,000. Sheet BIOG Van Mijenfjorden*. Norsk Polarinstitutt.

Hodgkins, R., 1997. Glacier hydrology in Svalbard, Norwegian high arctic. *Quaternary Science Reviews*, 16(9), pp.957-973. Available at: http://helios.hampshire.edu/~srNS/Svalbard/Hodgkins_Glacier%20Hydrology%20in%20Svalbard,%20Norway%20High%20Arctic.pdf (Accessed: 18.02.2020).

Hodson, A., 1994. *Climate, hydrology and sediment transfer process interactions in a sub-polar glacier basin, Svalbard* (Doctoral dissertation, University of Southampton).

Hughes, A.L., Gyllencreutz, R., Lohne, Ø.S., Mangerud, J. and Svendsen, J.I., 2016. The last Eurasian ice sheets—a chronological database and time-slice reconstruction, DATED-1. *Boreas*, 45(1), pp.1-45.

Humlum, O., 2005. Holocene permafrost aggradation in Svalbard. *Geological Society, London, Special Publications*, 242(1), pp.119-129

Humlum, O., 2002. Modelling late 20th-century precipitation in Nordenskiold Land, Svalbard, by geomorphic means. *Norsk Geografisk Tidsskrift-Norwegian Journal of Geography*, 56(2), pp.96-103.

Humlum, O., Christiansen, H. H., Eckerstorfer, M., Farnsworth, W., Gilbert, G., Hancock, H., O'Neill, B., Prokop, A., Strand, S., (2016) *The 7-8 November 2016 Rainstorm in Longyearbyen, Svalbard* (UNIS, Arctic Geology Department, report no. 2016-02).

Humlum, O. E., B.; Hormes, A.; Fjordheim, K.; Hansen, O.; Heinemeier, J., 2005, Late-Holocene glacier growth in Svalbard, documented by subglacial relict vegetation and living soil microbes: The Holocene, v. 15, no. 3, p. 396-407.

Humlum, O., Instanes, A. and Sollid, J.L., 2003. Permafrost in Svalbard: a review of research history, climatic background and engineering challenges. *Polar research*, 22(2), pp.191-215. Available at: <https://www.tandfonline.com/doi/pdf/10.3402/polar.v22i2.6455> (Accessed: 20.10.2019).

Ingolfsson, O., 2004. Outline of the geography and geology of Svalbard. *University of Iceland and UNIS*. Available at: <http://helios.hampshire.edu/~srNS/Svalbard/Outline%20of%20the%20geology%20and%20geography%20of%20Svalbard.pdf> (accessed: 23.04.2019).

Ingólfsson, Ó., Möller, P. and Lokrantz, H., 2008. Late Quaternary marine-based Kara Sea ice sheets: a review of terrestrial stratigraphic data highlighting their formation. *Polar Research*, 27(2), pp.152-161. Available at: <https://www.tandfonline.com/doi/pdf/10.1111/j.1751-8369.2008.00060.x> (Accessed: 24.04.2020).

Isaksen, K., Nordli, Ø., Førland, E.J., Łupikasza, E., Eastwood, S. and Niedzwiedź, T., 2016. Recent warming on Spitsbergen—Influence of atmospheric circulation and sea ice cover. *Journal of Geophysical Research: Atmospheres*, 121(20), pp.11-913.

Jansson, P., Rosqvist, G. and Schneider, T., 2005. Glacier fluctuations, suspended sediment flux and glacio-lacustrine sediments. *Geografiska Annaler: Series A, Physical Geography*, 87(1), pp.37-50.

Johannesen, R. M., 2018. Bødalen. Bachelor thesis. Svalbard: University Centre in Svalbard.

Johnson, T.C., Brown, E.T. and Shi, J., 2011. Biogenic silica deposition in Lake Malawi, East Africa over the past 150,000 years. *Palaeogeography, Palaeoclimatology, Palaeoecology*, 303(1-4), pp.103-109.

Kastner, S., Enters, D., Ohlendorf, C., Haberzettl, T., Kuhn, G., Lücke, A., Mayr, C., Reyss, J.L., Wastegård, S. and Zolitschka, B., 2010. Reconstructing 2000 years of hydrological variation derived from laminated proglacial sediments of Lago del Desierto at the eastern margin of the South Patagonian Ice Field, Argentina. *Global and Planetary Change*, 72(3), pp.201-214.

Kaufman, D.S., 2009. An overview of late Holocene climate and environmental change inferred from Arctic lake sediment. *Journal of Paleolimnology*, 41(1), pp.1-6.

Ketterer, E. M., *Plutonium chronology of sediments from Pyramid Lake (NZ), Bodalen 2012, Linnevatnet 2012 H4, and Vardeborgsletta Lake 7* (29.01.2013).

Killingtveit, Å., Pettersson, L.E. and Sand, K., 2003. Water balance investigations in Svalbard. *Polar Research*, 22(2), pp.161-174. Available at: <https://www.tandfonline.com/doi/pdf/10.3402/polar.v22i2.6453> (Accessed: 04.04.2020).

Larsson, S., 1982. Geomorphological effects on the slopes of Longyear Valley, Spitsbergen, after a heavy rainstorm in July 1972. *Geografiska Annaler: Series A, Physical Geography*, 64(3-4), pp.105-125.

Lie, Ø., Dahl, S.O., Nesje, A., Matthews, J.A. and Sandvold, S., 2004. Holocene fluctuations of a polythermal glacier in high-alpine eastern Jotunheimen, central-southern Norway. *Quaternary Science Reviews*, 23(18-19), pp.1925-1945. Available at:
https://d1wqxts1xzle7.cloudfront.net/50769499/Holocene_fluctuations_of_a_polythermal_g20161207-19384-1wodcfz.pdf?1481132414=&response-content-disposition=inline%3B+filename%3DHolocene_fluctuations_of_a_polythermal_g.pdf&Expires=1594895725&Signature=P2PRWggBHpHvAWMkpP0d6g5ZgYTgG4nbmHEjXx7fKHt27ljI33C4vG88NhY560XvhZAtIdbzpkVSKZCoPJgfBaY180Pi9oWtHcRj-a2Lv7s3PMMkeZoPe76HpljAxzITF4Aew3aa06zXcjsfTi6R0oCB464cIVnOm9KKZky5y8WfwczImuqEISezuUcphOX3xk9n7m1d3u5CPWvplIoBueYz6FVHjXI7~Uy~~xMuxlcivvWa0OG-i~VsC5XXwP6lJE2EA1fCS5-U-9dr37-9VIMjkC4jQocwL~aJtYTvxQ7nPKG3qCHZJKicfo~Ca5nK02NZrqshpnyl6KoOtHGaw_&Key-Pair-Id=APKAJLOHF5GGSLRBV4ZA (Accessed: 28.04. 2020).

Lindelof, J.A., 2012. Using Sedimentary and Geochemical Proxies for Little Ice Age Climate Climate Change Reconstructions, South Mainland Shetland.

Lund, D.C., Lynch-Stieglitz, J. and Curry, W.B., 2006. Gulf Stream density structure and transport during the past millennium. *Nature*, 444(7119), pp.601-604.

Majewski, W. and Zajaczkowski, M., 2007. Benthic foraminifera in Adventfjorden, Svalbard: Last 50 years of local hydrographic changes. *The Journal of Foraminiferal Research*, 37(2), pp.107-124. Available at: <http://citesexr.ist.psu.edu/viewdoc/download?doi=10.1.1.861.8526&rep=rep1&type=pdf> (Accessed 10th of March, 2020). Miller, G.H., Geirsdóttir, Á., Zhong, Y., Larsen, D.J., Otto-Bliesner, B.L., Holland, M.M., Bailey, D.A., Refsnider, K.A., Lehman, S.J., Southon, J.R. and Anderson, C., 2012. Abrupt onset of the Little Ice Age triggered by volcanism and sustained by sea-ice/ocean feedbacks. *Geophysical Research Letters*, 39(2). Available at: <https://agupubs.onlinelibrary.wiley.com/doi/pdf/10.1029/2011GL050168> (Accessed: 14.07.2020).

Major, H. and Nagy, J., 1972. Geology of the Adventdalen map area: with a geological map, Svalbard C9G 1: 100 000. Available at: <https://brage.npolar.no/npolar-xmlui/bitstream/handle/11250/173948/Skrifter138.pdf?sequence=2> (Accessed: 14.07.2020).

Mangerud, J. and Svendsen, J.I., 1990. Deglaciation chronology inferred from marine sediments in a proglacial lake basin, western Spitsbergen, Svalbard. *Boreas*, 19(3), pp.249-272.

Mann, M.E., Zhang, Z., Rutherford, S., Bradley, R.S., Hughes, M.K., Shindell, D., Ammann, C., Faluvegi, G. and Ni, F., 2009. Global signatures and dynamical origins of the Little Ice Age and Medieval Climate Anomaly. *Science*, 326(5957), pp.1256-1260.

- Moore, J.J., Hughen, K.A., Miller, G.H. and Overpeck, J.T., 2001. Little Ice Age recorded in summer temperature reconstruction from varved sediments of Donard Lake, Baffin Island, Canada. *Journal of Paleolimnology*, 25(4), pp.503-517. Available at: https://notendur.hi.is/~oi/AG-326%202006%20readings/Anthropocene/Moore_JOPL2001.pdf (Accessed: 22.03.2020).
- Mulder, T. and Alexander, J., 2001. The physical character of subaqueous sedimentary density flows and their deposits. *Sedimentology*, 48(2), pp.269-299.
- Matthews, J.A., Dahl, S.O., Nesje, A., Berrisford, M.S. and Andersson, C., 2000. Holocene glacier variations in central Jotunheimen, southern Norway based on distal glaciolacustrine sediment cores. *Quaternary Science Reviews*, 19(16), pp.1625-164.
- Naeher, S., Gilli, A., North, R.P., Hamann, Y. and Schubert, C.J., 2013. Tracing bottom water oxygenation with sedimentary Mn/Fe ratios in Lake Zurich, Switzerland. *Chemical Geology*, 352, pp.125-133.
- Nesje, A., Bakke, J., Dahl, S.O., Lie, Ø. and Bøe, A.G., 2007. A continuous, high-resolution 8500-yr snow-avalanche record from western Norway. *The Holocene*, 17(2), pp.269-277.
- Nesje, A., Lie, Ø. and Dahl, S.O., 2000. Is the North Atlantic Oscillation reflected in Scandinavian glacier mass balance records?. *Journal of Quaternary Science: Published for the Quaternary Research Association*, 15(6), pp.587-601.
- Nesje, A., Matthews, J.A., Dahl, S.O., Berrisford, M.S. and Andersson, C., 2001. Holocene glacier fluctuations of Flatebreen and winter-precipitation changes in the Jostedalsbreen region, western Norway, based on glaciolacustrine sediment records. *The Holocene*, 11(3), pp.267-280.
- Nesse, W.D., 2000. Introduction to Mineralogy: Oxford University Press. *New York*, pp.346-349.
- Nordli, P.Ø., Hanssen-Bauer, I. and Førland, E.J., 1996. *Homogeneity analyses of temperature and precipitation series from Svalbard and Jan Mayen*. Norske meteorologiske institutt.
- Nordli, Ø., Przybylak, R., Ogilvie, A.E. and Isaksen, K., 2014. Long-term temperature trends and variability on Spitsbergen: the extended Svalbard Airport temperature series, 1898–2012. *Polar research*, 33(1), p.21349.
- Nordli, Ø., Wyszyński, P., Gjelten, H., Isaksen, K., Łupikasza, E., Niedźwiedź, T. and Przybylak, R., 2020. Revisiting the extended Svalbard Airport monthly temperature series, and the compiled corresponding daily series 1898–2018.
- Normandeau, A., Joyal, G., Lajeunesse, P., Francus, P., Lamoureux, S. and Lapointe, F., 2016. Late-Holocene Mass Movements in High Arctic East Lake, Melville Island (Western Canadian Arctic Archipelago). In *Submarine Mass Movements and Their Consequences* (pp. 311-320). Springer, Cham.
- Nowak, A. and Hodson, A., 2013. Hydrological response of a High-Arctic catchment to changing climate over the past 35 years: a case study of Bayelva watershed, Svalbard. *Polar Research*, 32(1), p.19691.
- Norwegian Metrological Institute. (2020) eKlima. Available at: http://sharki.oslo.dnmi.no/portal/page?_pageid=73,39035,73_39049&_dad=portal&_schema=PORTAL (Accessed: 24.06.2020).
- Norwegian Polar Institute. (2020). *Børdalen 75°05'N and 78°06'N. 2D dynamic map*. Available at: <https://toposvalbard.npolar.no/> (Accessed: 02.08.2020).
- Ojala, A.E.K., Francus, P., Zolitschka, B., Besonen, M. and Lamoureux, S.F., 2012. Characteristics of sedimentary varve chronologies—a review. *Quaternary Science Reviews*, 43, pp.45-60.
- Praet, N., Van Daele, M., Collart, T., Moernaut, J., Vandekerkhove, E., Kempf, P., Haeussler, P.J. and De Batist, M., 2020. Turbidite stratigraphy in proglacial lakes: Deciphering trigger mechanisms using a statistical approach. *Sedimentology*.
- Retelle, M., Dowey, C. and Dulin, I. 2013, Laminated Sediments from a Proglacial Lake in Bodalen, Nordenskiöldland, Svalbard: Implications for late Little Ice Age and 20th Century Glacier Dynamics and Glacial-Lacustrine Sediment Production, Abstract, 43rd International Arctic Workshop, Amherst, Ma, USA

Romanovsky, V.E., Drozdov, D.S., Oberman, N.G., Malkova, G.V., Kholodov, A.L., Marchenko, S.S., Moskalenko, N.G., Sergeev, D.O., Ukraintseva, N.G., Abramov, A.A. and Gilichinsky, D.A., 2010. Thermal state of permafrost in Russia. *Permafrost and Periglacial Processes*, 21(2), pp.136-155. Available at: <https://onlinelibrary.wiley.com/doi/pdf/10.1002/ppp.683> (Accessed: 20.10.2019).

Rothwell, R.G., Hoogakker, B., Thomson, J., Croudace, I.W. and Frenz, M., 2006. Turbidite emplacement on the southern Balearic Abyssal Plain (western Mediterranean Sea) during Marine Isotope Stages 1–3: an application of ITRAX XRF scanning of sediment cores to lithostratigraphic analysis. *Geological Society, London, Special Publications*, 267(1), pp.79-98. Sabatier et al., 2017

Rubensdotter, L. and Rosqvist, G., 2009. Influence of geomorphological setting, fluvial-, glaciofluvial-and mass-movement processes on sedimentation in alpine lakes. *The Holocene*, 19(4), pp.665-678. Available at: https://www.researchgate.net/profile/Lena_Rubensdotter/publication/235430173_Influence_of_geomorphological_setting_fluvial-_glaciofluvial-_and_mass-movement_processes_on_sedimentation_in_alpine_lakes/links/0fcfd51190c7d89fa2000000/Influence-of-geomorphological-setting-fluvial-glaciofluvial-and-mass-movement-processes-on-sedimentation-in-alpine-lakes.pdf (Accessed at: 20.04. 2020).

Rubensdotter, L., Trøyen, P., Eckerstorfer, M., Christiansen, H. and Stalsberg, K., Landforms and sediments in Todalen and upper Gangdalen and Bødalen, Svalbard. Scale 1: 25 000. Available at: https://www.ngu.no/upload/Publikasjoner/Kart/Svalbard/kart_todalen_engelsk.pdf (Accessed: 13.05.2019).

Rutter, N., Hodson, A., Irvine-Fynn, T. and Solås, M.K., 2011. Hydrology and hydrochemistry of a deglaciating high-Arctic catchment, Svalbard. *Journal of Hydrology*, 410(1-2), pp.39-50.

Røthe, T.O., Bakke, J., Vasskog, K., Gjerde, M., D'Andrea, W.J. and Bradley, R.S., 2015. Arctic Holocene glacier fluctuations reconstructed from lake sediments at Mitrahalvøya, Spitsbergen. *Quaternary Science Reviews*, 109, pp.111-125. Available at: V (Accessed: 25.03.2020).

Santisteban, J.I., Mediavilla, R., Lopez-Pamo, E., Dabrio, C.J., Zapata, M.B.R., García, M.J.G., Castano, S. and Martínez-Alfaro, P.E., 2004. Loss on ignition: a qualitative or quantitative method for organic matter and carbonate mineral content in sediments?. *Journal of Paleolimnology*, 32(3), pp.287-299. Available at: https://eprints.ucm.es/10760/1/2004_1_Loss_ignition_JP.pdf (Accessed: 25.09.2019).

Schiefer, E., Menounos, B. and Slaymaker, O., 2006. Extreme sediment delivery events recorded in the contemporary sediment record of a montane lake, southern Coast Mountains, British Columbia. *Canadian Journal of Earth Sciences*, 43(12), pp.1777-1790. Available at: https://www.researchgate.net/profile/Erik_Schiefer/publication/237169390_Extreme_sediment_delivery_events_recorded_in_the_contemporary_sediment_record_of_a_montane_lake_southern_Coast_Mountains_British_Columbia/links/5410b0eb0cf2f2b29a41142f.pdf (Accessed: 12.07.2020).

Serreze, M.C., Walsh, J.E., Chapin, F.S., Osterkamp, T., Dyurgerov, M., Romanovsky, V., Oechel, W.C., Morison, J., Zhang, T. and Barry, R.G., 2000. Observational evidence of recent change in the northern high-latitude environment. *Climatic change*, 46(1-2), pp.159-207.

Smith, N.D. and Ashley, G., 1985. Proglacial lacustrine environment.

Smith, M.W. and Riseborough, D.W., 2002. Climate and the limits of permafrost: a zonal analysis. *Permafrost and Periglacial Processes*, 13(1), pp.1-15. Available at: <http://www.aari.ru/docs/pub/080118/Smith02.pdf> (Accessed: 22.11.2019).

Snowball, I. and Sandgren, P., 1996. Lake sediment studies of Holocene glacial activity in the Kårsa valley, northern Sweden: contrasts in interpretation. *The Holocene*, 6(3), pp.367-372.

Snyder, J.A., Werner, A. and Miller, G.H., 2000. Holocene cirque glacier activity in western Spitsbergen, Svalbard: sediment records from proglacial Linnévatnet. *The Holocene*, 10(5), pp.555-563.

Spielhagen, R.F., Werner, K., Sørensen, S.A., Zamelczyk, K., Kandiano, E., Budeus, G., Husum, K., Marchitto, T.M. and Hald, M., 2011. Enhanced modern heat transfer to the Arctic by warm Atlantic water. *Science*, 331(6016), pp.450-453. Available at: https://www.researchgate.net/profile/Katrine_Husum/publication/49791240_Enhanced_Modern_Heat_Transfer/

[to the Arctic by Warm Atlantic Water/links/0c96052dbcae5d9150000000/Enhanced-Modern-Heat-Transfer-to-the-Arctic-by-Warm-Atlantic-Water.pdf](https://www.researchgate.net/publication/0c96052dbcae5d9150000000/Enhanced-Modern-Heat-Transfer-to-the-Arctic-by-Warm-Atlantic-Water.pdf) (Accessed: 12.04.2020).

Sturm, M., 1979. Origin and composition of clastic varves. In *Moraines and varves; origin, genesis, classification, Proceedings of an INQUA symposium on genesis and lithology of Quaternary deposits, Zurich, 1979* (pp. 281-285).

Svendsen, J.I. and Mangerud, J., 1997. Holocene glacial and climatic variations on Spitsbergen, Svalbard. *The Holocene*, 7(1), pp.45-57.

Tjallingii, R., Röhl, U., Kölling, M. and Bickert, T., 2007. Influence of the water content on X-ray fluorescence core-scanning measurements in soft marine sediments. *Geochemistry, Geophysics, Geosystems*, 8(2).

Van Der Bilt, W.G., Bakke, J., Vasskog, K., D'Andrea, W.J., Bradley, R.S. and Ólafsdóttir, S., 2015. Reconstruction of glacier variability from lake sediments reveals dynamic Holocene climate in Svalbard. *Quaternary Science Reviews*, 126, pp.201-218. Available at: <https://www.sciencedirect.com/science/article/pii/S0277379115301025> (Accessed: 10.07.2020).

Vikhamar-Schuler, D., Førland, E.J., Lutz, J. and Gjelten, H.M., 2019. Evaluation of downscaled reanalysis and observations for Svalbard. *Norwegian Centre for Climate Services*. Available at: https://www.researchgate.net/profile/Herdís_Gjelten2/publication/331648373_Evaluation_of_downscaled_reanalysis_and_observations_for_Svalbard_-_Background_report_for_Climate_in_Svalbard_2100/links/5c86340892851c69506baae9/Evaluation-of-downscaled-reanalysis-and-observations-for-Svalbard-Background-report-for-Climate-in-Svalbard-2100.pdf (Accessed at: 08.04.2020).

Vasskog, K., Nesje, A., Støren, E.N., Waldmann, N., Chapron, E. and Ariztegui, D., 2011. A Holocene record of snow-avalanche and flood activity reconstructed from a lacustrine sedimentary sequence in Oldevatnet, western Norway. *The Holocene*, 21(4), pp.597-614.

White, J.W., Gorodetzky, D., Cook, E.R. and Barlow, L.K., 1996. Frequency analysis of an annually resolved, 700 year paleoclimate record from the GISP2 ice core. In *Climatic Variations and forcing mechanisms of the last 2000 years* (pp. 193-212). Springer, Berlin, Heidelberg.

Wickström, S., Jonassen, M.O., Cassano, J.J. and Vihma, T., 2019. Present Temperature, Precipitation and Rain-on-Snow Climate in Svalbard. *Journal of Geophysical Research: Atmospheres*, p.e2019JD032155. Available at: https://www.researchgate.net/profile/Siiri_Wickstroem/publication/341450093_Present_Temperature_Precipitation_on_and_Rain-on-Snow_Climate_in_Svalbard/links/5ed8d30e92851c9c5e7baf23/Present-Temperature-Precipitation-and-Rain-on-Snow-Climate-in-Svalbard.pdf (Accessed: 14.07.2020).

Woo, M.K., Kane, D.L., Carey, S.K. and Yang, D., 2008. Progress in permafrost hydrology in the new millennium. *Permafrost and Periglacial Processes*, 19(2), pp.237-254. Available at: https://d1wqxts1xzle7.cloudfront.net/51926853/Progress_in_Permafrost_Hydrology_in_the_20170224-24473-10hvnp.pdf?1487977948=&response-content-disposition=inline%3B+filename%3DProgress_in_permafrost_hydrology_in_the.pdf&Expires=1594736760&Signature=N~aFWwEFIsag1HDWXvPlSQL4~LP6xTBIsvpDcr1q1aG4C6t3sw8OnJ94D5Z~NbFCzyT-o58DQhUOjEHGH0y~6SgxSM8KLXosXzdTd9EE7B36LaWS4i4R0kWmanMmqcYY7hz7oRux7OlrzFHvS0_6A-stkHTqyZ0LyB8qBGawpcpSrphz7luhzoalNddfZ0MU1qKGm3HsEpGsxpQj-DgLKbG-uO4sD-EgQ0GCJYaBeG589NXRIVIUbWvY7vRGeFbU2MCpGOMVvBnF25XahaxWafzaoAn6e4b4m1oVtForsh~oN08ZEpiSGkGHqHNTWK8kfCtH0iFQGeOvqiLc6VLURUw_&Key-Pair-Id=APKAJLOHF5GGSLRBV4ZA (accessed: 23.11.2019).

Worsley, D., Aga, O.J., Dalland, A., Elverhøi, A. & Thon, A. 1986: The geological history of Svalbard, evolution of an arctic archipelago. Statoil, Aske Trykkeri, Stavanger, 121 p.

Zolitschka, B., 2007. Varved lake sediments. In: Elias, S.A. (Ed.), Encyclopaedia of Quaternary Science. Elsevier, Amsterdam, pp. 3105 – 3114.

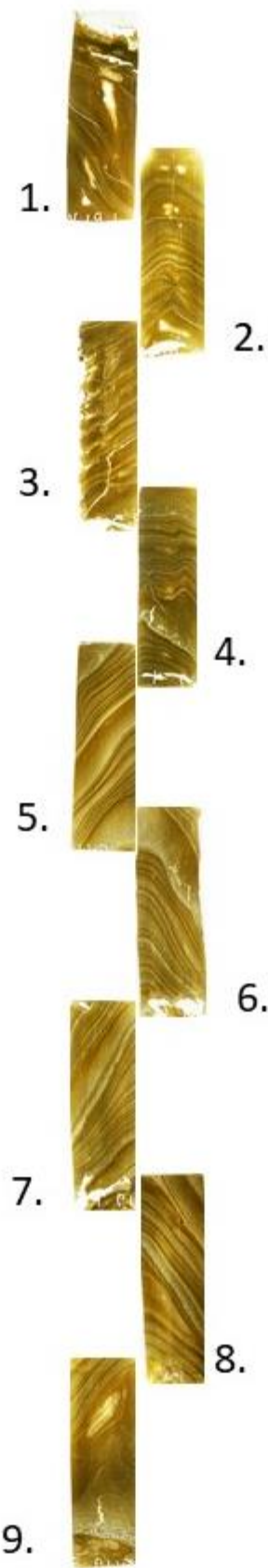
Zolitschka, B., Francus, P., Ojala, A.E. and Schimmelmann, A., 2015. Varves in lake sediments—a review. *Quaternary Science Reviews*, 117, pp.1-41.

Åkerman, H.J., 2005. Relations between slow slope processes and active-layer thickness 1972–2002, Kapp Linné, Svalbard. *Norsk Geografisk Tidsskrift-Norwegian Journal of Geography*, 59(2), pp.116-128.

APPENDIX A - VARVE

Surface core BVS-2019-thin section. The scans overlap using distinctive

1 reconstructed from scanned
are aligned 1cm or less
marker beds.



Varve count, thickness and year AD from surface core of 2019.

DEPTH	THICKNESS	YEAR			
0,8	0,8	2018	28,35	0,2	1977
1,7	0,9	2017	28,5	0,15	1976
6,2	4,5	2016	28,65	0,15	1975
6,7	0,5	2015	31,25	2,6	1974
7,9	1,2	2014	31,6	0,35	1973
8,35	0,45	2013	31,9	0,3	1972
8,75	0,4	2012	32	0,1	1971
9,05	0,3	2011	32,45	0,45	1970
9,8	0,75	2010	32,65	0,2	1969
10,2	0,4	2009	32,95	0,3	1968
10,7	0,5	2008	33,65	0,7	1967
12,1	1,4	2007	33,75	0,1	1966
12,7	0,6	2006	33,85	0,1	1965
13,3	0,6	2005	34,25	0,4	1964
14,1	0,8	2004	34,45	0,2	1963
14,5	0,4	2003	34,75	0,3	1962
15,6	1,1	2002	34,85	0,1	1961
16,2	0,6	2001	34,95	0,1	1960
17,6	1,4	2000	35,2	0,25	1959
18	0,4	1999	35,3	0,1	1958
18,6	0,6	1998	36,5	1,2	1957
19,45	0,85	1997	37,05	0,55	1956
19,7	0,25	1996	37,25	0,2	1955
20,05	0,35	1995	37,7	0,45	1954
20,8	0,75	1994	38,3	0,6	1953
22,8	2	1993	38,65	0,35	1952
23,4	0,6	1992	38,85	0,2	1951
23,6	0,2	1991	39,2	0,35	1950
23,9	0,3	1990	39,3	0,1	1949
24,1	0,2	1989	39,55	0,25	1948
24,4	0,3	1988	39,8	0,25	1947
24,75	0,35	1987	40,15	0,35	1946
24,95	0,2	1986	41,35	1,2	1945
25,15	0,2	1985	42,15	0,8	1944
25,45	0,3	1984	42,65	0,5	1943
26,6	1,15	1983	43,05	0,4	1942
27,1	0,5	1982	43,65	0,6	1941
27,4	0,3	1981	45,85	2,2	1940
27,5	0,1	1980	46,65	0,8	1939
27,85	0,35	1979	47,05	0,4	1938
28,15	0,3	1978	47,55	0,5	1937
			50,75	3,2	1936

APPENDIX B – GRAIN SIZE

Grain size distribution measured by Coulter LS, running average of D90 and observations throughout surface core of 2019.

DEPTH	MEDIAN	MEAN	D90	RA-90	OBSERVASJONS
0,5	4,13864	5,24673	11,6538	10,8994291	
1	3,10434	4,01922	8,83035	10,3879373	
1,5	3,36457	4,12447	8,69557	9,99260909	
2	4,68237	5,7967	12,5596	9,67234091	
3	4,51079	5,31483	11,3517	9,27918091	
4	3,45994	4,13581	8,5337	8,86132727	
5	3,09987	3,37428	6,02739	8,51548727	
6	4,02801	4,10665	7,30519	8,42805273	
7	4,06312	4,27665	8,13085	8,34711909	
8	3,41346	3,88706	7,32904	7,98271545	
9	3,19448	3,58673	7,05741	7,68142091	
10	4,12232	4,31532	7,84956	7,75761636	
11	3,87119	4,22426	7,86857	8,05260091	
12	3,85205	4,20266	7,8053	8,14350364	
13	4,18587	4,57658	8,55116	8,22791091	
14	4,04793	4,35556	8,03746	8,45532545	
15	4,9336	5,15707	9,37185	8,53348818	
16	4,88832	5,10659	9,27222	8,63788636	
17	4,60756	4,67254	8,30512	8,79782909	
18	5,0562	5,1376	9,05933	9,00857455	
19	4,94886	5,34032	9,8306	9,11932	
20	4,5191	4,57372	7,9172	9,66035091	
21	5,14928	5,12346	8,99794	10,5765736	
22	5,25158	5,38931	9,62794	12,5447627	
23	5,44295	5,60237	10,1235	13,6149882	
24	5,40055	5,50235	9,76936	14,4769491	
25	5,09983	6,20995	13,9888	15,4433855	Black coarser grains
26	6,87148	9,23374	19,4503	16,6615036	
27	8,94928	15,6844	30,9223	17,4633091	
28	6,92145	9,38958	20,0776	17,90536	
29	6,64733	8,86012	18,5409	18,6539964	
30	7,16838	9,6634	20,4614	19,5866182	
31	7,15221	9,8168	21,3165	19,9524273	
32	5,78367	8,20307	17,8178	19,8088273	
33	4,95637	6,21796	14,4905	19,5827545	
34	6,16022	8,57733	18,3585	20,2293818	
35	7,09059	9,50138	20,0282	20,1350364	
36	6,36175	8,59556	18,0127	19,6472455	2 mm gravel
37	6,21475	8,47011	17,8707	19,3805909	
40	8,78641	14,1931	28,4355	18,7720727	
41	6,88493	12,9627	27,1905	18,5876	
42	5,9422	8,24005	17,5031	18,3595909	

43	5,8278	6,95751	15,0957	17,6437727	
44	6,76105	8,89429	18,3833	16,9892182	
45	4,68043	5,46294	11,1241	20,0311727	
46	6,18882	6,68348	12,4613	22,1979182	
47	5,48964	7,20044	15,8504	23,3929818	
48	5,02669	5,9975	12,1542	25,4687182	
49	3,97865	5,53487	10,8126	27,7633091	
50	12,0128	31,2994	51,3322	29,7590273	sand
51	17,4092	26,5427	52,2697	32,4146727	sand
52	8,48848	18,4417	40,3362	34,9487545	sand

APPENDIX C – MAGNETIC SUSCEPTIBILITY

Magnetic susceptibility measurements and running average from surface core of 2019.

DEPTH	MS	RA-MS	DEPTH	MS	RA-MS
2	9,9	9,75454545	27	13,1	12,7545455
3	1	9,76454545	28	12,2	12,8636364
4	9,2	9,71909091	29	12,7	12,9545455
5	10,3	9,61909091	30	13	13,0181818
6	9,8	9,63727273	31	13,4	13,0818182
7	9,6	9,61909091	32	13,6	13,1
8	10,01	9,71	33	13,3	13,0909091
9	9,4	9,80090909	33	13,1	13,1
10	8,8	9,84636364	34	13	13,0454545
11	10,1	9,91	35	13,4	13,0454545
12	9,7	10,0190909	36	13,3	12,9090909
13	10,9	10,1554545	37	13	12,6909091
14	10	10,1909091	38	12,3	12,5363636
15	9,7	10,3363636	39	12,1	12,4363636
16	11	10,5727273	40	13	12,1636364
17	11	10,7545455	41	11,9	11,7090909
18	11,1	10,9727273	42	11,2	11,4545455
19	10,4	11,1	43	11,6	11,3545455
20	11	11,3454545	44	12	11,3
21	11,4	11,6545455	45	10	11,1363636
22	12,1	11,8454545	46	8,4	10,8909091
23	12,1	11,9545455	47	10,5	10,7454545
24	12,3	12,1	48	11,9	10,6636364
25	12,7	12,3363636	50	11,7	10,5454545
26	13,1	12,5545455	51	10,3	10,3909091

APPENDIX D - DRY BULK DENSITY, WATER CONTENT AND LOSS-ON-IGNITION

Dry Bulk Density, Water content and Loss-On-Ignition all with running average from surface core from 2019.

DEPTH	DBD	WC	LOI	RA-DBD	RA-WC	RA-LOI
0,5	0,9735	31,02104443	5,197740113	1,002990909	32,9095393	5,066790783
1,5	1,0781	33,93185439	4,943882757	1,013845455	33,17270165	5,050935538
2,5	0,9387	36,65564478	4,857782039	1,036172727	33,35577766	5,025091959
3,5	1,1198	34,65600747	4,849080193	1,0347	33,74319045	4,989404789
4,5	1,0842	33,86604855	5,026747833	1,0413	34,15412413	4,944445074
5,5	0,9711	36,76911056	4,870765112	1,041109091	34,6174221	4,89493034
6,5	1,0929	33,91583021	5,023332418	1,029481818	35,00526944	4,864267976
7,5	1,2191	33,03488053	4,91346075	1,033027273	35,00054141	4,842880502
8,5	0,9573	35,28258518	4,805181239	1,057090909	34,69616195	4,843193637
9,5	1,0461	35,54131493	4,703183252	1,066018182	34,51764378	4,857659999
10,5	0,9714	36,11732211	4,653078032	1,053327273	34,53312236	4,829917039
11,5	0,8456	35,28736512	4,860454115	1,106409091	33,66168771	4,885220181
12,5	1,1171	33,87984611	4,708620535	1,1299	33,47971616	4,863824684
13,5	1,2034	33,30747063	4,861226525	1,131772727	33,3498663	4,848335798
14,5	1,218	32,69230769	5,008210181	1,146045455	33,28773413	4,810447074
15,5	0,9446	34,03631285	4,72157527	1,16	32,88047216	4,864105973
16,5	1,555	27,18332943	5,479099678	1,180690909	32,20953365	4,949856177
17,5	1,3513	31,9141432	4,787981943	1,221872727	31,77334055	4,956031659
18,5	1,2397	31,60653205	4,743083004	1,236845455	31,29719172	4,947839358
19,5	1,1143	34,59913135	4,388405277	1,220709091	30,91483889	4,887835965
20,5	1,1996	31,06143325	5,293431144	1,235618182	30,48947771	4,846963286
21,5	1,199	28,73699851	5,596330275	1,2651	29,99098817	4,837563099
22,5	1,2986	30,48924098	4,928384414	1,241027273	30,34681852	4,736864518
23,5	1,2818	28,64220899	4,618505227	1,213027273	30,14136031	4,708519009
24,5	1,0259	29,1015895	4,2011892	1,215427273	29,72570718	4,704554265
25,5	1,382	28,01333472	4,558610709	1,232136364	29,24617994	4,753815851
26,5	1,2689	28,55292793	4,618173221	1,245772727	29,20335996	4,6956158
27,5	1,2902	31,09746328	4,371415284	1,265690909	29,2028629	4,625345338
28,5	1,0433	29,65410289	4,476181348	1,2536	29,11822536	4,607833883
29,5	1,2661	27,03434763	4,699470816	1,261036364	29,26736403	4,589313807
30,5	1,2981	29,32433168	4,930282721	1,273981818	29,34140287	4,649366149
31,5	1,3496	30,5904135	4,653230587	1,242454545	29,25404127	4,756585324
32,5	1,4181	28,73153081	4,823355194	1,246790909	29,47480581	4,744136809
33,5	1,1656	29,55822808	4,735758408	1,242018182	28,95720088	4,778621543
34,5	1,3636	30,28273429	4,414784394	1,251690909	28,95190388	4,774172501
35,5	1,1683	29,9160168	4,861764958	1,246781818	29,00972377	4,715204326
36,5	1,0352	27,05235713	5,738021638	1,244327273	29,06182261	4,674660891
37,5	1,3166	30,98133781	4,481239556	1,246536364	28,84038304	4,681736071
38,5	1,2377	25,40380906	4,750747354	1,236645455	28,71807735	4,730671383
39,5	1,1497	29,59583588	4,427241889	1,237245455	28,85195033	4,711960955

40,5	1,2121	27,67036639	4,050820889	1,225709091	28,79069906	4,710508125
41,5	1,2711	29,89741893	4,484304933	1,2086	29,23737421	4,659955229
42,5	1,3739	28,15457826	4,731057573	1,225	29,60642054	4,470363923
43,5	1,3093	27,38616827	5,361643626	1,229009091	29,27470285	4,428432119
44,5	1,1722	31,03083078	4,529943696	1,248836364	29,20989393	4,471136661
45,5	1,2367	29,60897035	4,398803267	1,2719	28,55063226	4,831094215
46,5	0,9801	34,82944345	4,305683094	1,290390909	28,45168534	4,928461867
47,5	1,2156	31,11186671	3,652517275	1,303518182	28,15027909	4,986421879
48,5	1,3607	27,33244326	4,019989711	1,3073	28,0073129	5,021949833
49,5	1,4558	24,69091097	5,220497321	1,316954545	27,93420217	5,000151782
50,5	1,4034	22,3439575	8,386774975	1,339072727	27,52975848	5,053962815
51,5	1,4155	26,58195021	5,121865065	1,355327273	27,25457483	5,119695706

APPENDIX E – ITRAX

Measurements in kcps from surface core from 2019.

DEPTH	K KCPS	CA KCPS	TI KCPS	MN KCPS	FE KCPS	ZR KCPS
0,8	0,12606895	0,01399766	0,07309389	0,01813845	2,12507877	0,01440274
0,9	0,11785996	0,01702937	0,0715512	0,01689017	2,09438077	0,01661176
1	0,12382097	0,01447198	0,07430183	0,01618273	2,08327169	0,01428704
1,1	0,11932872	0,01782241	0,07517981	0,01890804	2,08404578	0,01316325
1,2	0,13151199	0,01459756	0,07499665	0,01473149	2,06124727	0,01522254
1,3	0,1343921	0,01565906	0,07571511	0,01654878	2,04070466	0,01543663
1,4	0,1287966	0,01168866	0,0716373	0,01642611	2,08022669	0,01120163
1,5	0,12788114	0,01407346	0,07306871	0,01999913	2,08779574	0,01211276
1,6	0,12533183	0,01470908	0,07015101	0,01845163	2,07633056	0,01275077
1,7	0,13348555	0,01545622	0,07368051	0,01870554	2,04263634	0,01681742
1,8	0,13424441	0,01278727	0,07294459	0,01634662	2,01423738	0,01195237
1,9	0,13269934	0,01351649	0,07370229	0,01435301	2,01422093	0,01030247
2	0,13717373	0,010763	0,07586387	0,01468474	2,02797508	0,01363894
2,1	0,13088982	0,01453845	0,07637064	0,01506393	2,05141005	0,01142932
2,2	0,13387104	0,01380792	0,07272169	0,01446544	2,04900715	0,01363258
2,3	0,13606608	0,01361979	0,07569966	0,01410307	2,04621941	0,01612407
2,4	0,13850937	0,01414433	0,07531967	0,01331231	2,07282361	0,01541426
2,5	0,13176974	0,01432565	0,07512229	0,01677149	2,09818309	0,01528651
2,6	0,13111043	0,01379881	0,08244461	0,01806469	2,09781047	0,01345057
2,7	0,13069333	0,01417676	0,07751971	0,01960615	2,09195501	0,0144353
2,8	0,12964724	0,01439564	0,07487463	0,02161508	2,09281515	0,01154245
2,9	0,13237716	0,01304273	0,07076003	0,01975908	2,05555074	0,01195944
3	0,12811728	0,01353168	0,07498807	0,01812899	2,0587674	0,0130546
3,1	0,13070928	0,01510863	0,07380154	0,01741629	2,05403405	0,00979667
3,2	0,13778824	0,01281548	0,07344928	0,01608474	2,07135696	0,0131642
3,3	0,1282776	0,01369744	0,07709701	0,0170457	2,07196591	0,01156673
3,4	0,12518384	0,01340946	0,07089714	0,01924907	2,08962713	0,015356
3,5	0,12664438	0,01480485	0,07636869	0,01806104	2,08162202	0,01024617
3,6	0,1259897	0,01527279	0,07225371	0,01799853	2,06675897	0,01440748
3,7	0,12691561	0,01178502	0,07796244	0,0188215	2,06906972	0,01230304
3,8	0,13075594	0,01239741	0,07287257	0,01732181	2,07192225	0,0100216
3,9	0,1258261	0,01498855	0,07321498	0,0170619	2,05403654	0,01978316
4	0,12606466	0,01277594	0,07717713	0,01772988	2,06857292	0,01599166
4,1	0,12536191	0,01292079	0,07683333	0,01629143	2,05790588	0,01222938
4,2	0,12506436	0,0126566	0,07194955	0,01810537	2,04045821	0,01939248
4,3	0,12034447	0,01420703	0,07405141	0,01766043	2,05057702	0,01197762
4,4	0,13140723	0,01223491	0,07598523	0,01665665	2,02313901	0,01339401
4,5	0,12298474	0,01228554	0,06953186	0,01525994	2,02495905	0,01582033
4,6	0,12818587	0,01166129	0,07328062	0,01647599	2,0222183	0,01329564
4,7	0,12678094	0,01459822	0,06694139	0,01569418	2,05278155	0,01757924
4,8	0,12747079	0,01146447	0,06988492	0,01493455	2,04884477	0,01216727

4,9	0,12927673	0,01506987	0,07004863	0,01498226	2,00311035	0,01287949
5	0,12504931	0,01512163	0,0706991	0,01726934	2,00403244	0,01477098
5,1	0,12574561	0,01307018	0,07061404	0,01557018	2,00372807	0,01390351
5,2	0,12152056	0,01274506	0,06974377	0,0169049	1,99659247	0,01132894
5,3	0,12597622	0,01038339	0,0700213	0,01628506	1,99662762	0,01127086
5,4	0,12366046	0,01400685	0,06905598	0,0152519	2,0001334	0,01391792
5,5	0,11805432	0,01362507	0,07069945	0,01500089	2,00550328	0,00980827
5,6	0,12422052	0,01251695	0,07243561	0,01554451	1,98757343	0,01229101
5,7	0,12354625	0,01113795	0,069601	0,01306137	1,99852389	0,00890141
5,8	0,11889483	0,01475045	0,06876114	0,01604278	1,99006239	0,01185383
5,9	0,11575747	0,0142769	0,06371728	0,0156429	1,96611439	0,01083987
6	0,11832914	0,01406352	0,06854801	0,01620564	1,9587408	0,01369098
6,1	0,11047386	0,01269274	0,06026702	0,01443212	1,87044002	0,01631252
6,2	0,11469371	0,01564419	0,06935286	0,01709946	1,97198599	0,01205148
6,3	0,11979024	0,01331509	0,06803466	0,01595987	1,93871409	0,0125855
6,4	0,11801128	0,01261294	0,06843095	0,01366784	1,90836124	0,01275054
6,5	0,11952899	0,01124195	0,0683848	0,01595201	1,98049322	0,01301933
6,6	0,12234325	0,01350514	0,0708909	0,01881863	2,02577046	0,01036132
6,7	0,1101204	0,01168707	0,05964435	0,01501184	1,85920105	0,0122412
6,8	0,11044394	0,01422384	0,06782164	0,01506054	1,86986908	0,01634019
6,9	0,11632454	0,01517479	0,06903133	0,01801424	1,96788158	0,01261463
7	0,11763885	0,01293144	0,06344776	0,01702484	1,98553354	0,01097777
7,1	0,11791586	0,01375607	0,06878033	0,0163	1,95279597	0,01469826
7,2	0,12108442	0,01268905	0,06381983	0,01769912	1,97869551	0,01741818
7,3	0,1218697	0,01223875	0,06830164	0,01459236	1,97194502	0,01082659
7,4	0,12474052	0,01302133	0,07161729	0,01542744	1,98485563	0,01226647
7,5	0,11751316	0,01313606	0,06838336	0,01773605	1,99042064	0,00905771
7,6	0,11783394	0,01275547	0,06548438	0,01716535	2,00275025	0,01469961
7,7	0,11788483	0,01236388	0,07047411	0,0154073	1,98654239	0,01288697
7,8	0,11453284	0,01178595	0,06700884	0,02005513	1,98887938	0,01382948
7,9	0,11898409	0,01305632	0,06837892	0,01562947	1,99675975	0,01405699
8	0,11861184	0,01359639	0,06222962	0,01430948	1,98825767	0,01720941
8,1	0,11681171	0,01271875	0,07067036	0,01400975	1,99277996	0,01300564
8,2	0,11868396	0,01195965	0,06974063	0,01657061	2,00254563	0,01666667
8,3	0,11733041	0,01324314	0,07326601	0,01533918	2,00585938	0,01814977
8,4	0,11721927	0,01363571	0,0673652	0,01483183	1,99186642	0,01234391
8,5	0,11468937	0,01327181	0,07496908	0,01531729	2,01241557	0,01531729
8,6	0,11281661	0,01458918	0,07156774	0,01458918	1,99101839	0,01344865
8,7	0,11032518	0,01371944	0,06190363	0,01533349	2,00949442	0,01371944
8,8	0,11541554	0,01220378	0,0650868	0,01579869	2,00714252	0,01414313
8,9	0,11132129	0,01489643	0,06909108	0,01607869	2,01792301	0,01035657
9	0,10989011	0,01179078	0,07069754	0,01485639	2,00037731	0,01674291
9,1	0,10985916	0,01253521	0,06924883	0,0156338	1,9900939	0,01723005
9,2	0,11747045	0,01407394	0,06919685	0,01444924	1,97917058	0,01027397
9,3	0,11532497	0,01376944	0,0725598	0,01522628	1,97974529	0,00944593
9,4	0,11566728	0,01614942	0,07227449	0,01671114	1,98665918	0,01025137
9,5	0,11415568	0,0142636	0,0732886	0,01571811	2,0137944	0,0106977
9,6	0,11496564	0,0116415	0,06872692	0,015522	1,99672729	0,01584927

9,7	0,11666511	0,01500982	0,06850276	0,01613205	1,98672028	0,01234452
9,8	0,11296876	0,01382338	0,07173213	0,01503759	2,03381124	0,00910662
9,9	0,11445979	0,01172039	0,07092693	0,01651086	2,02125483	0,0113018
10	0,11293758	0,01222449	0,06996666	0,01509539	2,02296722	0,01120578
10,1	0,11612457	0,01361015	0,06855825	0,01411765	1,99331027	0,01407151
10,2	0,1127313	0,01527387	0,07267777	0,01467399	2,00978266	0,01190531
10,3	0,11425528	0,0127362	0,0733605	0,01500556	1,98754168	0,01079103
10,4	0,11981693	0,01290618	0,07276888	0,01487414	1,98237986	0,01395881
10,5	0,12006963	0,01328508	0,06999863	0,01566723	1,95968666	0,01204819
10,6	0,11821306	0,01214204	0,07413517	0,01713631	1,96815579	0,01282932
10,7	0,12408227	0,01231246	0,07127548	0,01477496	1,96497788	0,00916595
10,8	0,12540442	0,0117111	0,07213488	0,01526544	1,96764639	0,01449077
10,9	0,12372866	0,012668	0,07015075	0,01684526	1,97988558	0,01343988
11	0,11983397	0,01534019	0,07223425	0,01574626	1,97162065	0,01335499
11,1	0,12252147	0,01133043	0,07256868	0,0151522	1,96155748	0,01470258
11,2	0,11969319	0,01409204	0,06863182	0,01676775	1,96584017	0,01253122
11,3	0,117071	0,01277543	0,07015357	0,01736034	1,96728244	0,00952593
11,4	0,11857479	0,01261718	0,07063841	0,01652672	1,95210805	0,013328
11,5	0,11809389	0,01302831	0,06712891	0,01753301	1,96223999	0,01391158
11,6	0,11592729	0,01410943	0,06908753	0,01649786	1,94152771	0,01282675
11,7	0,12000351	0,01114475	0,06945724	0,01768242	1,94717213	0,01456715
11,8	0,12116827	0,01341929	0,06354427	0,01657677	1,96097005	0,01561198
11,9	0,1245418	0,01329329	0,06646646	0,01550148	1,94704765	0,01196838
12	0,12673642	0,01485845	0,06598382	0,01758396	1,96461227	0,01437489
12,1	0,12861666	0,01380705	0,0708381	0,01521414	1,99560285	0,00844253
12,2	0,12187322	0,0141061	0,07280852	0,01962588	2,0186183	0,01686599
12,3	0,11520273	0,01541291	0,07750241	0,02027323	2,0200543	0,00875733
12,4	0,11626273	0,01295223	0,07253249	0,02190903	2,02735335	0,01238145
12,5	0,11050526	0,01253243	0,06829075	0,01895255	2,03706961	0,01037773
12,6	0,10956851	0,01379523	0,06862356	0,02031822	2,04610164	0,01150337
12,7	0,11274777	0,01406582	0,07470807	0,0207891	2,05551132	0,01256193
12,8	0,11631729	0,01643276	0,06795168	0,01980814	2,037973	0,01092556
12,9	0,11333245	0,0135487	0,07140651	0,01981553	2,02965709	0,01646145
13	0,11214995	0,01358324	0,06619625	0,02041896	2,03845645	0,01115766
13,1	0,11056076	0,01587653	0,06996285	0,0174686	2,03117814	0,01105608
13,2	0,1159717	0,01339504	0,06595167	0,01998131	1,99830893	0,01076944
13,3	0,1191742	0,0149743	0,07044126	0,02042353	2,04762538	0,01240475
13,4	0,11983145	0,01400228	0,0716794	0,01984023	2,03766131	0,01242209
13,5	0,12225123	0,01376045	0,06977567	0,01716738	2,03460024	0,00933587
13,6	0,1181778	0,01278196	0,06784609	0,01937196	2,0305617	0,01256081
13,7	0,12368224	0,0143355	0,06907503	0,02245159	2,04362401	0,00952759
13,8	0,11910232	0,01488779	0,06750309	0,02314897	2,05800495	0,01276727
13,9	0,1194857	0,01268012	0,07479495	0,02358679	2,0545777	0,010818
14	0,12105147	0,01678816	0,07174729	0,02429865	2,07453059	0,0072896
14,1	0,11487198	0,01534549	0,07199228	0,02165907	2,04875482	0,00947036
14,2	0,1140156	0,01511785	0,07850826	0,02134797	2,06447959	0,01241668
14,3	0,10997864	0,01682393	0,0753071	0,02158626	2,06008546	0,01393092
14,4	0,10837684	0,0153462	0,07264472	0,02183882	2,03150965	0,01657208

14,5	0,10910222	0,0166141	0,07107636	0,01901293	2,05148594	0,01279375
14,6	0,10703741	0,01604019	0,0748689	0,01991804	2,05944564	0,01581986
14,7	0,11223809	0,01672672	0,07077717	0,01917345	2,02807064	0,0129899
14,8	0,11708861	0,01323765	0,0687734	0,01907648	1,99723658	0,01506507
14,9	0,11603883	0,01487221	0,06937394	0,01847894	2,00071244	0,01228961
15	0,12260571	0,01473412	0,07197393	0,01768094	1,99334732	0,01714515
15,1	0,12337923	0,01421379	0,07173729	0,01626342	2,01292162	0,01309985
15,2	0,12422943	0,01447333	0,0703118	0,0195658	2,02050389	0,0105423
15,3	0,12574425	0,01435173	0,07206967	0,0178619	2,02697059	0,01661779
15,4	0,12063857	0,01441649	0,07168443	0,01702561	2,03794278	0,00933092
15,5	0,12121755	0,01392122	0,07520143	0,01951656	2,05465533	0,01060877
15,6	0,11581758	0,0137931	0,07190211	0,01895439	2,04062291	0,01432703
15,7	0,11881495	0,012956	0,07300464	0,0215786	2,02675216	0,01613973
15,8	0,11683574	0,01512725	0,07194341	0,02011034	2,005517	0,00854245
15,9	0,12279682	0,01422564	0,07578062	0,01753601	2,00339984	0,01248099
16	0,12366024	0,01384423	0,07435691	0,01902465	2,02929618	0,01259378
16,1	0,12347372	0,01526279	0,07330561	0,02008494	2,05808706	0,01216599
16,2	0,11881929	0,01526483	0,0725849	0,01742038	2,0634788	0,0168485
16,3	0,11535935	0,01445277	0,07576753	0,01747471	2,06700828	0,01094907
16,4	0,11713628	0,01415361	0,07645552	0,02131724	2,05331481	0,01306821
16,5	0,11984096	0,01469381	0,06530101	0,02057133	2,03051126	0,01512598
16,6	0,11482503	0,01412513	0,0659597	0,02163309	2,05488865	0,01034995
16,7	0,11495723	0,01547756	0,06437958	0,02160684	2,0361143	0,00837816
16,8	0,1172502	0,01362554	0,07183173	0,02143046	2,06274804	0,00859864
16,9	0,11588712	0,01215051	0,07547252	0,02007665	2,08300671	0,01201986
17	0,11771935	0,01343107	0,07290524	0,01992714	2,12763903	0,01430892
17,1	0,1038281	0,0159805	0,07335681	0,01990791	2,10071325	0,01300108
17,2	0,09607281	0,01542186	0,07746795	0,02093607	2,12301623	0,0164978
17,3	0,09911736	0,01652707	0,08105917	0,02215617	2,13653967	0,01567144
17,4	0,09676261	0,01535629	0,07835302	0,01989134	2,12195232	0,02456109
17,5	0,09509437	0,01648723	0,07707554	0,01887472	2,10986981	0,01828911
17,6	0,0944452	0,01674173	0,08243483	0,02133661	2,0833902	0,01751513
17,7	0,10042774	0,01333273	0,08163451	0,02238806	2,05201129	0,01710957
17,8	0,1050462	0,01943287	0,07215981	0,020973	2,07043849	0,01490306
17,9	0,10640496	0,01724758	0,07554797	0,01881962	2,11255839	0,01329501
18	0,10414148	0,01687934	0,07624804	0,02064025	2,11511081	0,01535706
18,1	0,10828456	0,01674921	0,0754615	0,01787483	2,10805943	0,0087348
18,2	0,1091505	0,015625	0,07628412	0,01908226	2,09949713	0,01131466
18,3	0,10984187	0,01554451	0,07270528	0,01885947	2,05335304	0,01554451
18,4	0,11113087	0,01546942	0,0738798	0,02058144	2,08179232	0,01462482
18,5	0,10393321	0,01424171	0,07741417	0,01812581	2,08549489	0,01580428
18,6	0,101514	0,01536332	0,07400295	0,01768568	2,04827833	0,01710509
18,7	0,09883017	0,01609072	0,0761956	0,0209762	2,04379006	0,01550805
18,8	0,10286488	0,01403113	0,07714866	0,02165576	2,05973382	0,01493345
18,9	0,11122043	0,01556281	0,07302893	0,01958768	2,06462144	0,01153795
19	0,10823184	0,01560139	0,07649569	0,0207574	2,05942751	0,01573473
19,1	0,1143022	0,01611328	0,07293146	0,01922053	2,06294389	0,01260653
19,2	0,12021736	0,01336243	0,07460692	0,01679213	2,06814841	0,01567859

19,3	0,11863501	0,01421125	0,07118991	0,01790885	2,10152804	0,01162739
19,4	0,11502358	0,01513586	0,07406243	0,01917808	2,12494947	0,01365372
19,5	0,10842015	0,01298877	0,07739142	0,01781446	2,09110179	0,01371037
19,6	0,11194198	0,0154061	0,07112933	0,01959548	2,07811163	0,00828866
19,7	0,11400054	0,01235342	0,07488139	0,01902247	2,09900636	0,00989168
19,8	0,11263271	0,0146311	0,06927469	0,02060844	2,09077527	0,0133375
19,9	0,11635863	0,01510574	0,07735028	0,02021504	2,09938689	0,01204016
20	0,11131874	0,01388147	0,07354512	0,01957644	2,08030788	0,01241324
20,1	0,11331157	0,01631969	0,07233592	0,01931898	2,09368384	0,00988003
20,2	0,11920442	0,01670718	0,07235359	0,01966851	2,09264088	0,01029834
20,3	0,11261341	0,01448956	0,06760328	0,01990663	2,08874306	0,01087818
20,4	0,11820903	0,01413225	0,07523994	0,02056001	2,0929823	0,01113851
20,5	0,11134445	0,01706261	0,07695673	0,02143763	2,14201339	0,01365009
20,6	0,10932645	0,01654339	0,07715874	0,02306447	2,11952383	0,01382993
20,7	0,11383958	0,01430628	0,07318882	0,02276792	2,11606403	0,01295416
20,8	0,11110622	0,01430647	0,07047586	0,02152573	2,1272175	0,0168156
20,9	0,10271232	0,0144064	0,07612272	0,02063139	2,13766118	0,01636283
21	0,09968861	0,0155693	0,07243107	0,0213006	2,09206192	0,01678776
21,1	0,08818862	0,01831784	0,07866697	0,02221718	2,05617774	0,01623215
21,2	0,08661707	0,0190135	0,07913107	0,02686691	2,01942684	0,02236613
21,3	0,10541621	0,01981098	0,0717012	0,02621774	2,03076154	0,01990185
21,4	0,10103149	0,01680105	0,0754921	0,0232422	2,05891627	0,01986397
21,5	0,10209577	0,01718799	0,06879684	0,02306691	2,07490015	0,01947673
21,6	0,10091328	0,01731621	0,07125418	0,01984809	2,0844561	0,01659282
21,7	0,10291935	0,01605866	0,07642481	0,01880257	2,08780532	0,01668841
21,8	0,10673021	0,01640966	0,0736861	0,0217147	2,07935081	0,01533067
21,9	0,10437847	0,01653789	0,07238715	0,02218607	2,07076047	0,01653789
22	0,10524642	0,01485351	0,07172383	0,01885078	2,059732	0,01526232
22,1	0,10572787	0,01919855	0,07004754	0,02119085	2,05089427	0,01639122
22,2	0,10875439	0,01711249	0,07930289	0,02125552	2,04458255	0,01364496
22,3	0,10804257	0,01737842	0,07818043	0,02236293	2,05029413	0,01333693
22,4	0,11212928	0,01584436	0,06906514	0,02058412	2,06175236	0,01295536
22,5	0,11554124	0,01485658	0,07558062	0,02143464	2,05387748	0,00836801
22,6	0,1154274	0,01566324	0,07351044	0,02144796	2,08436791	0,01290437
22,7	0,112536	0,01565875	0,07343413	0,02096832	2,08490821	0,01345392
22,8	0,11369603	0,01493618	0,07594822	0,01977913	2,06313931	0,01380465
22,9	0,11158875	0,0162547	0,07701952	0,01970267	2,11252911	0,01043346
23	0,10596116	0,01825211	0,07705449	0,02126416	2,11265959	0,01694839
23,1	0,10481689	0,01664261	0,074779	0,02061158	2,13499008	0,01781526
23,2	0,11337014	0,01714465	0,0743683	0,02154302	2,11525515	0,01983753
23,3	0,10843266	0,01711623	0,07007796	0,02079039	2,1315082	0,01389013
23,4	0,1061182	0,01696986	0,07353607	0,02194769	2,11725043	0,01543126
23,5	0,10926601	0,01593088	0,07510913	0,02196121	2,11705144	0,01899105
23,6	0,11187808	0,01671896	0,07099955	0,02102196	2,13325863	0,01156432
23,7	0,10638681	0,016485	0,06873255	0,01815152	2,14588776	0,01292676
23,8	0,10051268	0,01695449	0,08252384	0,02082209	2,14116748	0,0159651
23,9	0,09163549	0,01902914	0,08175142	0,01935246	2,08138192	0,02129232
24	0,09964862	0,01662312	0,07874583	0,02162357	2,09888278	0,02527255

24,1	0,10068496	0,01589291	0,07565922	0,02104132	2,04253033	0,02359314
24,2	0,10637544	0,01648133	0,07850782	0,0200257	2,07996987	0,01940543
24,3	0,11069619	0,01582644	0,06637326	0,02222815	2,11620877	0,01564862
24,4	0,10718706	0,01701733	0,07620226	0,02236563	2,17269272	0,01710573
24,5	0,10615683	0,01534798	0,07396137	0,0247861	2,19436359	0,01618594
24,6	0,09544826	0,01796621	0,08136062	0,02068566	2,17654139	0,01043199
24,7	0,09397839	0,01546877	0,08084114	0,02448101	2,17616464	0,01555845
24,8	0,0870428	0,01844586	0,0865918	0,02448924	2,15812024	0,01664186
24,9	0,08757969	0,01912556	0,08776055	0,0227879	2,14332866	0,02256183
25	0,08055743	0,02211733	0,09022252	0,02490447	2,09521241	0,02562374
25,1	0,08377404	0,02082651	0,07591145	0,02485141	2,00781579	0,02316657
25,2	0,09556575	0,01947293	0,08252384	0,02365533	2,10388559	0,02086706
25,3	0,09958711	0,01858002	0,07746163	0,02297819	2,0755767	0,01512432
25,4	0,10538107	0,01648819	0,07755724	0,02123751	2,10954792	0,016533
25,5	0,10586334	0,0156236	0,07834246	0,02289665	2,15560744	0,01396247
25,6	0,10000904	0,01807665	0,08215835	0,02444866	2,13006146	0,0188449
25,7	0,10026696	0,01692231	0,07578843	0,02171847	2,08578797	0,01678657
25,8	0,1065526	0,01473552	0,07730551	0,02293188	2,12625969	0,01236172
25,9	0,10670143	0,01433772	0,0783406	0,02170884	2,1637377	0,01249494
26	0,10343108	0,01513847	0,08666093	0,02365952	2,14798532	0,02211848
26,1	0,09601704	0,01572341	0,07938738	0,02319996	2,10612171	0,02011872
26,2	0,09418647	0,01813894	0,08393797	0,02534918	2,1004444	0,01659713
26,3	0,10279766	0,01803142	0,07509992	0,02244632	2,04637978	0,01877498
26,4	0,10549649	0,01434065	0,07387469	0,02429315	2,10115359	0,01628591
26,5	0,11045222	0,01715631	0,07478159	0,02168304	2,11538636	0,01932914
26,6	0,11082521	0,01638678	0,0762008	0,02248104	2,11606176	0,01358794
26,7	0,10511415	0,01509977	0,07190365	0,02390796	2,13436994	0,01613338
26,8	0,10633505	0,01563486	0,07866991	0,02667388	2,11917635	0,01676129
26,9	0,10885609	0,01723517	0,0798308	0,02439024	2,12618126	0,01768518
27	0,11051781	0,01615364	0,0768644	0,02144844	2,11581262	0,02265997
27,1	0,11034113	0,01694461	0,0758707	0,02441096	2,11744981	0,01605043
27,2	0,1148364	0,01887046	0,07333035	0,02142537	2,10672344	0,01676378
27,3	0,11472172	0,01665171	0,0763465	0,02244165	2,13025135	0,01674147
27,4	0,10877006	0,01617994	0,0778326	0,02280304	2,1254834	0,01657999
27,5	0,11409957	0,01655148	0,07540608	0,02487124	2,17629969	0,01505481
27,6	0,10735437	0,01533634	0,07858216	0,02377796	2,21652082	0,00795545
27,7	0,1009489	0,01612688	0,08593576	0,02169555	2,1771729	0,01951263
27,8	0,09420257	0,01806932	0,08137919	0,02327041	2,16791463	0,02367395
27,9	0,09229516	0,01606117	0,07627924	0,02406913	2,16065692	0,02244039
28	0,09190691	0,01917384	0,08662386	0,02181537	2,16199845	0,01953819
28,1	0,09385306	0,01809271	0,08501283	0,02390986	2,12843532	0,02184866
28,2	0,08664143	0,01523264	0,08119461	0,02446455	2,10861337	0,02400295
28,3	0,07871653	0,01786704	0,08024007	0,02349954	2,1011542	0,02451524
28,4	0,08368259	0,01909286	0,08116792	0,02463444	2,06342554	0,02314427
28,5	0,0800388	0,01842786	0,08211713	0,02438574	2,04082764	0,0294661
28,6	0,07378834	0,02002083	0,07539758	0,02257668	1,98139909	0,03156948
28,7	0,08278723	0,02168686	0,07722408	0,02522276	2,01296497	0,02668427
28,8	0,07714094	0,0218894	0,07618088	0,02457757	1,96188556	0,02256144

28,9	0,07321258	0,021449	0,06982841	0,02235462	1,97669209	0,0306959
29	0,07085498	0,01955598	0,07619273	0,02309873	2,01006141	0,02966462
29,1	0,06980639	0,01847382	0,07478201	0,02172521	1,9230504	0,02433617
29,2	0,08092784	0,020806	0,07549203	0,02441425	2,0450328	0,02235239
29,3	0,09070632	0,01937732	0,08080855	0,02355948	2,04934944	0,02142193
29,4	0,10548445	0,01626392	0,07563646	0,02425727	2,06329991	0,02056092
29,5	0,09935254	0,01696152	0,08480759	0,02247857	2,11371512	0,0181014
29,6	0,09869561	0,01815197	0,07890176	0,02280398	2,1198121	0,01860805
29,7	0,10544591	0,0188231	0,07899306	0,02430556	2,11403509	0,01891447
29,8	0,101777758	0,01791249	0,08272562	0,02360985	2,10929809	0,01517776
29,9	0,10471864	0,01632855	0,08132788	0,02258108	2,11938284	0,0184877
30	0,10498348	0,01781727	0,0810485	0,02130035	2,13414307	0,01161025
30,1	0,10073471	0,0171727	0,08086218	0,02252811	2,12782155	0,01354342
30,2	0,10598652	0,01788468	0,08277168	0,0238756	2,18752478	0,01951456
30,3	0,10279314	0,01732112	0,08179922	0,02190079	2,13625646	0,01419244
30,4	0,10320781	0,0176812	0,08021775	0,02164035	2,130247	0,01543168
30,5	0,10125388	0,01743742	0,07703025	0,02224619	2,12574716	0,01936992
30,6	0,09838257	0,01791204	0,07895558	0,02321437	2,15394555	0,01648621
30,7	0,10461223	0,01964549	0,0785373	0,02335134	2,16957628	0,0154485
30,8	0,10316014	0,01626739	0,07747011	0,02204542	2,13013912	0,01737855
30,9	0,10773555	0,01833512	0,07624019	0,02261777	2,12718594	0,01597074
31	0,10906649	0,01627034	0,07665832	0,02342214	2,13105668	0,01180047
31,1	0,1054387	0,01792147	0,075199	0,02139014	2,12224841	0,01098412
31,2	0,1060417	0,01595081	0,08006594	0,02486188	2,14034931	0,01358938
31,3	0,10291893	0,01592952	0,07461956	0,02327134	2,14799324	0,01842129
31,4	0,09906817	0,01707611	0,08056534	0,02394222	2,13424584	0,01640733
31,5	0,11096699	0,01771178	0,0709813	0,02079793	2,09643081	0,0169067
31,6	0,10692927	0,01641261	0,0776114	0,02216826	2,12248752	0,0193354
31,7	0,11331419	0,015925	0,07316526	0,0230576	2,11672349	0,01408577
31,8	0,10710259	0,01533258	0,0778354	0,02511838	2,13271702	0,02385569
31,9	0,09920492	0,020103	0,08212866	0,02565956	2,10331587	0,01793459
32	0,10206572	0,01518781	0,07851557	0,02332414	2,11160331	0,02431858
32,1	0,10354187	0,0150631	0,07088253	0,02515041	2,10679875	0,01651061
32,2	0,10679174	0,01736268	0,07368991	0,025345	2,11747993	0,0189411
32,3	0,10345912	0,01603774	0,07915544	0,02457323	2,12111411	0,01221923
32,4	0,10790756	0,01631577	0,08005901	0,02145635	2,12332931	0,0182379
32,5	0,10510309	0,01677177	0,07415359	0,0202603	2,13377164	0,01373049
32,6	0,10939117	0,01691941	0,07595734	0,02227422	2,11546596	0,01916933
32,7	0,11237617	0,01819893	0,08086423	0,02420548	2,13066475	0,00963737
32,8	0,111158722	0,01700589	0,07614712	0,02374576	2,13046777	0,01410462
32,9	0,10681226	0,01783949	0,07315539	0,02224319	2,10955334	0,01527815
33	0,10594536	0,01665242	0,07840137	0,02128809	2,10788064	0,01368198
33,1	0,1123454	0,0168653	0,07654599	0,0222622	2,11310996	0,01740499
33,2	0,11035753	0,01585519	0,07343694	0,0228171	2,11664571	0,0190442
33,3	0,10599946	0,0157385	0,07393956	0,02259887	2,12021343	0,01555914
33,4	0,11486487	0,01651155	0,07530875	0,02232862	2,11714695	0,01409522
33,5	0,10924294	0,01667797	0,07358192	0,02115254	2,10879096	0,01482486
33,6	0,11110109	0,0162323	0,07913247	0,02358193	2,10573541	0,0175399

33,7	0,10957361	0,0176688	0,07126116	0,02321284	2,1015956	0,01582079
33,8	0,10766302	0,01682235	0,07490371	0,02328567	2,0934083	0,0132808
33,9	0,11131534	0,01412176	0,06895006	0,02398458	2,07791626	0,01636331
34	0,11278691	0,01622549	0,07417993	0,02172192	2,14180811	0,01385103
34,1	0,10644056	0,01501894	0,07694389	0,0209273	2,14685189	0,01767996
34,2	0,10538579	0,01760911	0,07384174	0,02294112	2,1764047	0,01451743
34,3	0,10157342	0,01600469	0,07867094	0,02195573	2,1693792	0,01753753
34,4	0,09417366	0,01582408	0,07948311	0,02407617	2,14191793	0,02017683
34,5	0,09741324	0,02076692	0,07878678	0,02431916	2,11904545	0,02158667
34,6	0,09470497	0,01968432	0,07731486	0,02381389	2,08516105	0,01794072
34,7	0,0933861	0,01987809	0,08060408	0,02447234	2,08183224	0,01928675
34,8	0,0975123	0,01587302	0,07402766	0,02450571	2,11050775	0,0176831
34,9	0,10289783	0,0194549	0,07972428	0,02639336	2,11087933	0,02163167
35	0,10212844	0,0178131	0,07344478	0,02452727	2,10518864	0,02160409
35,1	0,10637814	0,01827522	0,06941856	0,02595809	2,12992681	0,01827522
35,2	0,10792313	0,01903726	0,08086302	0,02338863	2,11404225	0,0206237
35,3	0,10660729	0,01694992	0,07788785	0,021994	2,10006362	0,01599564
35,4	0,104897	0,01526925	0,07336466	0,024485	2,1123961	0,01657933
35,5	0,10442766	0,01736692	0,07399032	0,02207046	2,09755325	0,01695988
35,6	0,11060138	0,01848656	0,07589935	0,0221657	2,0758085	0,01798692
35,7	0,10601772	0,01684778	0,07506164	0,02360515	2,04323806	0,02022646
35,8	0,11142011	0,01636654	0,07444723	0,02461819	2,07189423	0,01987691
35,9	0,10148616	0,01758851	0,07726219	0,02449666	2,06149162	0,02004272
36	0,10517946	0,01976374	0,07328487	0,02471604	2,06706043	0,01985461
36,1	0,10485119	0,0185674	0,07290434	0,02339128	2,06894512	0,01610995
36,2	0,10093907	0,01778342	0,07743955	0,02408928	2,07476296	0,01678537
36,3	0,09931849	0,01835529	0,07505679	0,02385279	2,06819627	0,01844616
36,4	0,10263027	0,01765585	0,07478836	0,02426547	2,05744941	0,02064376
36,5	0,10826211	0,01732013	0,07045629	0,02374169	2,08515353	0,01641568
36,6	0,10230248	0,01571106	0,08243792	0,02361174	2,07891648	0,01476298
36,7	0,1051426	0,01702223	0,0749607	0,02250168	2,101819	0,01477656
36,8	0,10418438	0,01888566	0,07970463	0,02398747	2,10669054	0,01754308
36,9	0,1072778	0,01713746	0,08460777	0,02370457	2,10021591	0,01533825
37	0,10371365	0,01713647	0,07543624	0,02255034	2,10067114	0,01628635
37,1	0,10809607	0,01822395	0,07476719	0,02214499	2,09045137	0,01929332
37,2	0,10870729	0,01494335	0,08087251	0,02364172	2,10344366	0,01703988
37,3	0,10783789	0,01580075	0,07779861	0,02209427	2,10681128	0,01450634
37,4	0,10821527	0,01626125	0,07881137	0,02254299	2,12857525	0,0162167
37,5	0,10773136	0,01554289	0,07593302	0,02302485	2,13302752	0,01692349
37,6	0,11140441	0,01369066	0,07874368	0,02272829	2,12464767	0,01601718
37,7	0,11018408	0,01337571	0,07831192	0,02454421	2,1339337	0,0196442
37,8	0,10884773	0,01645475	0,07510229	0,02345022	2,11676713	0,01588279
37,9	0,10849431	0,01600953	0,07510805	0,02363941	2,13813178	0,01706801
38	0,11359134	0,01470524	0,07616783	0,0232466	2,12204464	0,01043455
38,1	0,11122971	0,01565488	0,07698466	0,02379364	2,12759618	0,01778964
38,2	0,10691741	0,01302256	0,07729661	0,02176312	2,14885446	0,01284598
38,3	0,10485617	0,01612832	0,07701825	0,02403782	2,12964518	0,01877955
38,4	0,10905295	0,01536958	0,07755864	0,02274343	2,13850391	0,01936745

38,5	0,10389957	0,01673789	0,08155271	0,02621973	2,14302885	0,01549145
38,6	0,10417038	0,0183568	0,07690251	0,02365888	2,14988416	0,0183568
38,7	0,09963165	0,01544402	0,08072605	0,02618382	2,12199885	0,02050326
38,8	0,10550136	0,01687319	0,0756657	0,02605677	2,12118815	0,02038844
38,9	0,10536884	0,01562636	0,07948494	0,02584024	2,19262331	0,01601921
39	0,10151928	0,01831035	0,07675419	0,02511636	2,21344516	0,01514885
39,1	0,09853918	0,0189907	0,07401505	0,02324037	2,21243913	0,01053564
39,2	0,09777679	0,01662961	0,08328146	0,02449978	2,18008004	0,01831925
39,3	0,08911338	0,01844503	0,08496437	0,02412736	2,16167584	0,02083521
39,4	0,09156506	0,02036809	0,08119834	0,02228616	2,14796548	0,01995707
39,5	0,09130596	0,02085268	0,07960245	0,0241501	2,13185027	0,02048114
39,6	0,08872173	0,02022986	0,08091945	0,01976266	2,10152308	0,0230798
39,7	0,08817001	0,01709563	0,07948052	0,0231405	2,05567887	0,01770956
39,8	0,08941683	0,01833232	0,08151335	0,0230557	2,02880793	0,0400318
39,9	0,08751826	0,01771366	0,07989408	0,02022462	2,00808072	0,02629657
40	0,08684152	0,01627438	0,07375028	0,01954719	2,00668012	0,02304416
40,1	0,09074874	0,017065	0,07822559	0,02054855	2,02434077	0,02350295
40,2	0,09036629	0,01715012	0,07164938	0,01994495	2,07753547	0,02083422
40,3	0,09157872	0,01468878	0,07374542	0,02175318	2,05397372	0,01744562
40,4	0,09038004	0,01269729	0,06533815	0,01979543	2,02226435	0,01997178
40,5	0,09832378	0,01676224	0,07640053	0,02112925	2,11526246	0,01945302
40,6	0,09827579	0,01570658	0,0799807	0,02215593	2,18799632	0,01399553
40,7	0,10243171	0,01778543	0,073569	0,02219869	2,19952337	0,01438722
40,8	0,10441144	0,01551762	0,07528264	0,0237198	2,18780758	0,01534028
40,9	0,10123884	0,01753919	0,0694463	0,02277874	2,16140491	0,01673993
41	0,10408045	0,01686468	0,07711476	0,02238241	2,16375206	0,01432831
41,1	0,10242177	0,01759255	0,07771163	0,0212185	2,16545056	0,01665249
41,2	0,09761321	0,01516841	0,07329913	0,02194959	2,16181129	0,01659603
41,3	0,10831539	0,01583244	0,07656082	0,02381593	2,16585935	0,01888231
41,4	0,09907641	0,01702584	0,07426066	0,02043101	2,06535125	0,01571975
41,5	0,10582059	0,01547592	0,07290573	0,02200411	2,11869436	0,01921936
41,6	0,09905618	0,01597241	0,07450767	0,02259733	2,12060986	0,01547327
41,7	0,10579973	0,01454463	0,07458088	0,02170367	2,16198459	0,01558677
41,8	0,09939112	0,01616225	0,07449857	0,02166905	2,15768267	0,01258059
41,9	0,10775378	0,01486104	0,07502357	0,02056301	2,14452476	0,01400799
42	0,10733904	0,01688429	0,07528141	0,02368303	2,12971634	0,01445295
42,1	0,10484199	0,01876215	0,07333062	0,02540802	2,1170939	0,02188164
42,2	0,10180018	0,01714672	0,0759676	0,02592259	2,10009001	0,01827183
42,3	0,09944876	0,01879631	0,07062172	0,02349539	2,09994578	0,01707934
42,4	0,10015812	0,01707703	0,07183194	0,02299526	2,09017393	0,01861306
42,5	0,10282194	0,01834488	0,07519138	0,02455044	2,08982199	0,0159442
42,6	0,10207651	0,01784994	0,07929318	0,02318698	2,11777369	0,01574203
42,7	0,10558562	0,01587586	0,06945128	0,02383614	2,12960064	0,01475784
42,8	0,1079028	0,01612545	0,07169828	0,02234463	2,11816445	0,01616987
42,9	0,10971018	0,01505998	0,08020314	0,0191752	2,14171264	0,0141844
43	0,10246262	0,01710642	0,07726473	0,02220756	2,13764292	0,01649077
43,1	0,10044604	0,01609236	0,07280917	0,02238937	2,14487493	0,01185062
43,2	0,10355831	0,01595559	0,07545025	0,0219444	2,14753453	0,01333275

43,3	0,10387842	0,01686652	0,07871041	0,02182984	2,16163746	0,01585628
43,4	0,10372154	0,01440455	0,07302977	0,02044659	2,16304729	0,01768827
43,5	0,10380027	0,01604065	0,07149801	0,02015024	2,14966858	0,0142289
43,6	0,10488893	0,01744469	0,07225191	0,01987369	2,16830809	0,01351411
43,7	0,10051501	0,01597416	0,07441515	0,02156075	2,18736906	0,01579958
43,8	0,10125637	0,01849411	0,06628888	0,02262344	2,16802847	0,01440872
43,9	0,10129904	0,01793291	0,07514325	0,02103836	2,19188208	0,0136465
44	0,10436416	0,01622683	0,07605261	0,0213084	2,24865488	0,01567171
44,1	0,10196749	0,01398631	0,07643285	0,02014542	2,28691189	0,01347305
44,2	0,10376273	0,01683215	0,07802446	0,0202838	2,29518047	0,01819576
44,3	0,10138209	0,0168684	0,08013563	0,02086016	2,31363207	0,00909949
44,4	0,10120513	0,016198	0,08392726	0,019524	2,2905706	0,0121809
44,5	0,10180917	0,01922241	0,08036879	0,02100548	2,22501522	0,01452553
44,6	0,09687405	0,01608754	0,07974016	0,02123207	2,13502202	0,01974975
44,7	0,10003367	0,01653901	0,06977527	0,02238869	2,11892938	0,01830654
44,8	0,10483193	0,0184874	0,07340336	0,02142857	2,1352521	0,01109244
44,9	0,10123415	0,01603121	0,07396412	0,02145977	2,16769159	0,01488613
45	0,10819205	0,01747121	0,08097149	0,02376947	2,16655882	0,01043958
45,1	0,11011712	0,01633606	0,07588919	0,02268897	2,15553827	0,01828083
45,2	0,10378468	0,01733374	0,07521449	0,02190671	2,16458342	0,01829189
45,3	0,10511745	0,01821171	0,07340918	0,02245101	2,18354458	0,01509712
45,4	0,10919092	0,01524602	0,07549376	0,02130977	2,18087318	0,0131237
45,5	0,10956635	0,01582044	0,0758771	0,02227065	2,16809763	0,01141861
45,6	0,103975	0,0163754	0,08288947	0,02460712	2,1550821	0,01241361
45,7	0,10377609	0,01605058	0,07693668	0,02113548	2,15294482	0,01534312
45,8	0,11105233	0,01617952	0,07763523	0,02455584	2,15178768	0,01573866
45,9	0,11452231	0,01497599	0,07201691	0,02356517	2,17711316	0,01783905
46	0,10999474	0,01377676	0,07555283	0,02031415	2,19217269	0,01180239
46,1	0,10497238	0,01657459	0,08339911	0,02407261	2,18372358	0,01539069
46,2	0,10473805	0,01680128	0,07515225	0,02388459	2,16658748	0,01451216
46,3	0,10265586	0,01599552	0,07730448	0,02121238	2,09084246	0,01405536
46,4	0,11212309	0,0168204	0,06670026	0,02267266	2,19238819	0,01131695
46,5	0,10637481	0,01702509	0,06315071	0,02099334	2,06195597	0,01655573
46,6	0,10392071	0,01409692	0,06656388	0,02110132	1,99339207	0,01555066
46,7	0,10104204	0,01344852	0,0535269	0,02057357	1,94812077	0,01522978
46,8	0,10348116	0,01443621	0,05653098	0,02124247	1,9835696	0,01122816
46,9	0,10965351	0,01640846	0,0641346	0,02186407	2,10565551	0,00812094
47	0,113163	0,01690699	0,06522472	0,01943672	2,09701493	0,00885404
47,1	0,111928	0,01542232	0,06874551	0,01973212	2,08797059	0,00938015
47,2	0,1097098	0,01514257	0,0711996	0,02206006	2,1042686	0,01265396
47,3	0,11084327	0,01332149	0,06275903	0,02000338	2,11346528	0,01632411
47,4	0,10867619	0,0140695	0,06514602	0,01965466	2,12231934	0,01257728
47,5	0,11457502	0,016764	0,06793832	0,02155372	2,21574724	0,01373892
47,6	0,10765762	0,01295428	0,06640729	0,02122204	2,13745689	0,01326377
47,7	0,10515968	0,01266984	0,06929093	0,01983486	2,13499935	0,01000481
47,8	0,11364915	0,01553104	0,0682241	0,02093878	2,19978369	0,00934458
47,9	0,10821495	0,0131196	0,07363482	0,02063513	2,18958252	0,01437943
48	0,10924756	0,01409511	0,07009913	0,02032707	2,22920239	0,01334226

48,1	0,09677717	0,01449811	0,06944316	0,02013113	2,15583156	0,01191246
48,2	0,09918304	0,01647696	0,06595374	0,01950615	2,14498807	0,01390674
48,3	0,10436501	0,01562781	0,0737381	0,02191486	2,2362134	0,01266391
48,4	0,09858902	0,01514335	0,07697493	0,02129954	2,23227285	0,00957131
48,5	0,09801738	0,01621742	0,07320116	0,02102918	2,23956338	0,01349967
48,6	0,09194475	0,01941425	0,07376466	0,02273698	2,1471021	0,0200788
48,7	0,0890955	0,01770697	0,07293029	0,02326668	2,15370959	0,01429639
48,8	0,09359076	0,01926044	0,07676126	0,02356131	2,19363284	0,0119209
48,9	0,09053631	0,0149742	0,07316624	0,0209178	2,18535754	0,01819941
49	0,08846468	0,01750249	0,07984946	0,02267162	2,18663281	0,01750249
49,1	0,09123678	0,01643105	0,07911244	0,02223575	2,1555566	0,01493306
49,2	0,09063054	0,01828889	0,07717719	0,02120937	2,13635276	0,01718772
49,3	0,09196533	0,01761537	0,08006559	0,02220661	2,17877723	0,01625674
49,4	0,08656702	0,01660256	0,07731633	0,01903695	2,11509811	0,01397342
49,5	0,0939679	0,02040339	0,07777622	0,02264963	2,17361599	0,01895269
49,6	0,08883046	0,020893	0,0792995	0,02314663	2,15841119	0,01723086
49,7	0,08798954	0,0196051	0,08322831	0,02217243	2,16402931	0,01825141
49,8	0,08657886	0,0227541	0,0794033	0,02431195	2,15153661	0,02020488
49,9	0,08789044	0,02162086	0,07832286	0,02298096	2,14346684	0,01782197
50	0,08361799	0,02110336	0,08137195	0,02475317	2,15497637	0,01740677
50,1	0,08158163	0,01902954	0,0793129	0,02157607	2,1508473	0,020000185
50,2	0,0894958	0,0197479	0,08347339	0,02287582	2,13132586	0,02329599
50,3	0,09000141	0,02114096	0,08386069	0,02193784	2,11020485	0,02123471
50,4	0,08812188	0,01999524	0,08978815	0,02332778	2,1154487	0,02032849
50,5	0,09125118	0,01956726	0,07841016	0,02285983	2,11312324	0,02436501
50,6	0,08118308	0,02165197	0,08335299	0,02448229	2,06939007	0,02146328
50,7	0,08300005	0,01915024	0,08582318	0,02503176	2,06761398	0,02234979
50,8	0,08350344	0,02425825	0,07453121	0,02629955	2,04742464	0,02682174
50,9	0,08110927	0,02047879	0,0855653	0,02526665	2,04678834	0,02735245
51	0,08186143	0,02359757	0,08322736	0,02661203	2,05298855	0,02816636
51,1	0,07750624	0,02335547	0,0799548	0,02505062	2,01718699	0,02439139
51,2	0,08235349	0,02304774	0,08478943	0,02496838	2,01456879	0,03794444
51,3	0,08298419	0,0219482	0,07560465	0,02437631	1,9737669	0,03346982
51,4	0,08347979	0,02261585	0,08519101	0,02705578	1,9883452	0,02372584
51,5	0,07882456	0,02254771	0,08450769	0,0288777	1,95846232	0,02619785
51,6	0,07169793	0,02396296	0,07842857	0,02367655	1,90324121	0,02792496

Running average of ITRAX measurements from surface core from 2019.

DEPTH	RA-K	RA-CA	RA-TI	RA-MN	RA-FE	RA-ZR
0,8	0,12575704	0,01486967	0,07366436	0,0174629	2,10128389	0,01464888
0,9	0,12600501	0,01465976	0,07353194	0,01730723	2,09720642	0,01435787
1	0,12616975	0,01466665	0,07352965	0,01747638	2,09381706	0,01414969
1,1	0,12610274	0,01473132	0,07326212	0,01750485	2,0893854	0,01399951
1,2	0,12677698	0,01486392	0,07331545	0,01755641	2,08189064	0,01421902
1,3	0,1275202	0,01475389	0,07330187	0,01739352	2,07181415	0,01399626
1,4	0,12812296	0,01471014	0,07335718	0,01704938	2,06173616	0,01362351
1,5	0,12987876	0,01414047	0,07374924	0,01684889	2,05569928	0,01335326
1,6	0,13052138	0,01414651	0,07393732	0,01674718	2,05280277	0,01309346
1,7	0,13184341	0,01378156	0,07371385	0,01634331	2,04961744	0,01313613
1,8	0,13225742	0,01369267	0,07377776	0,01628618	2,04825127	0,01321809
1,9	0,13263172	0,01355497	0,07374181	0,01599196	2,05117118	0,01321605
2	0,132902	0,0137947	0,07405863	0,01602336	2,05280358	0,01358741
2,1	0,13319558	0,01376973	0,07491099	0,0158475	2,05371401	0,01370903
2,2	0,13368299	0,01372133	0,07558087	0,01595245	2,05513441	0,01386216
2,3	0,13333405	0,01362492	0,07568942	0,01621696	2,05969612	0,01338262
2,4	0,1331643	0,01364814	0,07549083	0,01652718	2,06345188	0,01338327
2,5	0,13274775	0,01364952	0,07560772	0,01687045	2,06750156	0,01363346
2,6	0,13216007	0,01404458	0,07542023	0,01711877	2,06987056	0,01328416
2,7	0,1327872	0,01388795	0,07515465	0,01721157	2,07168391	0,01344188
2,8	0,1322787	0,0138779	0,07555241	0,01744614	2,07377107	0,01325407
2,9	0,13128941	0,01385878	0,07511582	0,01791396	2,07771723	0,01318425
3	0,13021077	0,01391883	0,07521118	0,01834567	2,07851709	0,01271442
3,1	0,12968532	0,01400493	0,0749504	0,01845721	2,07566035	0,01263451
3,2	0,12930397	0,01382186	0,07454293	0,01852602	2,07304755	0,01253019
3,3	0,12930966	0,0136601	0,07412047	0,01831835	2,07122639	0,01212894
3,4	0,12896228	0,013714	0,07396959	0,01790442	2,06770106	0,0128781
3,5	0,12838842	0,01368975	0,07455296	0,01771995	2,0688849	0,01324466
3,6	0,12813793	0,01363422	0,07472071	0,0175529	2,06880658	0,01316964
3,7	0,12762476	0,0134113	0,07455235	0,01761554	2,06757241	0,01404199
3,8	0,12603896	0,01353781	0,07460709	0,01775879	2,06568332	0,01393412
3,9	0,12632347	0,01340485	0,07450601	0,01772342	2,06124452	0,01410024
4	0,12612355	0,01330268	0,0743819	0,01736077	2,0553656	0,01414245
4,1	0,12626369	0,0130169	0,07410117	0,01721668	2,04996526	0,01441967
4,2	0,12633562	0,01295557	0,07361823	0,01700719	2,04869459	0,01470801
4,3	0,12638609	0,01292643	0,07288391	0,01665383	2,04685595	0,01469567
4,4	0,12625162	0,01316938	0,07262718	0,01644114	2,04060033	0,01495548
4,5	0,126181	0,01318148	0,07239847	0,01646	2,0360545	0,01449983
4,6	0,126152	0,01320823	0,07180182	0,01626367	2,03015951	0,01430999
4,7	0,12580278	0,01319225	0,07115732	0,01631944	2,02458557	0,01422814
4,8	0,12588568	0,0129856	0,07098202	0,01615395	2,02060097	0,01348981
4,9	0,12618713	0,0129674	0,07052789	0,01593499	2,01601518	0,0136662
5	0,12497323	0,01309378	0,07004737	0,01578447	2,01441194	0,01334022

5,1	0,12508558	0,01311481	0,07031135	0,01581034	2,01101324	0,01301937
5,2	0,12466379	0,01306724	0,06997683	0,01549992	2,00885921	0,0126199
5,3	0,12394687	0,01308108	0,07014227	0,01553161	2,00315746	0,01209941
5,4	0,12288203	0,01333675	0,06958157	0,01559601	1,99563652	0,01197873
5,5	0,12188679	0,01324527	0,06944515	0,01570722	1,99160292	0,01205251
5,6	0,12056175	0,01302446	0,06849678	0,01544929	1,97945816	0,01219265
5,7	0,11955703	0,01325846	0,06838213	0,01558832	1,97657252	0,01202428
5,8	0,11939973	0,01331028	0,06822676	0,01550241	1,97131085	0,01213851
5,9	0,11867564	0,01351297	0,06808218	0,01526448	1,96328663	0,01227303
6	0,11830006	0,01326161	0,06802116	0,01532813	1,96150116	0,01219134
6,1	0,11868996	0,01325071	0,06803857	0,01567519	1,96334363	0,01224162
6,2	0,11740813	0,01317527	0,06687572	0,01562677	1,95167341	0,01223709
6,3	0,11621701	0,0134558	0,06671396	0,01580851	1,93997752	0,01291334
6,4	0,11598335	0,01349438	0,06673853	0,01598774	1,93796108	0,0129825
6,5	0,11615438	0,01337206	0,06671402	0,01611337	1,93972646	0,01299504
6,6	0,11611681	0,01334411	0,06673514	0,01612194	1,93918602	0,01308661
6,7	0,11708141	0,01334378	0,06705813	0,01641894	1,94902743	0,01318713
6,8	0,11773377	0,01303419	0,06696256	0,01619103	1,9490237	0,01307577
6,9	0,1181838	0,01300749	0,06728825	0,01614262	1,95321839	0,01304677
7	0,11813851	0,01305504	0,06728393	0,01651246	1,96067834	0,01271106
7,1	0,11798442	0,01319263	0,06702025	0,01662276	1,9627017	0,01286381
7,2	0,11757911	0,01308888	0,06698236	0,01631264	1,95913551	0,01309341
7,3	0,11798024	0,01309787	0,06765186	0,01677112	1,97092445	0,0132378
7,4	0,11875661	0,01299174	0,06770252	0,01682284	1,98245997	0,01303024
7,5	0,11896455	0,01284824	0,06708419	0,01648605	1,98431234	0,01344795
7,6	0,11888935	0,01282891	0,06774079	0,01621195	1,98497111	0,0136323
7,7	0,11895918	0,0126656	0,06782809	0,01623655	1,9894938	0,01381125
7,8	0,11861791	0,01271597	0,06868683	0,01602201	1,99196324	0,01387775
7,9	0,11819514	0,01284297	0,0686017	0,01604378	1,99377428	0,01401569
8	0,1172814	0,01286574	0,06890641	0,01603377	1,99627973	0,01429304
8,1	0,11685444	0,01299784	0,0691959	0,01574769	1,99633407	0,01469222
8,2	0,11617183	0,01308547	0,06887038	0,01558115	1,99694718	0,01460311
8,3	0,11594735	0,01307092	0,06838062	0,01561673	1,99881992	0,01471731
8,4	0,11565539	0,01335369	0,06856992	0,01525524	2,00146025	0,01440159
8,5	0,11482866	0,01323864	0,0687807	0,01518496	2,00178911	0,01464576
8,6	0,11403297	0,01314217	0,06941881	0,01530535	2,00195604	0,01464764
8,7	0,11409285	0,01326537	0,06928485	0,01534531	2,00071883	0,01439931
8,8	0,11378749	0,0134299	0,06954114	0,01522309	1,99864607	0,01374288
8,9	0,11363629	0,0136941	0,069451	0,01534782	1,9969006	0,01302484
9	0,11335779	0,01375118	0,0699895	0,01542839	1,99889405	0,01287518
9,1	0,1133829	0,01360297	0,06942203	0,015447	1,99746784	0,01292355
9,2	0,11373276	0,01364121	0,06914339	0,01558726	1,99707711	0,01282317
9,3	0,11397309	0,01365066	0,07003689	0,01556036	1,99928773	0,01240382
9,4	0,1138862	0,01360672	0,07056781	0,0156251	2,00057066	0,01214552
9,5	0,11403314	0,01336381	0,07064741	0,01553571	2,00102923	0,01222272
9,6	0,11459991	0,01352921	0,07045293	0,01546855	2,00038677	0,01197987
9,7	0,11486101	0,01377818	0,07076465	0,0153813	2,00217666	0,0114958
9,8	0,11456872	0,01365657	0,07114316	0,01543187	2,00293767	0,0115428

9,9	0,11497708	0,01357809	0,07116217	0,01539986	2,00317717	0,01195307
10	0,1153773	0,01331769	0,07095528	0,01530496	2,00072512	0,01211641
10,1	0,11574615	0,01312483	0,07103224	0,01543389	1,99657616	0,0123102
10,2	0,11657493	0,01318582	0,07126392	0,01536598	1,99368985	0,01170262
10,3	0,11736942	0,01288594	0,07159412	0,01528719	1,99195586	0,01189774
10,4	0,11834759	0,0127809	0,07145035	0,01545153	1,98705353	0,01229167
10,5	0,11883615	0,01310998	0,0715692	0,01538202	1,98254133	0,01247832
10,6	0,11970741	0,0130287	0,07180575	0,01538718	1,97695863	0,01279621
10,7	0,12003183	0,01307251	0,07181244	0,0156281	1,97446135	0,01265619
10,8	0,12042635	0,01284538	0,07158296	0,01587231	1,97059769	0,01243988
10,9	0,12081903	0,01283456	0,0713355	0,0160106	1,96737645	0,01267051
11	0,12066239	0,01284566	0,07082278	0,01625232	1,96554555	0,01266622
11,1	0,12028582	0,0129206	0,07073995	0,01632783	1,96389474	0,012737
11,2	0,12044859	0,01282994	0,07031469	0,01637747	1,96198713	0,01289498
11,3	0,12018368	0,01293056	0,06961185	0,01654127	1,96162278	0,01348099
11,4	0,12010526	0,01307439	0,06909654	0,01656273	1,95975017	0,01325168
11,5	0,12037869	0,01327353	0,06871773	0,01662989	1,95836169	0,01333668
11,6	0,12117712	0,01313415	0,0685908	0,01658151	1,96054189	0,01289009
11,7	0,12111818	0,01338648	0,06861261	0,01698821	1,96572924	0,01308676
11,8	0,12070996	0,01350656	0,06941902	0,01730689	1,97065779	0,01274368
11,9	0,12063648	0,01352263	0,06963529	0,01772041	1,97611879	0,01300328
12	0,11990289	0,01351493	0,06942186	0,01794094	1,98384256	0,01273507
12,1	0,11912785	0,01358465	0,06955774	0,01819414	1,99146635	0,01251614
12,2	0,1188388	0,01358069	0,0700687	0,01858425	2,0018285	0,01249207
12,3	0,11850369	0,01406141	0,06993183	0,0187775	2,01008312	0,01216101
12,4	0,11779134	0,01407318	0,07064658	0,01907193	2,0163274	0,01223824
12,5	0,11666481	0,01409954	0,07062201	0,01951898	2,02463729	0,01216454
12,6	0,1151943	0,01419209	0,07098374	0,01950849	2,03068873	0,01186283
12,7	0,11404475	0,01415464	0,07053952	0,01994187	2,03093474	0,01207436
12,8	0,11379939	0,01423356	0,07032432	0,02001438	2,03357175	0,0116688
12,9	0,11422018	0,01410532	0,06979495	0,01997502	2,03517238	0,01200196
13	0,11476459	0,0141788	0,06954433	0,01954396	2,03583119	0,01172508
13,1	0,11546209	0,01420148	0,06950391	0,01958209	2,03523956	0,01192355
13,2	0,11674516	0,0142506	0,06954495	0,01977603	2,03501432	0,01174393
13,3	0,11732285	0,01432532	0,06888995	0,01999056	2,03524102	0,0117626
13,4	0,11761089	0,01398417	0,06951207	0,02033408	2,03675054	0,01175282
13,5	0,11831262	0,01427867	0,06954305	0,02074163	2,04082995	0,01091901
13,6	0,11856008	0,01443887	0,07006996	0,02085437	2,04176616	0,01076562
13,7	0,11887415	0,0143699	0,07084682	0,02120704	2,04479357	0,01088931
13,8	0,11832933	0,01468162	0,07169731	0,02135294	2,05040961	0,01117672
13,9	0,11734775	0,01471543	0,07189763	0,02148161	2,04894455	0,01155557
14	0,11637237	0,01495287	0,0718428	0,0214064	2,05020133	0,01158936
14,1	0,11498929	0,01516012	0,07230583	0,02165646	2,05246	0,01217881
14,2	0,11444932	0,01551873	0,07257229	0,02163841	2,05223355	0,01221782
14,3	0,1138499	0,01541893	0,07254487	0,02133158	2,04801651	0,01272123
14,4	0,1135714	0,01541751	0,07271494	0,02090704	2,0428081	0,0126778
14,5	0,11385503	0,01560424	0,07245849	0,02037014	2,0372417	0,013253
14,6	0,11406665	0,0153702	0,07245758	0,01963966	2,03164088	0,0137812

14,7	0,11491733	0,01529092	0,07230481	0,01944937	2,02907262	0,01387865
14,8	0,11598357	0,01522127	0,07171948	0,01913245	2,02566271	0,01426057
14,9	0,11695265	0,01500241	0,07139015	0,01871785	2,02364974	0,01384239
15	0,11811999	0,01487287	0,07162258	0,01850673	2,02575389	0,01330027
15,1	0,11873048	0,01461641	0,07169764	0,01850141	2,02476634	0,01343966
15,2	0,11980116	0,01433603	0,07152817	0,01865237	2,02179421	0,01346874
15,3	0,12021913	0,01419063	0,07163419	0,01873754	2,01974387	0,01306443
15,4	0,12073806	0,01428044	0,07227121	0,0185975	2,02030417	0,01282951
15,5	0,12143091	0,01418699	0,0727242	0,01864711	2,02290269	0,01285716
15,6	0,12150982	0,01423505	0,07284527	0,01886566	2,02878812	0,01240451
15,7	0,12109528	0,0143306	0,07292232	0,01897083	2,03338423	0,01274529
15,8	0,12028891	0,01432873	0,0734183	0,01878074	2,0376119	0,01278227
15,9	0,11950637	0,01431072	0,07381701	0,01909486	2,04000683	0,01245958
16	0,11943386	0,01433593	0,0732367	0,0194172	2,03933124	0,01298641
16,1	0,11885272	0,01435447	0,07239654	0,01960961	2,03935245	0,01296288
16,2	0,11877451	0,0145076	0,07171268	0,01985074	2,03894257	0,01242207
16,3	0,11863226	0,01456847	0,07160605	0,01983727	2,04221493	0,01173652
16,4	0,11854602	0,01429785	0,07192688	0,01983421	2,04925945	0,01205265
16,5	0,11808443	0,01422562	0,07166548	0,02005158	2,06055392	0,01221882
16,6	0,11628151	0,01441983	0,07157456	0,02013188	2,06704638	0,01225585
16,7	0,11379052	0,01443429	0,07195295	0,02020926	2,07294903	0,01264965
16,8	0,11199943	0,01454904	0,07272334	0,02063978	2,07959093	0,01254265
16,9	0,11030882	0,01463118	0,07295838	0,02085948	2,08458584	0,0137801
17	0,10830501	0,01484332	0,07301475	0,02063743	2,08972721	0,01425473
17,1	0,10599631	0,0150295	0,07457237	0,020707	2,09453438	0,01447193
17,2	0,10468746	0,01495746	0,07599735	0,02077563	2,0942728	0,01508644
17,3	0,10378646	0,01531704	0,07670465	0,02071801	2,09739318	0,01567961
17,4	0,10280053	0,01564631	0,07704249	0,02048066	2,1019214	0,01610655
17,5	0,10173274	0,0160762	0,07711299	0,0205319	2,10483995	0,01640993
17,6	0,10087503	0,01637785	0,07734538	0,02034533	2,10305999	0,0159032
17,7	0,10135889	0,01634554	0,0776115	0,02027027	2,10294943	0,01574988
17,8	0,10261062	0,01635669	0,07717853	0,02008149	2,09661642	0,01566322
17,9	0,10370276	0,01626054	0,07652586	0,01993833	2,09163938	0,01556807
18	0,10435463	0,01615921	0,07644051	0,01977782	2,08832507	0,014772
18,1	0,10493824	0,01605704	0,07616118	0,01966973	2,08272585	0,01466436
18,2	0,10533687	0,01599785	0,07559398	0,01963696	2,07912583	0,0144819
18,3	0,10555843	0,01606134	0,07518617	0,01957039	2,07982788	0,01428407
18,4	0,10611972	0,01570952	0,07526518	0,01944445	2,07929906	0,01397815
18,5	0,1062858	0,01555987	0,07535134	0,01962062	2,07446898	0,01419994
18,6	0,1072095	0,01549023	0,07504983	0,01949155	2,06972653	0,0139499
18,7	0,1082943	0,01518234	0,07497214	0,01939312	2,06609826	0,01458115
18,8	0,10915653	0,01505381	0,07450903	0,01928645	2,06628289	0,01460958
18,9	0,1096276	0,01501667	0,07463241	0,01931541	2,07279165	0,01443769
19	0,10938117	0,01479115	0,07495165	0,01906387	2,07363797	0,01435456
19,1	0,11010924	0,01489701	0,0743803	0,01919748	2,07296676	0,01367132
19,2	0,11124438	0,01462338	0,07446016	0,019319	2,0775784	0,01301556
19,3	0,11249915	0,01449069	0,07383099	0,01928557	2,08184978	0,01281823
19,4	0,11372586	0,01458838	0,07384931	0,01915459	2,08545461	0,01255521

19,5	0,11373479	0,01443553	0,07389624	0,01915357	2,08688065	0,01263478
19,6	0,11419659	0,01450083	0,07351808	0,01902281	2,08999486	0,01210253
19,7	0,11464224	0,01455482	0,07346555	0,01906353	2,09269459	0,0118927
19,8	0,11395098	0,01465729	0,07282885	0,01934667	2,09456683	0,0114563
19,9	0,11391225	0,0146501	0,07319703	0,01958768	2,09378994	0,01141185
20	0,11357778	0,01482526	0,07346015	0,0197931	2,09534121	0,01141152
20,1	0,11366017	0,01514841	0,073439	0,02027037	2,09792503	0,01142239
20,2	0,11383268	0,01504843	0,07362623	0,02055878	2,10137525	0,01184653
20,3	0,11356956	0,01522598	0,07322572	0,02078634	2,1039399	0,01247598
20,4	0,11266771	0,01520555	0,07384827	0,02078843	2,10820225	0,01275101
20,5	0,11115225	0,01524769	0,07340107	0,02088712	2,10753635	0,01318261
20,6	0,10904952	0,015651	0,07386669	0,02112719	2,1053427	0,01352978
20,7	0,10662274	0,01589589	0,07448443	0,02181336	2,09859206	0,01466488
20,8	0,10536927	0,01617805	0,07442513	0,02240875	2,09296667	0,01553792
20,9	0,10431637	0,01638819	0,07514229	0,02271198	2,09025514	0,01635481
21	0,10285152	0,01666598	0,07455656	0,02293988	2,08861131	0,01711284
21,1	0,10190324	0,01668904	0,07403814	0,02279538	2,08337883	0,01738036
21,2	0,10132077	0,01664497	0,07397142	0,02240793	2,08049533	0,01764022
21,3	0,10067447	0,01683619	0,07401663	0,02231218	2,07715776	0,01785626
21,4	0,10006285	0,01703904	0,07419038	0,02237221	2,0720253	0,01783102
21,5	0,10029323	0,01707969	0,07379048	0,02221034	2,06494083	0,01773097
21,6	0,10084225	0,01740962	0,0735738	0,02220036	2,06119832	0,01769492
21,7	0,10271187	0,01730004	0,07363161	0,02211294	2,06014421	0,01745972
21,8	0,10465964	0,0171514	0,07354519	0,02170349	2,06295033	0,01663889
21,9	0,10526992	0,0167908	0,07330555	0,02119134	2,06576767	0,01600739
22	0,10658899	0,01661403	0,07331359	0,02102702	2,0653096	0,0149623
22,1	0,10780095	0,01647541	0,0737421	0,02087984	2,06617031	0,01436481
22,2	0,10885756	0,01632474	0,07394028	0,02098168	2,06621141	0,01407946
22,3	0,10983726	0,01622269	0,07389695	0,02107046	2,06396904	0,0138173
22,4	0,11027895	0,01620861	0,07419999	0,02088755	2,06698525	0,0133721
22,5	0,11042283	0,01636444	0,07462429	0,02080373	2,07079427	0,01340942
22,6	0,11038378	0,01652709	0,07490204	0,02096381	2,07763591	0,0136415
22,7	0,11107853	0,01634037	0,07529483	0,02099582	2,0834869	0,0139548
22,8	0,11104928	0,01634071	0,0744562	0,02095354	2,09138923	0,01397709
22,9	0,11087434	0,01630357	0,07403399	0,02091579	2,09747617	0,01416749
23	0,11061404	0,01631144	0,07458344	0,02104098	2,10250335	0,01471619
23,1	0,11028103	0,01648074	0,07416698	0,02100346	2,10971982	0,01500676
23,2	0,10945916	0,01655545	0,07373263	0,02070379	2,11531254	0,01500879
23,3	0,10836613	0,01667324	0,07455897	0,02069049	2,12042702	0,01523708
23,4	0,10636062	0,01704533	0,07508653	0,0206517	2,12208543	0,01591778
23,5	0,10527516	0,01707882	0,07524347	0,02082633	2,12084486	0,01726679
23,6	0,1047955	0,01686435	0,07511662	0,02080607	2,11446947	0,01787086
23,7	0,10493719	0,01684969	0,07545561	0,02075281	2,10946764	0,01801542
23,8	0,1046941	0,01672985	0,07472879	0,0208151	2,10955433	0,01763461
23,9	0,10458087	0,01672086	0,07528554	0,0209583	2,11329837	0,01792693
24	0,10458438	0,01657342	0,0753242	0,02121634	2,12030866	0,01799554
24,1	0,10332822	0,01675845	0,07589252	0,02110038	2,12571684	0,01721745
24,2	0,10170098	0,01664479	0,07678721	0,02141484	2,12961739	0,01758055

24,3	0,09994243	0,01682305	0,07841078	0,02199099	2,13072943	0,01791828
24,4	0,0987667	0,01702042	0,07888684	0,0221697	2,1309259	0,01851799
24,5	0,09775961	0,01730117	0,07965694	0,02267443	2,13218322	0,01891175
24,6	0,09631646	0,01768329	0,07939927	0,02296787	2,1239044	0,0187203
24,7	0,09585108	0,01800875	0,08002333	0,02320551	2,12948215	0,01847247
24,8	0,09523396	0,01819954	0,07992822	0,02347392	2,12908277	0,01808328
24,9	0,09475077	0,0182597	0,08094495	0,02338386	2,12847724	0,01816368
25	0,09463043	0,018133	0,08113951	0,02343213	2,12692403	0,01787793
25,1	0,09407154	0,01838106	0,08188469	0,02340146	2,12107839	0,01811965
25,2	0,0945096	0,01828616	0,08137813	0,02349535	2,11282807	0,01869734
25,3	0,09565271	0,0182195	0,08105671	0,02335452	2,10829126	0,01840673
25,4	0,09743986	0,01784603	0,0803066	0,02310176	2,10880194	0,01802974
25,5	0,09888089	0,01748357	0,08020663	0,02318099	2,10922527	0,01798943
25,6	0,10028631	0,0169023	0,07922162	0,02302604	2,11021703	0,01748898
25,7	0,1012329	0,01665798	0,0799513	0,02307129	2,11863781	0,01689176
25,8	0,10189034	0,01652693	0,0792764	0,02296138	2,11341001	0,01670157
25,9	0,10242756	0,01614153	0,07895031	0,02308092	2,11573518	0,01680717
26	0,10288857	0,01620227	0,07869798	0,02312142	2,11626595	0,01706136
26,1	0,10333965	0,01627165	0,07850328	0,02308364	2,11267088	0,01702731
26,2	0,10380375	0,01600103	0,07757104	0,02303449	2,11306256	0,01678081
26,3	0,1043554	0,01588399	0,07783299	0,02348498	2,11609787	0,01677851
26,4	0,10456481	0,01611123	0,07806256	0,02361756	2,11609074	0,01726246
26,5	0,10491175	0,01627631	0,07792836	0,02359388	2,11173392	0,01818656
26,6	0,10553994	0,0164405	0,07694744	0,0236622	2,10895796	0,01763491
26,7	0,10725079	0,0167266	0,0763968	0,02350087	2,10901266	0,01732992
26,8	0,10911763	0,0165914	0,07570666	0,02323655	2,11172239	0,01734304
26,9	0,10966057	0,01642308	0,07595509	0,02326898	2,11891362	0,0171435
27	0,11044267	0,01662406	0,07609431	0,02332153	2,12574509	0,01703158
27,1	0,11016105	0,01645861	0,07643981	0,02351198	2,13493913	0,01599761
27,2	0,1092632	0,01643499	0,07732481	0,02344057	2,14049469	0,01653622
27,3	0,10827124	0,01670494	0,07818622	0,02338261	2,14354421	0,01722172
27,4	0,10699489	0,0167437	0,07796889	0,02314582	2,14731517	0,017738
27,5	0,10545406	0,01691994	0,07858644	0,02291174	2,15057127	0,01790646
27,6	0,10393908	0,01709622	0,07932721	0,0231355	2,15171879	0,0178327
27,7	0,10178456	0,01694059	0,0798112	0,02314037	2,15091548	0,01855566
27,8	0,09850094	0,01684937	0,08043935	0,02332894	2,15040919	0,01926034
27,9	0,0956792	0,01707129	0,08087767	0,02352828	2,14433411	0,01984241
28	0,09306726	0,01727565	0,08126717	0,02367216	2,13663813	0,02101388
28,1	0,08940261	0,01759104	0,08126639	0,02346356	2,1189199	0,02251521
28,2	0,08716923	0,01816836	0,08114293	0,02359491	2,10041482	0,02421783
28,3	0,08500487	0,01869223	0,08025612	0,02385691	2,08084325	0,02449499
28,4	0,08309669	0,01899947	0,07920605	0,02377366	2,06345938	0,02513335
28,5	0,08114758	0,01931718	0,07919819	0,02368544	2,04976888	0,0257901
28,6	0,07913844	0,01925354	0,07812166	0,02367724	2,02804633	0,02622628
28,7	0,07796342	0,01950021	0,07725613	0,0237231	2,02046428	0,02627208
28,8	0,07833296	0,019877	0,07722104	0,02364082	2,01507665	0,02603744
28,9	0,08076641	0,01973126	0,07680253	0,0237097	2,01163535	0,02567795
29	0,08219095	0,0195375	0,0771334	0,02351372	2,01620713	0,02521951

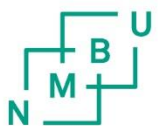
29,1	0,08388702	0,01951242	0,0768411	0,02336992	2,02338754	0,02423242
29,2	0,08676498	0,01940353	0,07716796	0,02352709	2,03544535	0,02308196
29,3	0,08849138	0,01906041	0,0776681	0,02338046	2,04420291	0,02203591
29,4	0,09099844	0,01855488	0,07813601	0,02319896	2,05852084	0,02166557
29,5	0,0938867	0,01822472	0,07915602	0,02310312	2,07283457	0,01993052
29,6	0,09660304	0,01800806	0,07958051	0,02305124	2,08354004	0,01846495
29,7	0,09989214	0,0179545	0,08030685	0,02324673	2,10758316	0,01802662
29,8	0,1018799	0,01763769	0,08088023	0,02301824	2,11587622	0,01728481
29,9	0,1030164	0,0174835	0,08082652	0,02284377	2,12323055	0,01674024
30	0,1026318	0,01759018	0,08095322	0,02266095	2,12890757	0,01663197
30,1	0,10254362	0,01767659	0,08042122	0,02272784	2,13256488	0,01648513
30,2	0,1030815	0,01781237	0,08038809	0,0227776	2,1370889	0,0161979
30,3	0,1028737	0,01758003	0,08024964	0,02257213	2,1385529	0,01605827
30,4	0,10341533	0,01761845	0,07966006	0,02248194	2,14017907	0,01613036
30,5	0,10381045	0,01761316	0,07923555	0,0225584	2,14124033	0,01552243
30,6	0,10385183	0,01762263	0,07870378	0,02256656	2,14015899	0,01546551
30,7	0,10433429	0,01751155	0,0786314	0,02277873	2,14129788	0,01546969
30,8	0,10405541	0,01733381	0,07789029	0,02272379	2,1377041	0,0153703
30,9	0,10371678	0,01731154	0,07777812	0,02290938	2,13752132	0,01557165
31	0,10442216	0,01731432	0,07693845	0,02283279	2,13444712	0,01570574
31,1	0,1049381	0,01722115	0,07699128	0,02282571	2,13415079	0,01570261
31,2	0,10629552	0,01704051	0,07646489	0,02281146	2,13076697	0,01548439
31,3	0,10652192	0,01664843	0,07640108	0,0229721	2,12741613	0,01624868
31,4	0,10616236	0,01699712	0,07682458	0,02330065	2,12497765	0,01629922
31,5	0,10564692	0,016711	0,07703143	0,02336487	2,12356105	0,01705812
31,6	0,10514482	0,01660125	0,07650636	0,02352199	2,12135578	0,01748631
31,7	0,10526783	0,01655045	0,07636917	0,02388152	2,12092228	0,01820968
31,8	0,10503305	0,01655836	0,0762864	0,02385528	2,11917363	0,01808512
31,9	0,10548656	0,01659347	0,07678089	0,02369028	2,11693145	0,01806845
32	0,10603519	0,0165658	0,07619801	0,02335556	2,11688834	0,0178251
32,1	0,10589193	0,01649377	0,07665037	0,02348977	2,11861881	0,01803079
32,2	0,1063871	0,01665616	0,07694608	0,02367497	2,11936219	0,01714915
32,3	0,10623011	0,01675443	0,07721716	0,02373753	2,12061167	0,01715086
32,4	0,10620371	0,01698233	0,07679171	0,02347615	2,11850589	0,01637109
32,5	0,10681648	0,01666864	0,07645286	0,02307874	2,11892086	0,01598449
32,6	0,107751	0,01682114	0,07627381	0,0229822	2,11905783	0,01535598
32,7	0,1083706	0,01689314	0,07650603	0,02277008	2,11995301	0,01558631
32,8	0,10829858	0,01674549	0,07652872	0,02252043	2,12020151	0,01527885
32,9	0,10933546	0,01678856	0,07617902	0,02231638	2,11984086	0,0154494
33	0,10945686	0,01682149	0,0755902	0,02228876	2,11851919	0,01513912
33,1	0,11000213	0,01677245	0,07604282	0,02259073	2,11597044	0,01548543
33,2	0,11001872	0,01684058	0,0756159	0,02267606	2,1147095	0,01518102
33,3	0,10959025	0,01671543	0,07507403	0,02259244	2,11132255	0,01551224
33,4	0,10956553	0,01645324	0,07441976	0,02261415	2,10654514	0,01571758
33,5	0,11010868	0,01630651	0,0745129	0,02256676	2,10947739	0,01558784
33,6	0,1101537	0,01615801	0,0743804	0,02253396	2,11302023	0,01595129
33,7	0,10952101	0,01622563	0,07413456	0,02259568	2,1187743	0,01568878
33,8	0,10872245	0,01623922	0,07461038	0,02251737	2,12356825	0,01555182

33,9	0,10764738	0,016247	0,07511434	0,02265167	2,12554139	0,01597161
34	0,10606087	0,01663385	0,07543052	0,02283263	2,12571398	0,01665265
34,1	0,10473924	0,01690716	0,07576988	0,02307457	2,12356581	0,01693591
34,2	0,10312878	0,01723859	0,07590366	0,02315552	2,12139279	0,01709471
34,3	0,1020323	0,01707534	0,07615516	0,02327305	2,12220299	0,01726401
34,4	0,1015991	0,01731466	0,07659339	0,02355557	2,12379126	0,01802318
34,5	0,10076393	0,01765024	0,077002	0,02360491	2,12627057	0,01849962
34,6	0,10018131	0,01783658	0,07656915	0,02399001	2,12519045	0,01890182
34,7	0,10031609	0,01820188	0,07692544	0,02421377	2,12220776	0,01916943
34,8	0,10042714	0,01814196	0,07729326	0,02412767	2,11526766	0,01930381
34,9	0,10072928	0,0180751	0,07681087	0,0243576	2,11008738	0,0192167
35	0,10166146	0,01821536	0,07631153	0,02417527	2,10605423	0,01892425
35,1	0,10286038	0,01800805	0,07604904	0,0239795	2,10212359	0,018597
35,2	0,10388882	0,01775018	0,0758442	0,02396052	2,09831241	0,0188048
35,3	0,10552827	0,01743095	0,07528449	0,02397378	2,09740896	0,01885845
35,4	0,10588953	0,0175869	0,07557853	0,02397296	2,09295295	0,01907296
35,5	0,10609695	0,01761498	0,07499313	0,02382047	2,08896941	0,01891141
35,6	0,10634448	0,01768355	0,074944	0,0237172	2,08567454	0,01841194
35,7	0,10585001	0,01763884	0,07567318	0,02354731	2,08065965	0,0182765
35,8	0,10506778	0,01757685	0,07514534	0,02358951	2,07649183	0,01807854
35,9	0,10470623	0,01764102	0,07486357	0,023796	2,07261781	0,0185011
36	0,10501215	0,01782747	0,07459918	0,02372843	2,07014122	0,01848622
36,1	0,10481895	0,01767693	0,07536714	0,02386854	2,06844696	0,0182865
36,2	0,1043227	0,01754381	0,07528181	0,02389909	2,07081156	0,01799465
36,3	0,10415603	0,01772908	0,0757039	0,02393385	2,07657996	0,01775071
36,4	0,10377946	0,01779916	0,07662758	0,02385079	2,07915466	0,0173381
36,5	0,10398195	0,01775806	0,07646159	0,02367385	2,08271643	0,01699661
36,6	0,1042471	0,01761808	0,07659634	0,02344012	2,08484288	0,01694559
36,7	0,10459766	0,01728862	0,07732072	0,02346289	2,08797911	0,01703013
36,8	0,10522482	0,01710838	0,07735337	0,02328152	2,0908926	0,01682294
36,9	0,10603362	0,01691801	0,07769469	0,02316245	2,0963816	0,01662026
37	0,10649735	0,01672593	0,07779875	0,02304966	2,10325233	0,01628206
37,1	0,10678302	0,01639597	0,07855215	0,02295754	2,10684271	0,01624583
37,2	0,10749953	0,01618367	0,07817706	0,02304231	2,11184427	0,01668958
37,3	0,10783636	0,01613208	0,07818993	0,02312854	2,1132032	0,01679014
37,4	0,10822817	0,01587061	0,07777206	0,0230969	2,11606149	0,01674696
37,5	0,10880213	0,0156495	0,07700479	0,02305526	2,11804592	0,01630116
37,6	0,1094854	0,01551481	0,07714556	0,02316829	2,12049365	0,01643783
37,7	0,10937825	0,01504196	0,0773755	0,02313357	2,12580302	0,0158517
37,8	0,10902815	0,01514968	0,07702512	0,02316958	2,12818498	0,01600986
37,9	0,10913861	0,01511049	0,0770033	0,0232286	2,13106613	0,01645178
38	0,10874628	0,01515382	0,07725251	0,02356285	2,13238009	0,01638584
38,1	0,10842255	0,01540963	0,07734065	0,02362049	2,13391251	0,01651615
38,2	0,1073523	0,01556902	0,07752086	0,02393463	2,13367171	0,01692397
38,3	0,1069266	0,01588698	0,0772803	0,02407213	2,13251302	0,01699163
38,4	0,10661033	0,01581167	0,07767872	0,02428941	2,13940904	0,01700403
38,5	0,10597624	0,01602084	0,07782837	0,02442367	2,14625571	0,01682956
38,6	0,10460786	0,01641042	0,07763266	0,02442311	2,15447339	0,01683875

38,7	0,10338487	0,01649904	0,0782051	0,0244873	2,15924465	0,0168869
38,8	0,10176632	0,01699199	0,07890217	0,02470223	2,16041023	0,01761319
38,9	0,10055804	0,01737742	0,07928218	0,02454299	2,16207571	0,01772024
39	0,09894468	0,01787588	0,07946798	0,02467087	2,16147084	0,01782148
39,1	0,09756487	0,01819334	0,07941041	0,02408386	2,15769759	0,01851133
39,2	0,09611029	0,01807868	0,07964478	0,02403674	2,14913347	0,01845249
39,3	0,09518167	0,01834126	0,07971635	0,02375236	2,14066157	0,02022782
39,4	0,09354685	0,01841766	0,08010075	0,02322217	2,13037907	0,02076492
39,5	0,09186254	0,01847657	0,07957941	0,02265007	2,11347515	0,02140355
39,6	0,0908834	0,01836336	0,07971318	0,02223482	2,09628384	0,02216301
39,7	0,09014042	0,01819603	0,07949812	0,02193523	2,08401987	0,02309925
39,8	0,08957695	0,01801959	0,0786312	0,02168554	2,07255566	0,02301983
39,9	0,08969211	0,01749707	0,076847	0,02129173	2,05988189	0,02294133
40	0,09030653	0,01716927	0,07641084	0,02118656	2,05690889	0,02289551
40,1	0,09094016	0,01670144	0,07644522	0,02100527	2,06201307	0,02230591
40,2	0,09218652	0,01647922	0,075777	0,02122672	2,07092219	0,02151568
40,3	0,09366301	0,01633576	0,07539538	0,02127939	2,08293389	0,02130029
40,4	0,09473774	0,01626366	0,07429837	0,02125421	2,09498816	0,01918284
40,5	0,09624339	0,01618648	0,0740457	0,02145037	2,1091401	0,01809482
40,6	0,09765978	0,01630632	0,07440583	0,02160231	2,12357378	0,01751376
40,7	0,09828382	0,0161339	0,07395797	0,02172968	2,1360711	0,01688586
40,8	0,09991556	0,01601411	0,07440446	0,02208158	2,14410054	0,01670841
40,9	0,10059717	0,01622657	0,0744513	0,02196139	2,14513486	0,01655151
41	0,10200085	0,01647917	0,07513926	0,02216218	2,15390123	0,01648311
41,1	0,10206743	0,01640737	0,07496718	0,02229564	2,15438735	0,01612132
41,2	0,10275143	0,01630174	0,07447629	0,02225452	2,15202265	0,01626597
41,3	0,10247501	0,01615418	0,0745608	0,02220638	2,14821895	0,01610173
41,4	0,10277886	0,01609449	0,07453725	0,0219194	2,14428415	0,01598062
41,5	0,10333342	0,01603495	0,07506771	0,0220016	2,14140337	0,01577271
41,6	0,10340265	0,01620745	0,0747237	0,02227666	2,13716172	0,01645938
41,7	0,10334615	0,01616692	0,07456515	0,0227043	2,13121985	0,01660659
41,8	0,10351301	0,01649673	0,07432175	0,02284483	2,12559571	0,01665053
41,9	0,10277144	0,01660987	0,07389185	0,02277022	2,11871522	0,01662605
42	0,10311195	0,01672978	0,07397646	0,02314472	2,12093984	0,01664645
42,1	0,10277158	0,0169456	0,07455714	0,02325225	2,12085614	0,01633033
42,2	0,10336516	0,01693683	0,07409747	0,02336487	2,12167348	0,01626529
42,3	0,10355635	0,01708054	0,07383541	0,02342314	2,11768983	0,0163183
42,4	0,10449445	0,01698033	0,07435401	0,02319643	2,11623801	0,0164641
42,5	0,10401343	0,01718446	0,07455775	0,02334593	2,11561239	0,01668981
42,6	0,1033868	0,01711246	0,074333	0,02322833	2,11699044	0,01645323
42,7	0,1032701	0,01685732	0,0745257	0,02291345	2,11975777	0,01567606
42,8	0,10345903	0,01683185	0,07477504	0,02254138	2,125353	0,01545647
42,9	0,10384746	0,0164326	0,07499396	0,02226422	2,1310895	0,01551182
43	0,10417857	0,01633838	0,0749636	0,02200558	2,1364981	0,01511327
43,1	0,10436648	0,01625654	0,07469638	0,02158042	2,1436332	0,01489235
43,2	0,10422452	0,01608602	0,07425292	0,02143258	2,14996005	0,01489758
43,3	0,10383095	0,01632404	0,07396543	0,02132234	2,15345349	0,01486584
43,4	0,10323061	0,01648836	0,07427861	0,02120359	2,16015509	0,01463644

43,5	0,10274461	0,01659444	0,07390129	0,02139751	2,16987712	0,01477165
43,6	0,1026996	0,01631079	0,07382566	0,02121004	2,18344702	0,01449732
43,7	0,10300112	0,01637804	0,07429978	0,02101863	2,19711116	0,01507415
43,8	0,10280328	0,01646103	0,07472572	0,02092006	2,21221094	0,01468931
43,9	0,10256025	0,01640025	0,07519998	0,02071044	2,22393213	0,01435518
44	0,1023864	0,01683824	0,07586716	0,02076125	2,22956558	0,01406766
44,1	0,10175674	0,0168425	0,07661645	0,0208596	2,22823408	0,01456955
44,2	0,10131536	0,01676017	0,0763913	0,02108823	2,2237451	0,01500523
44,3	0,1017078	0,01698864	0,07629932	0,02107622	2,2190072	0,01457731
44,4	0,10170578	0,01676474	0,07699707	0,02097043	2,21897657	0,01462071
44,5	0,10233242	0,01672277	0,07752691	0,02121871	2,21667446	0,01432917
44,6	0,10285542	0,0167327	0,07751205	0,02134422	2,20820931	0,01456636
44,7	0,10302062	0,01703701	0,07740129	0,02150434	2,19708854	0,01500444
44,8	0,10314377	0,01716243	0,07698172	0,02170135	2,18693983	0,01472274
44,9	0,10385366	0,01701494	0,07655973	0,02174223	2,17487084	0,01508858
45	0,10461378	0,01698061	0,0758279	0,02199192	2,16373693	0,01501928
45,1	0,10481067	0,01672179	0,07605705	0,02231935	2,15737937	0,01482729
45,2	0,10543813	0,01671843	0,07580219	0,02231056	2,15900872	0,01442669
45,3	0,10643982	0,01668575	0,07651673	0,02250758	2,16199584	0,01419324
45,4	0,10732077	0,01636653	0,07639069	0,02270181	2,16580139	0,01480657
45,5	0,10811718	0,01616158	0,07653512	0,02259767	2,16802694	0,01452623
45,6	0,10782449	0,01608007	0,07675581	0,02262522	2,16958737	0,01497633
45,7	0,10733548	0,01612237	0,07668882	0,02273392	2,17059185	0,01463373
45,8	0,10723286	0,01600071	0,07687882	0,0226708	2,16388812	0,01424859
45,9	0,10786974	0,01587423	0,07626892	0,02269095	2,16469209	0,01390494
46	0,10761373	0,01603596	0,07514682	0,02266218	2,15388143	0,01421694
46,1	0,10710049	0,01587928	0,07430016	0,02255588	2,13799911	0,01459258
46,2	0,10683385	0,0156132	0,07163084	0,02218919	2,11918444	0,01484859
46,3	0,10680704	0,01546644	0,06977577	0,02219892	2,1037867	0,01447451
46,4	0,10667988	0,01548725	0,06854844	0,02195421	2,09959286	0,01378199
46,5	0,10655563	0,01566279	0,06793097	0,0215789	2,0923112	0,01296517
46,6	0,10673205	0,01581239	0,06731213	0,02152599	2,08283829	0,01274496
46,7	0,10716273	0,01568221	0,06620308	0,02134303	2,07561511	0,01249617
46,8	0,10771775	0,01536586	0,06507642	0,02099019	2,07078581	0,01266089
46,9	0,10826505	0,01519077	0,06397111	0,02084858	2,07364735	0,01252652
47	0,10848795	0,01518564	0,06408366	0,02074686	2,0757709	0,0127467
47,1	0,10860457	0,01481557	0,06437971	0,02076765	2,08263462	0,01244743
47,2	0,10871721	0,01468583	0,06462763	0,02065251	2,09550801	0,01194326
47,3	0,10986331	0,01487515	0,06596374	0,02068571	2,11838646	0,01140825
47,4	0,11029365	0,01475546	0,06751863	0,0206305	2,1371149	0,01169473
47,5	0,11025675	0,01454516	0,06806086	0,02049078	2,14834644	0,01216939
47,6	0,10876713	0,01432617	0,06844435	0,0205539	2,1536934	0,01244743
47,7	0,1076085	0,01442205	0,06819056	0,02053336	2,15887681	0,01285894
47,8	0,10712261	0,01446616	0,06842133	0,02052016	2,17087179	0,01285984
47,9	0,10600858	0,01463178	0,06971368	0,02063799	2,18167248	0,01224595
48	0,1050396	0,01482705	0,07044597	0,02076295	2,19233103	0,0123298
48,1	0,1029823	0,01506798	0,07097564	0,02087052	2,18609056	0,01290616
48,2	0,10129484	0,01550004	0,07156864	0,0210564	2,18756808	0,01300003

48,3	0,10024312	0,01609919	0,07224776	0,02139517	2,1928984	0,01317422
48,4	0,09814195	0,01604856	0,07269704	0,02139326	2,19158693	0,01397921
48,5	0,09634647	0,01644701	0,07326201	0,02157839	2,19131877	0,01426312
48,6	0,09470913	0,01665937	0,0740814	0,02175191	2,1846237	0,01440774
48,7	0,09415034	0,01700398	0,0747845	0,02184993	2,1828529	0,01488731
48,8	0,09349419	0,01710747	0,07606739	0,02209543	2,18592464	0,01510095
48,9	0,09187619	0,01719609	0,07639268	0,0218338	2,17491416	0,01521999
49	0,09145608	0,01767427	0,07646553	0,02195654	2,16958172	0,01607284
49,1	0,09062091	0,01809933	0,07701992	0,02214903	2,16220425	0,01641204
49,2	0,09026135	0,01811668	0,07788026	0,02209771	2,16374309	0,01624592
49,3	0,09003256	0,01857551	0,07846871	0,02219273	2,16354554	0,01678305
49,4	0,08951435	0,01879009	0,07861067	0,02213997	2,158985	0,01731951
49,5	0,08888541	0,01934729	0,07935665	0,02248864	2,15622307	0,01724745
49,6	0,08825968	0,01948611	0,07930787	0,02238905	2,15296985	0,01747467
49,7	0,08810141	0,01978764	0,07970432	0,02244723	2,15076705	0,01823493
49,8	0,08804422	0,02004692	0,08031191	0,02251346	2,14838997	0,01860284
49,9	0,08769481	0,02026327	0,08119578	0,02261538	2,14263283	0,018973
50	0,08812064	0,02053279	0,08129522	0,02296292	2,1424533	0,01991769
50,1	0,08695839	0,0206463	0,0818022	0,02312952	2,13297821	0,02014593
50,2	0,08642835	0,02048787	0,08239526	0,0233009	2,12472392	0,02061128
50,3	0,08602052	0,02091088	0,08160462	0,02367609	2,1141235	0,02139041
50,4	0,08552329	0,02070403	0,0821648	0,02376288	2,10460093	0,02204018
50,5	0,08497519	0,02088373	0,08261066	0,02409298	2,09637563	0,02298058
50,6	0,08441958	0,02108847	0,08248183	0,02412002	2,08384932	0,02361555
50,7	0,08448975	0,02145376	0,08297969	0,02442841	2,07146036	0,02524669
50,8	0,08389779	0,02165379	0,08226435	0,02456482	2,05713682	0,02617159
50,9	0,08330491	0,02178787	0,08238529	0,02503009	2,04605867	0,02639805
51	0,0824597	0,02201991	0,08190525	0,02553463	2,03178718	0,02693163
51,1	0,08068213	0,02241952	0,08190693	0,02560887	2,012707	0,02725526
51,2	0,07981985	0,02262961	0,08145925	0,02553562	1,99760256	0,02784269
51,3	0,07879238	0,02306713	0,08078701	0,02541242	1,98265958	0,02834952
51,4	0,07771915	0,02304029	0,08114132	0,02517397	1,96955199	0,02844982
51,5	0,07686358	0,02335703	0,08049252	0,02502941	1,95650225	0,02850186
51,6	0,07593962	0,02339025	0,08005627	0,02476255	1,94288886	0,02847992



Norges miljø- og biovitenskapelige universitet
Noregs miljø- og biovitenskapslelege universitet
Norwegian University of Life Sciences

Postboks 5003
NO-1432 Ås
Norway